AD-A123 522 PERSISTENT CURRENTS IN A ROTATING SUPERLEAK PARTIALLY FILLED WITH SUPERFLUID HELIUM(U) CALIFORNIA UNIV LOS ANGELES DEPT OF PHYSICS J S MARCUS DEC 82 TR-41 1/3

UNCLASSIFIED N00014-75-C-0246 F/G 20/4 NL

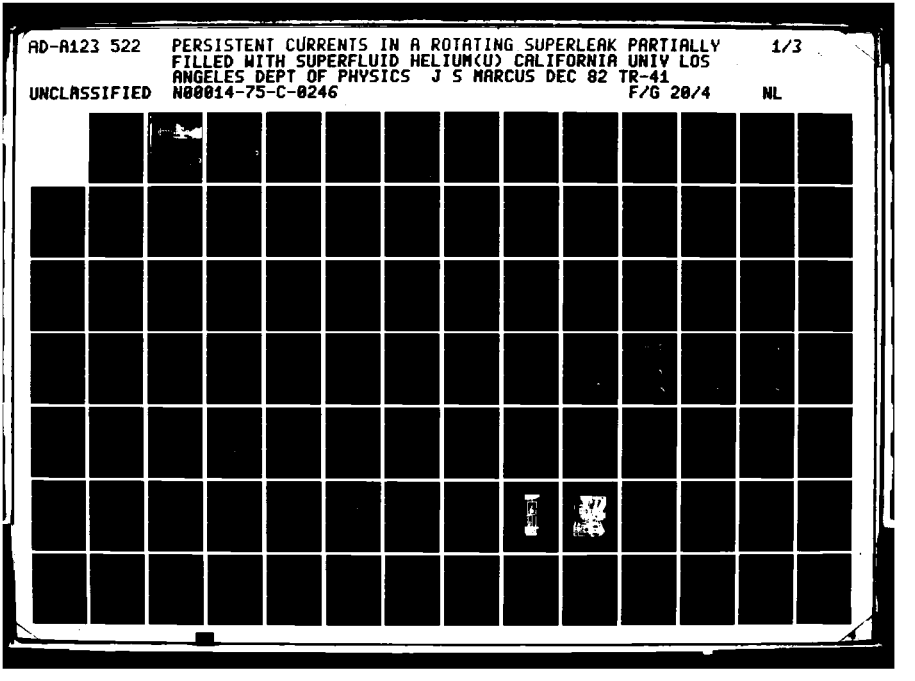

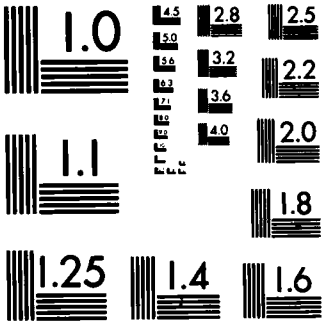

MICROCOPY RESOLUTION TEST CHART
NATIONAL BUREAU OF STANDARDS-1963-A

UCLA

Department of Physics

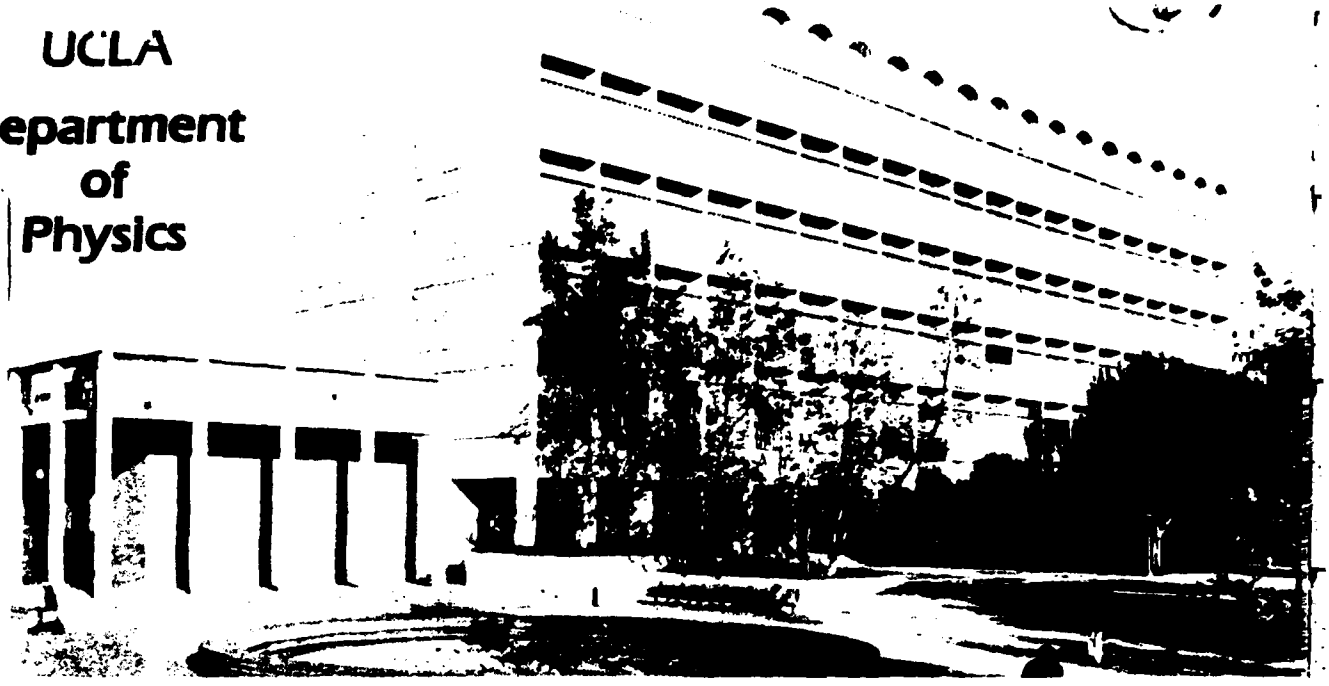

LOS ANGELES 90024

CALIFORNIA

TECHNICAL REPORT No. 41

December 1982

Submitted by

I. Rudnick, Project Director

Persistent Currents in a Rotating Superleak Partially Filled with Superfluid Helium

(6)

by

John Stanley Marcus

Office of Naval Research
Contract
N00014-75-C-0246
NR. No. 384-302

Department of Physics
University of California
Los Angeles, California 90024

UNCLASSIFIED

SECURITY CLASSIFICATION OF THIS PAGE (When Data Entered)

REPORT DOCUMENTATION PAGE	READ INSTRUCTIONS BEFORE COMPLETING FORM
1. REPORT NUMBER: 41	2. GOVT ACCESSION NO.: AD-A123522
	3. RECIPIENT'S CATALOG NUMBER:
4. TITLE (and Subtitle): PERSISTENT CURRENTS IN A ROTATING SUPERLEAK PARTIALLY FILLED WITH SUPERFLUID HELIUM	5. TYPE OF REPORT & PERIOD COVERED: Interim
	6. PERFORMING ORG. REPORT NUMBER: Technical Report #41
7. AUTHOR(s): John Stanley Marcus	8. CONTRACT OR GRANT NUMBER(s): N00014-75-C-0246
9. PERFORMING ORGANIZATION NAME AND ADDRESS: University of California at Los Angeles, Department of Physics, Los Angeles, California 90024	10. PROGRAM ELEMENT, PROJECT, TASK AREA & WORK UNIT NUMBERS: NR. No. 384-302
11. CONTROLLING OFFICE NAME AND ADDRESS: Office of Naval Research, Physics Division, Code 412, Arlington, Virginia 22217	12. REPORT DATE: December 1982
	13. NUMBER OF PAGES: 175
14. MONITORING AGENCY NAME & ADDRESS (if different from Controlling Office)	15. SECURITY CLASS. (of this report): UNCLASSIFIED
	15a. DECLASSIFICATION/DOWNGRADING SCHEDULE

16. DISTRIBUTION STATEMENT (of this Report)

APPROVED FOR PUBLIC RELEASE; DISTRIBUTION UNLIMITED

17. DISTRIBUTION STATEMENT (of the abstract entered in Block 20, if different from Report)

18. SUPPLEMENTARY NOTES

19. KEY WORDS (Continue on reverse side if necessary and identify by block number)

SUPERFLUIDITY	SURFACE TENSION SOUND
SUPERFLUID HELIUM	SUPERLEAK
CRYOGENIC	PERSISTENT CURRENTS
THIRD SOUND	ACOUSTIC SCATTERING
FIFTH SOUND	ACOUSTIC INDEX OF REFRACTION

20. ABSTRACT (Continue on reverse side if necessary and identify by block number)

See over

DD FORM 1 JAN 73 1473 EDITION OF 1 NOV 65 IS OBSOLETE
S/N 0102-LF-014-6601

UNCLASSIFIED

SECURITY CLASSIFICATION OF THIS PAGE (When Data Entered)

20. ABSTRACT

Persistent currents in a partially helium II filled rotating superleak have been investigated. Measurements were made using the acoustic doppler shift of the thickness wave in the helium II film which covers the alumina powder grains (1 micron) of the superleak. The superleak is contained in an annular resonator. Q's as high as 120 were observed. The acoustic index of refraction, n, has been measured as a function of filling fraction, f (f is the fraction of pores filled with liquid He II). Motivated by a model which treats the scattering from the powder and vapor separately an expression for the index of refraction, n, has been formulated. The data is in excellent agreement with this formulation for $0.3 < f < 1.0$. When $f = 1$ the system becomes a fourth sound resonator and the value of n is in excellent (1%) agreement with that from fourth sound.

The existence of a potential flow region (Landau region) was established and measured at low rotational speeds (below 0.5 Hz). This region is comparable to the Meissner region in irreversible high field type-II superconductors. The upper bound on this region ω_{c1} plays the same role as H_{c1} does in the type-II superconductor. At rotational velocities greater than ω_{c1} quantized vortices enter the system. These vortex lines are directly comparable to quantized magnetic flux lines in type-II superconductors. At even higher rotational velocities $\omega_s - \omega_n$ becomes a maximum at a rotational velocity ω_σ (about 1 Hz) was measured as a function of temperature and filling fraction.

The decay rates of persistent current velocities were measured over almost five decades of time. The persistent current velocity was found to decay at a logarithmic rate. This rate is determined by the initial persistent current velocity rather than the instantaneous velocity. The decay per decade ranged between 0.5 and 2.9 percent.

We found a one-to-one correspondence with our system and that of a helium II filled superleak and also to the analogous quantities in an irreversible type-II superconductor.

TABLE OF CONTENTS

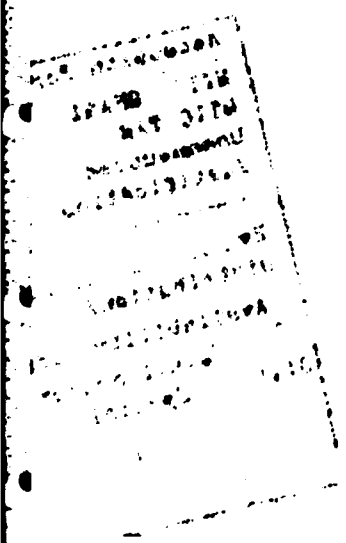

List of Figures and Tables

ACKNOWLEDGEMENTS

I would like to thank Professor Isadore Rudnick for not only suggesting my thesis problem but also for his friendship, continued support and enthusiasm which have made my studies so much more enjoyable.

I would also like to thank Professor Seth Putterman and Professor Gary Williams for their time and effort on my behalf and Professor Daniel Kivelson and Professor Richard Stern for being on by doctoral committee.

A special thanks also goes to the following people. Gabriel Briceno who helped take much of the data and made many helpful comments. Scott Hannahs who was never to busy to stop his work and help fix my computer problems or write new software. Steve Baker who spent many hours on the problems involved with the acoustic scattering correction. Also I would like to thank Harold Eaton who was always a valuable source of information and ideas and Bob (Bonzo) Keolian who was always around late at night for one thing or another.

Many thanks to the whole machine shop under the direction of Bud Knox and for the work and advice of Al Casillas, and Floyd Lacy. A special thanks to Pete

Goodman in the Student Shop.

I would also like to thank the following members of the Physics Department for their contributions; Ron Bohn, Barbra Yamadera Cabot, Curt Hamblin, Earl Kershaw Pedro Oillataguerre, Jackie Payne, and Gail Yamamoto.

A special thanks to Liz Muldawer-Gallagher for her help.

I would also like to thank my family and friends for their support and encouragement and finally I would like to thank Jacklyn for her help, support and love which makes everything worthwhile.

ABSTRACT OF THE DISSERTATION

Persistent Currents in a Rotating Superleak
Partially Filled with Superfluid Helium

by

John Stanley Marcus
Doctor of Philosophy in Physics
University of California, Los Angeles, 1983
Professor Isadore Rudnick, Chairman

Persistent currents in a partially helium II filled rotating superleak have been investigated. Measurements were made using the acoustic doppler shift of the thickness wave in the helium II film which covers the alumina powder grains (1 micron) of the superleak. The superleak is contained in an annular resonator. Q's as high as 120 were observed. The acoustic index of refraction, n, has been measured as a function of filling fraction, f (f is the fraction of pores filled with liquid He II). Motivated by a model which treats

the scattering from the powder and vapor separately an expression for the index of refraction, n, has been formulated. The data is in excellent agreement with this formulation for $0.3 < f < 1.0$. When $f = 1$ the system becomes a fourth sound resonator and the value of n is in excellent (1%) agreement with that from fourth sound.

The existence of a potential flow region (Landau region) was established and measured at low rotational speeds (below 0.5 Hz). This region is comparable to the Meissner region in irreversible high field type-II superconductors. The upper bound on this region Wc1 plays the same role as Hc1 does in the type-II superconductor. At rotational velocities greater than Wc1 quantized vortices enter the system. These vortex lines are directly comparable to quantized magnetic flux lines in type-II superconductors. At even higher rotational velocities $\omega_s - \omega_n$ becomes a maximum at a rotational velocity Wsig. The dependence of ω_σ (about 1 Hz) was measured as a function of temperature and filling fraction.

The decay rates of persistent current velocities were measured over almost five decades of time. Measurements were made both as a function of filling fraction and initial persistent current velocity. The

persistent current velocity was found to decay at a logarithmic rate. This rate is determined by the initial persistent current velocity rather than the instantaneous velocity. The decay per decade ranged between 0.5 and 2.9 percent.

We found a one-to-one correspondence with our system and that of a helium II filled superleak and also to the analogous quantities in an irreverisible type-II superconductor.

I. INTRODUCTION TO THE SUPERFLUID PROBLEM

Macroscopic quantum systems have captivated the attention of physicists since they were recognized in the early 1900's. Helium was first liquified by Kamerlingh Onnes in 1908. Only three years later superconducting properties were discovered by Kamerlingh Onnes in mercury. Then in 1938 Kapitza (Kapitza) and also Allen and Misener (Allen) observed that helium could pass through fine slits and capillaries respectively without measureable resistance. In such geometries any other liquid would be held almost immobile. These experiments are taken as the first recognition of superfluidity and the beginning of the study of superfluid helium as a macroscopic quantum system.

Helium gas is liquified under atmospheric presssure at 4.2 degrees above absolute zero (4.2 degrees Kelvin). It is the only liquid to exist at this extreme temperature, due to its large zero point motion and very low Van der Waals attraction to itself. Once liquified, helium behaves as a normal viscous fluid would, until it is cooled below 2.17 degrees Kelvin at its vapor pressure. This point on the helium phase diagram is

known as the lambda point. It is below this temperature, that helium is a superfluid and called helium II which distinguishes it from its normal phase helium I above 2.17 degrees Kelvin.

Research on helium II had begun in full swing after the experiments of Kapitza and of Allen and Misener had indicated that helium II had zero viscosity. However, Keesom and Macwood (Keesom) also measured the viscosity of helium in 1938 with a torsional oscillator. They reported no abrupt change at the lambda point but did observe a continual decrease in damping as the temperature was lowered below the lambda point. The conflicting results of the experimental determination of the viscosity of superfluid helium created a paradox which could not be resolved with classical hydrodynamic theory. Classical hydrodynamics uses five variables to describe the system. The vector velocity (three), entropy, and density are usually taken as the complete set of five variables.

I.B THE TWO FLUID MODEL

Physicists, to explain the apparent paradox, developed the two fluid theory. The roots of the two fluid model lie in the research of Fritz London (London) and Lazlo Tisza (Tisza) in 1938. In 1941 Lev Landau (Landau) formulated a thermohydrodynamic theory of helium II in which eight variables are taken as a complete set. This theory became known as the Two Fluid Model (Landau's two fluid equations). A velocity field for the superfluid component (three), a velocity field for the normalfluid component (three), entropy and density are used to make a total of eight variables. The two fluid theory describes helium II as two interpenetrating fluids. One which behaves as a normal fluid and the other a superfluid. The total density, ρ, is given by the sum of the normalfluid density, ρ_n, and the superfluid density, ρ_s.

$$\rho = \rho_n + \rho_s \qquad \{I.B.1\}$$

Each has its own vector velocity, Vn and Vs. The superfluid component carries no entropy and flows with zero viscosity. The normalfluid component behaves as a Navier-Stokes fluid and carries the entropy. Equations

I.B.2 through I.B.5 are the complete set of two fluid equations which describe the thermohydrodynamics of helium II in the absence of dissipation.

$$\frac{\partial \rho}{\partial t} + \nabla \cdot (\rho_n \vec{V}_n + \rho_s \vec{V}_s) = 0 \qquad \{I.B.2\}$$

$$\frac{\partial \rho s}{\partial t} + \nabla \cdot (\rho s \vec{V}_s) = 0 \qquad \{I.B.3\}$$

$$\frac{D_s V_s}{Dt} = - \nabla \mu \qquad \{I.B.4\}$$

$$\frac{\partial \rho V_i}{\partial t} + \frac{\partial}{\partial r_j} (\rho_n V_{ni} V_{nj} + \rho_s V_{si} V_{sj} + P \delta_{ij}) = 0 \qquad \{I.B.5\}$$

Landau added the restriction that the superfluid component flow was curl free:

$$\text{curl } V_s = 0 \qquad \{I.B.6\}$$

These equations had immediate consequence for all dynamic experiments in helium II. In many cases they were found to be a complete description. This was not, however, the case for the experiments of D. Osborne in 1950 (Osborne). In these experiments the free surface of rotating helium was observed. Since the restriction that the superfluid component be curl free in helium II, a surface contour different from the parabolic surface of helium I was expected. However, no difference was observed. The combination of the theoretical predictions of Landau and these experimental results

generated considerable work both experimental and theoretical in this area. What was now needed was a unifying theory, which kept the predictions of the two fluid equations and would be able to explain the, once again, apparently paradoxical experimental results.

In 1949, L. Onsager (Onsager) proposed that the circulation of the superfluid velocity field Vs was quantized in units of Planck's constant;

$$\oint \vec{V}_s \cdot d\vec{\ell} = \frac{nh}{m_{He}} \qquad \{I.B.7\}$$

This was to apply in multiply connected regions where the presence of non-superfluid vortex cores made it multiply connected (n = 1,2,3...). To satisfy Landau's restriction n must be zero in a simply connected region by Stokes Theorem;

$$\oint \vec{V}_s \cdot d\vec{\ell} = \int \text{curl } \vec{V}_s \cdot d\vec{a} = 0 \qquad \{I.B.8\}$$

Now, the failure of the Landau restriction to predict the surface contour, in a rotating bucket, may be explained by the entrance of vortices. Vortices with non-superfluid cores satisfy equation I.B.7 for n = 1,2,3... .

It should be pointed out, that by the circulation condition of equation I.B.7, the superfluid helium system becomes a macroscopically large quantum system.

It may be used to measure what is usually considered a microscopic parameter, Planck's constant, h. It may also be possible to look for shortcomings in the current quantum mechanical theories.

Vinen's experiment in 1961 (Vinen) was the first confirmation of the quantization of the circulation. He measured the values of circulation around a fine wire stretched in a cylindrical container. Whitmore and Zimmermann (Whitmore) extended Vinen's experiment and confirmed his results. In 1963, Rayfield and Reif (Rayfield) observed ions on vortex rings in helium and further solidified the evidence for the circulation being quantized as in equation I.B.7. In 1974 Williams and Packard (Williams 1974) photographed the vortices. They rotated a tiny bucket of superfluid helium to which electrons were added. The electrons were pinned to the vortex cores. Then a vertical electric field was applied and sent the electrons into a photomultiplier which was photographed.

I.C HISTORY OF PERSISTENT CURRENT EXPERIMENTS

Since the viscosity of the superfluid component had been measured to be zero, it should have been possible to establish persistent mass currents in helium II with very long lifetimes. This is analogous to establishing a persistent electric current in a superconducting ring of zero electrical resistance. A brief history of pertinent, persistent current experiments which preceeded the current work is now presented.

Hall's 1957 experiment (Hall) which measured the angular momentum of helium II in a rotating cell, was the first support for the existence of persistent mass currents. Lifetimes as long as 25 minutes were observed. In Vinen's work previously cited, he observed that the circulation around the wire could persist for as long as one hour.

Using a helium container, similar to the one Hall used in his experiment, Reppy and Depatie (Depatie) measured the residual angular momentum after the uniformly rotating container of helium II had been brought to rest. After a given waiting period, it was

warmed above the lambda point and its steady state velocity was measured. The value of the superfluid persistent current could then be calculated. They waited up to 12 hours before warming without any observable decay in the persistent current velocity.

Reppy and co-workers (Clow) and Mehl and Zimmermann (Mehl) developed gyroscopic techniques in which their cells were filled with tightly packed porous media or powder before the helium was introduced. The porous media served two purposes. It locked the normal component to the container and raised the limiting critical velocity. These were the first experiments in which the persistent current velocity could be measured non-destructively. Decay measurements of the velocity could also be made. However, all measurements were made with the cell at rest and hence the dynamics of bringing the helium into motion could not be studied.

The most complete study of persistent currents in helium filled porous media (superleak) is the work of Kojima and Co-workers (Kojima). In these experiments the doppler shift of fourth sound was used to measure the persistent current velocities. This non-destructive technique not only allowed measurements to be taken at rest but also while the cell was being rotated. This is analogous to being able to have an applied magnetic

field while measuring the magnetization of a superconductor. They measured lifetimes of persistent currents for five decades of time (1 to 10 to the 5th seconds). An extrapolation of their results indicated that there would only be a ten percent loss of velocity in the age of the universe (10 to the 17th seconds). They also showed a one-to-one correspondence between superfluid helium II in a superleak and a highly irreversible type II superconductor (Bean). See section IV.F for a more complete comparison.

The experiments so far described have all been in systems filled with helium II. However, superfluid research was also taking place on helium films. Investigators looked for persistent flow in film systems also. R.P. Henkel et al (Reppy) were the first to measure persistent currents in a superleak partially filled with helium II. Their 1969 experiment used the gyroscopic technique developed for studying filled superleaks (Clow). They reported persistent currents with low decay rates and measured critical velocities for several film thicknesses (3 to 9 atomic layers).

In 1974, H.J. Verbeek et al (Verbeek 1974) reported persistent currents in saturated films induced by rotation. They rotated a long coiled capillary tube (100 meters) about the coil's axis and brought it to

rest. The current was detected by warming a portion of the superleak in the flow path above the lambda point. This created oscillations in the remaining film. They found a critical velocity above which they needed to rotate in order to establish a persistent current. Since then H. J. Verbeek has published his dissertation (Verbeek) which is an excellent overview of persistent film flow experiments in general and also the work he has done at Kammerlingh Onnes Laboratory (along similar lines to his previous work).

Ekholm and Hallock (Hallock) generated persistent currents with a thermal drive (without rotation). They observed decay rates for various film thicknesses . They found that for very thin films, less than eight atomic layers, the decay rates deviated strongly from the previously observed log t behavior (Telschow).

The present work looks for the first time at a rotating superleak whose pores are partially filled with helium II. Many different aspects of the system were studied. This includes the study of decay rates of persistent currents, the Landau region, the vortex state, acoustic scattering and critical velocities.

I.D SOUND MODES IN SUPERFLUID HELIUM

A plethora of sound modes exist in helium II. The existence of these many modes can be attributed to the additional three variables needed to describe a superfluid (quantum fluid) over the five variables which describe a classical Navier-Stokes fluid. There are five independent sound modes in helium II. First and second sound exist in bulk helium II. Third sound exists in films of helium II. Third, fourth and fifth sound exist in systems in which the normal fluid velocity, Vn, is zero. Fifth sound also requires the helium to be pressure released as well as Vn to be locked. For completeness tabel I.D.1 list the velocities of the various sound modes in helium II and shows the relative motion of the superfluid component and the normalfluid component in the sound modes. Figure I.D.2 is a graph of the various sound speeds (first, second, fourth and fifth).

SOUND	NORMAL COMPONENT VELOCITY	SUPERFLUID COMPONENT VELOCITY	TYPE OF WAVE	WAVE VELOCITY
1st	→	→	PRESSURE DENSITY	$c_1 = \left[\left[\frac{dp}{d\rho}\right]_s\right]^{1/2}$
2nd	→	←	TEMPERATURE ENTROPY	$c_2 = \left[\frac{\rho_s\, Ts^2}{\rho_n\, c_p}\right]^{1/2}$
3rd	ZERO	⟲	SURFACE WAVE IN FILMS	$c_3 = \left[\frac{\rho_s}{\rho} fd\right]^{1/2}$
4th	ZERO	→	PRESSURE WAVE IN SUPERLEAK	$c_4 = \left[\frac{\rho_s}{\rho} c_1^2\right]^{1/2}$
5th	ZERO	→	THERMAL WAVE IN SUPERLEAK	$c_5 = \left[\frac{\rho_n}{\rho} c_2^2\right]^{1/2}$

Figure I.D.1 The Sound Modes which Propagate in Superfluid helium, He II.

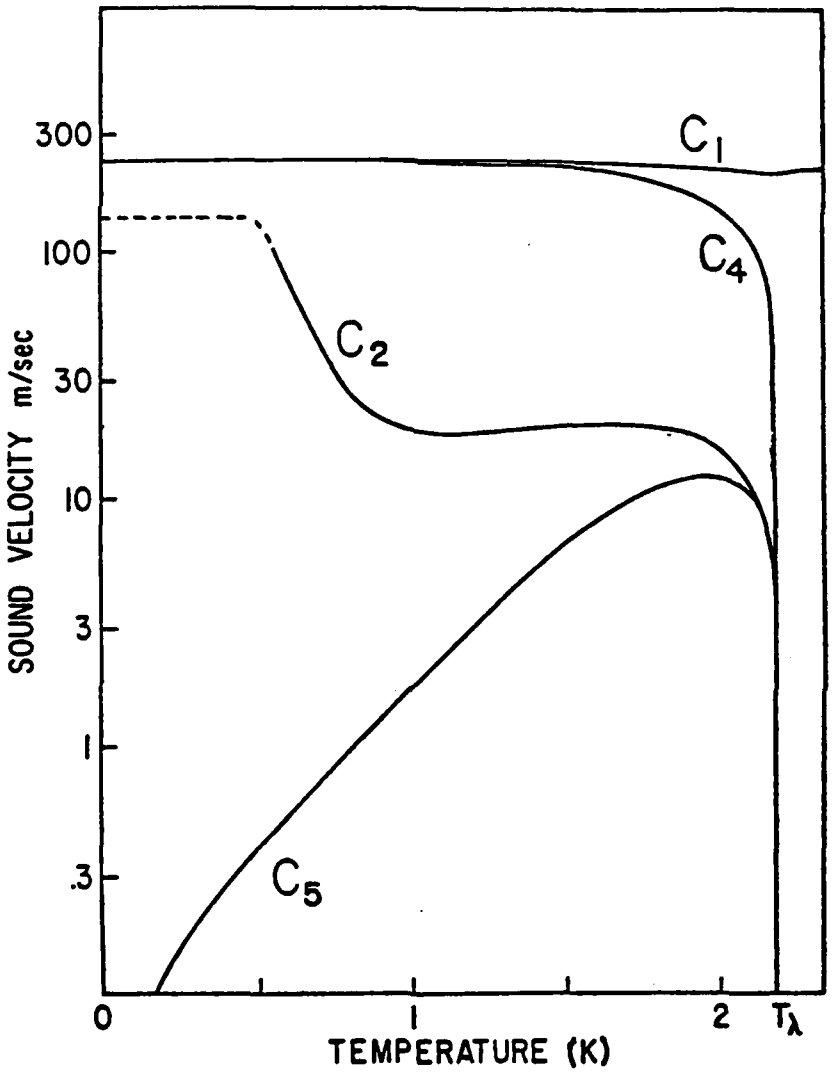

Figure I.D.2 Helium II Sound Speeds

Third sound exists only in helium II films. It is a surface or thickness wave of the film. The restoring force is provided by the Van der Waals force between the helium film and the substrate on which the film is adsorbed. Third sound will be discussed further in section II.

II ACOUSTICS OF A SUPERLEAK PARTIALLY FILLED WITH HELIUM

II.A INTRODUCTION

The acoustics of a superleak partially filled with superfluid helium were first investigated here at UCLA, in 1979. See R. Rosenbaum, G.A. Williams, D. Heckermann, J. Marcus, D. Scholler, J. Maynard and I. Rudnick, Journal of Low Temperature Physics, Volume 37, Number 5/6, 1979 , henceforth called Rosenbaum et al and also G.A. Williams, Ralph Rosenbaum, and Isadore Rudnick, Physical Review Letters, Volume 42, Number 19, 7 May 1979 (Williams 79). It was noted that the mode which propagated in a superleak whose pores were partially filled with helium had a very low velocity, on the order of 500 centimeters per second. This is an

order of magnitude less than fourth sound. The ability to measure changes in the velocity of a persistent current using doppler shifted sound varies inversely with the sound speed. Since this mode was an order of magnitude less than fourth sound it was hoped that the resolution in measuring persistent current velocities could be increased by a factor of ten. Persistent currents could be observed using a technique similar to the doppler shift techniques used by Kojima and co-workers with fourth sound in 1972 (Kojima). Once the experiment was decided upon, the experimental apparatus was designed and built. What follows is the theory and experimental results from this investigation.

II.B ACOUSTIC THEORY

The velocity of the sound mode observed in a superleak partially filled with superfluid helium has been found to be given by equation II.B.1 (Rosenbaum et al).

$$c^2 = c_3^2 + c_\sigma^2 + c_5^2 \qquad \{II.B.1\}$$

It is composed of three distinct parts. The first term is the velocity squared of isothermal third sound which has been studied extensively over the past twenty years (Atkins). The velocity of isothermal third sound is given in equation II.B.2.

$$c_3^2 = \frac{\langle \rho_s \rangle}{\rho} \frac{\partial \mu_{VDW}}{\partial d} d \qquad \{II.B.2\}$$

The next two terms were first observed in 1979 at UCLA (Rosenbaum et al). The first of which is the contribution to the speed from the surface tension and the final term being the contribution from fifth sound. Figure I.D.2 shows the speed of fifth sound as a function of temperature. Fifth sound can be related to the more familiar second sound speed as shown in equation II.B.3.

$$c_5^2 = \frac{\rho_n}{\rho} c_2^2 \qquad \text{(II.B.3)}$$

The speed of the surface tension contribution is given as

$$c_\sigma^2 = \frac{\rho_s}{\rho} \frac{\partial \mu_\sigma}{\partial d} d \qquad \text{(II.B.4)}$$

Where mu sigma is the surface tension chemical potential. It is interesting to note that in this system the surface tension is a restoring force while in many systems (film on the inside of a capillary tube) is is an anti-restorng force.

To measure the velocity of sound it is necessary to know the relationship between the sound speed, the wavelength and the frequency in the experimental cell. This is obtained by solving the wave equation for the cell's annular geometry. The exact solution of the wave equation in an annular wave guide has been treated elsewhere (Morse). In the present work the azimuthal resonance frequencies are given by equation II.B.5.

$$f_m = \frac{m}{2\pi r} \cdot c \qquad \text{(II.B.5)}$$

The geometeric average has been taken for r the cell radius;

$$2r^2 = r_{inner}^2 + r_{outer}^2 \qquad \{II.B.6\}$$

The mode number is denoted by m and the velocity by c. The limit used to yield equation II.B.5 is valid when the ratio of the inner and outer diameters tend towards one and only if the azimuthal mode be excited and/or detected. In the present work the ratio of the outer to inner radi is 1.274. The approximation of equation II.B.5 is fully justified. Equation II.B.5 holds until the wavelength becomes comparable to the height or width of the annular channel (whichever is larger). At these high mode numbers (m = 20) non-azimuthal modes may enter the system.

The experimental procedure is to measure the resonance frequencies and compute the sound speed from equation II.B.7.

$$C = 2\pi r \left(\frac{f_m}{m}\right) \qquad \{II.B.7\}$$

Figure II.B.1 shows the resonant frequencies divided by their mode number plotted against frequency from a typical run. This straight line of zero slope illustrates that the spectrum is harmonic as predicted by equation II.B.5. The observed speed of this mode is shown in figure II.B.2 from the data of Rosenbaum et al. The graph shows the sound speed plotted against the

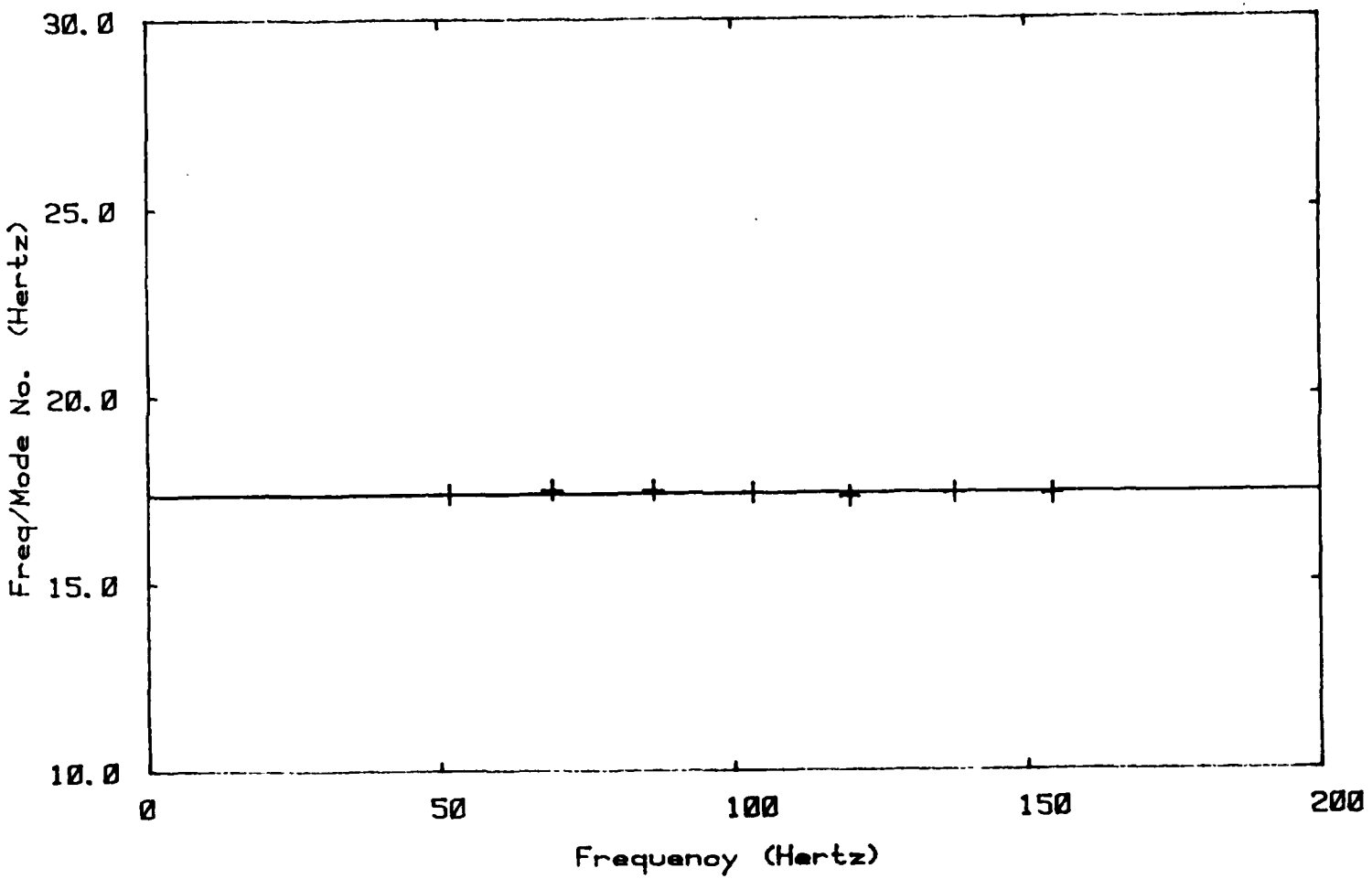

Figure II.B.1 Resonance Frequencies of the Cell.

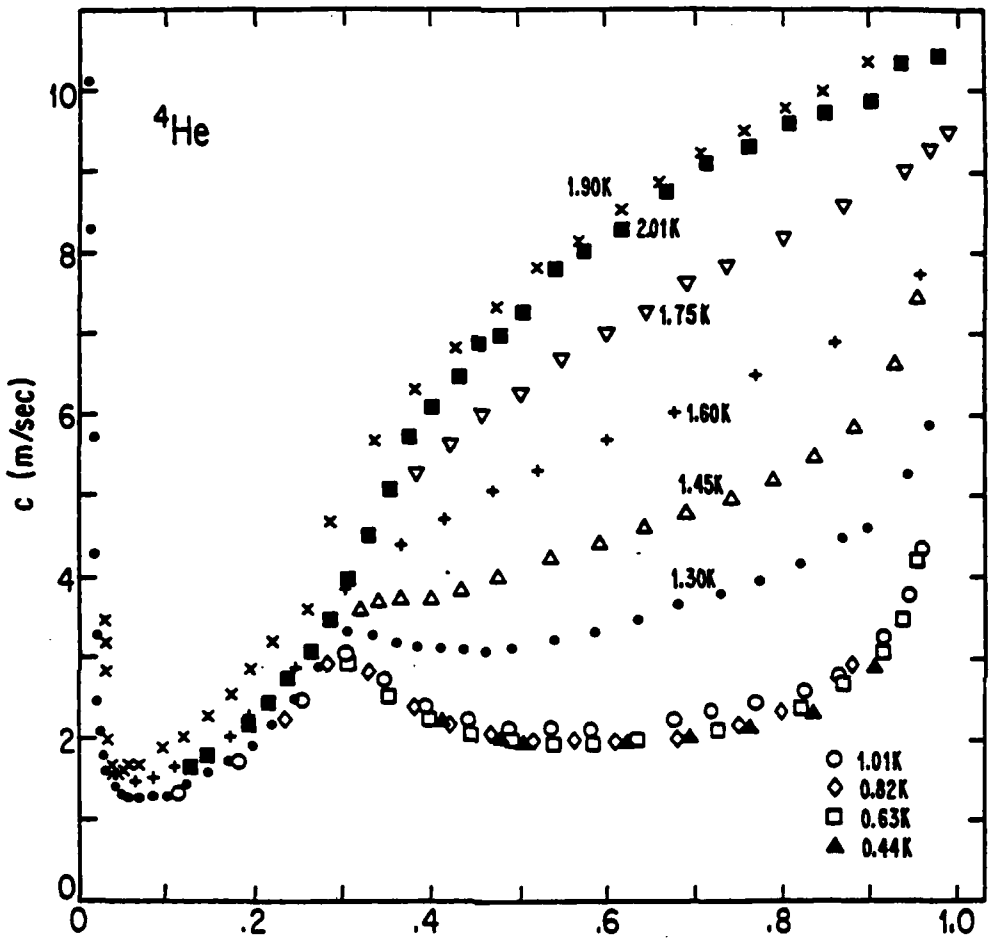

Figure II.B.2 Sound Speed vrs Filling Fraction, f (Rosenbaum et al)

filling fraction f for ten temperatures (0.44 to 1.90 degrees Kelvin). The filling fraction f is defined as zero when the cell is void of helium. As the cell is filled with helium the filling fraction increases and is one when the cell is filled.

There are three distinct regions. The first region being from a filling fraction of 0.0 to 0.05; in this region the sound speed is dominated by the velocity of third sound (equation II.B.2). This can be seen from the dependence of the sound velocity going as log Po/P as in equation II.B.8.

$$c_3^2 = \frac{3\langle\rho_s\rangle}{\rho}\left[\frac{KT\,\log(P_o/P)}{m_{He}}\right] \qquad \{II.B.8\}$$

The helium coats the powder in a uniformly thin film. This can be verified by looking at the pressure adsorption isotherm, figure II.B.3. Here the filling fraction is plotted against the difference in pressure of the helium bath Po and the reduced vapor pressure in the cell P. In the region from 1.0 to 0.1 the log Po-P has been seen to vary linearly with the filling fraction (Rosenbaum et al) and is consistent with figure II.B.3. The slope in this region is roughly three. This is the expected behavior from equation II.B.9 which shows the relation between Po-P and the film thickness, d.

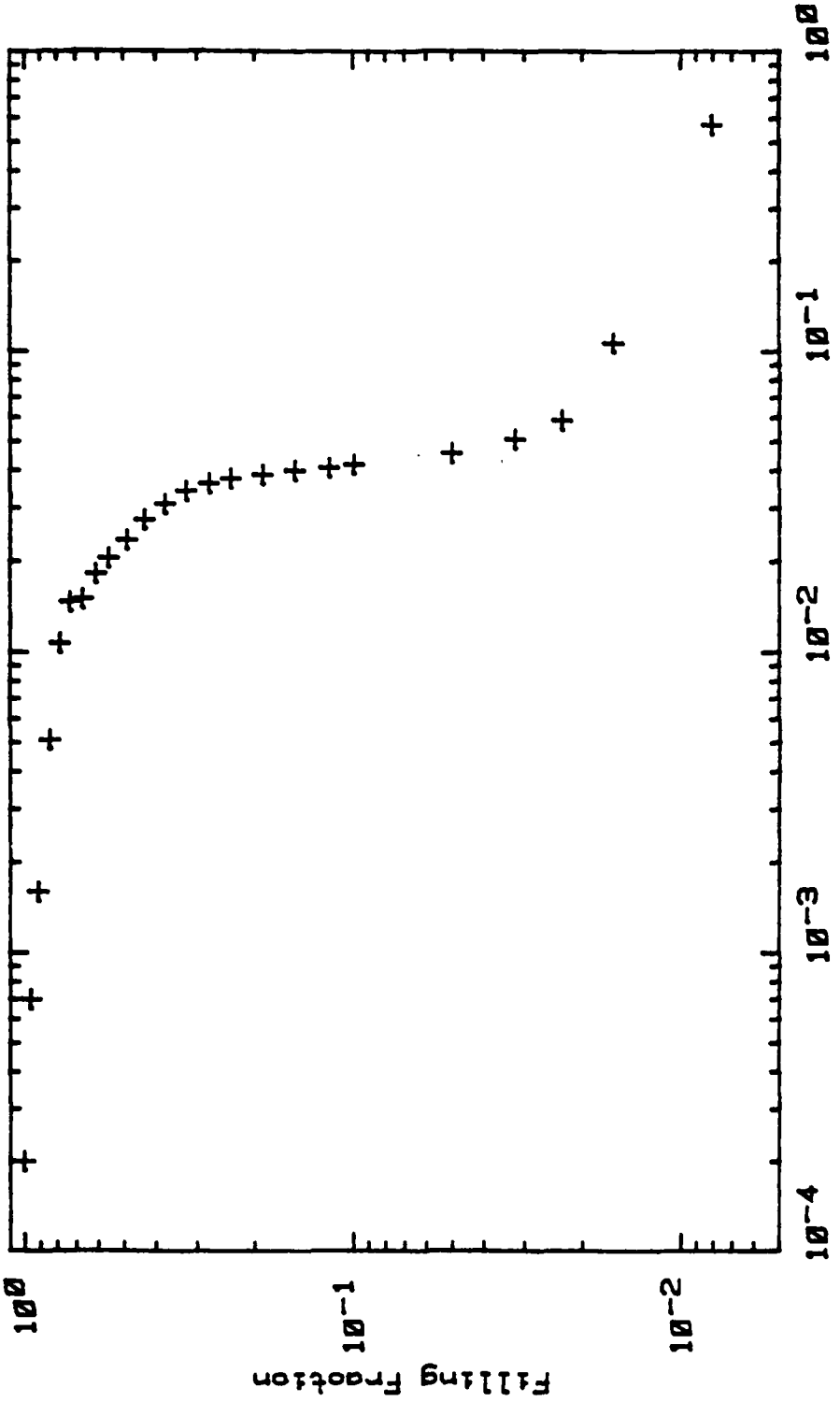

Figure II.B.3 Adsorption Isotherm T = 1.27°K.

$$d^3 = \frac{m\alpha/k}{T \log(P_o/P)} \qquad \{II.B.9\}$$

Equation II.B.9 relates the easily measurable quantities of temperature, T, the helium bath pressure, Po, and the cell pressure P to the film thickness d. Alpha is a measure of the Van der Waals attraction of the helium to the substrate. The derivation is presented in Superfluid Hydrodynamics (Putterman). The relationship between Po-P and the filling fraction is determined by monitoring the amount of helium metered into the cell.

The next region extends from a filling fraction of 0.05 to 0.3. In this region the sound speed is seen to deviate strongly from its log Po/P behavior which is characteristic of films. The pressure adsorbtion isotherm also has an abrupt change of slope at this point. This change is believed to be the onset of capillary condensation at the points where the powder particles are in contact with each other (Rosenbaum et al). The upturn in the sound velocity is from the surface tension contribution (equation II.B.4) becoming dominant over the third sound contribution. The strength of this term arises from the very strong curvature at the points of contact between the powder grains.

The third region is for filling fractions greater than 0.3. This marks the point where the smallest pores begin to fill up and continues until the cell is completely full of helium (f = 1.0). The slope of the filling isotherm is seen to gradually change slope at f = 0.3. The slope of the velocity versus filling curves are also seen to change slope at about f = 0.3.

The sound speed versus filling and temperature graphs are the acoustic basis on which the rest of the experiment is based. The resonance frequency at a given filling and temperature may be obtained from them. Also the initial instrument settings can be inferred from them as well.

II.C DOPPLER SHIFT IN A SUPERLEAK PARTIALLY FILLED WITH HELIUM II

Measuring doppler shifted sound is an ideal technique with which to measure flow velocities in a fluid. In a classical fluid (in one dimension) the speed of sound is given in equation II.C.1.

$$C = C_o \pm V \qquad \{II.C.1\}$$

When the velocity Co (fluid at rest) is known, the apparent velocity C can be measured and the velocity of the media V can be calculated. This is easily understood. If the fluid is at rest the speed of sound is given as the static value Co. If the fluid is moving in the direction of propagation then the observed sound speed C is the sum of the static speed plus the forward motion of the fluid as the sound is carried by the fluid. If the fluid is moving against the direction of propagation then it is the difference in velocities.

In an annular resonator (radius r) the resonance frequencies are given by equation II.B.5 when the fluid contained in the annulus is at rest. If the fluid is given a velocity V the new resonance frequencies are given by equation II.C.2.

$$f_m^{\pm} = \frac{m}{2\pi r} (C_o \pm V) \qquad \{II.C.2\}$$

These frequency doublets are easily understood. When the fluid is at rest, the clockwise and counterclockwise paths from the drive transducer to the receiver transducer are degenerate. The frequency doublet combines and there is a single resonance frequency. If a flow is introduced, the degeneracy is lifted as the clockwise and counterclockwise paths are no longer equivalent. The velocity of the sound is increased by the flow velocity in the direction of the flow. In the other direction it is reduced by the flow velocity.

The flow velocity of the fluid may again be solved for. In this case the frequency splitting of the m-th mode is used. Note that from equation II.C.2 that the frequency splitting divided by its mode number is a constant for a given flow. The flow velocity as a function of the frequency splitting divided by mode number is:

$$v = \frac{\Delta f}{m} \cdot \pi r \qquad \{II.C.3\}$$

Experimentally the frequency divided by mode number is easily obtained. A spectrum analyser may be used to continously monitor the splitting and hence the flow velocity.

In helium II, the same technique can be used to measure the flow velocity of the helium. The values of the doppler shifted velocities and hence the frequencies however depend on both the normalfluid and superfluid velocities. Remember that Helium II has two independent velocity fields and they both play a role in the doppler shift. A velocity measurement in Helium II, measures some combination of the two velocity fields, Vn and Vs.

The doppler shift for the various sound modes in helium II can be calculated from the Landau eqautions I.B.2 through I.B.6. The doppler shift coefficients dC/dVs are listed in table II.C.1 for first, second, third, fourth and fifth sound (Rudnick 76).

In the present work the normalfluid velocity Vn, is zero (as it is in third, fourth, and fifth sound). It is locked to the superleak by its viscosity. A doppler shift measurement then measures some fraction of the superfluid velocity which flows freely in the superleak.

$$c_1 = c_{10} + \left(\frac{\rho_s}{\rho} v_s + \frac{\rho_n}{\rho} v_n\right)$$

$$c_2 = c_{20} + \left(\frac{\rho_s}{\rho} v_s + \frac{\rho_n}{\rho} v_n\right) + \left(v_n - v_s\right)\left(\frac{2\rho_s}{\rho} - \frac{s}{\rho_n}\left(\frac{\partial \rho_n}{\partial T}\right)_P\left(\frac{\partial T}{\partial s}\right)_P\right)$$

$$c_3 = c_{30} + \frac{\langle \rho_s \rangle}{\rho} V_s$$

$$c_4 = c_{40} + \left(\frac{\rho_s}{\rho} + \frac{s[(\partial/\partial T)(\rho_n/\rho)]_P}{(\partial s/\partial T)_P} - \frac{\rho[\frac{\partial}{\partial \rho}(\rho_n/\rho)]_T}{(\partial \rho/\partial P)_T}\right) V_s$$

$$c_5 = c_{50} + \left(\frac{\rho_s}{\rho} - \frac{s\frac{\partial \rho_s}{\partial T}}{\rho\frac{\partial s}{\partial T}}\right) V_s$$

Table 11.C.1 Doppler Shift Coefficients

This is shown in equation II.C.4.

$$C = C_o \pm \frac{\partial C}{\partial V_s}(V_n - V_s) \qquad \{II.C.4\}$$

The coefficient of (Vn - Vs) is the doppler shift coefficient, dC/dVs. It is given by equation II.C.5 for the surface wave mode which propagates in a partially filled superleak.

$$\frac{\partial C}{\partial V_s} = \frac{\rho_s}{\rho} - \frac{s(\partial \rho_o/\partial T)}{\rho(\partial s/\partial T)} \qquad \{II.C.5\}$$

The doppler shift coefficient dC/dVs is shown as a function of temperature in figure II.C.2.

The doppler shift coefficient calculated above (equation II.C.5) is for adiabatic sound propagation (compared to isothermal). This is determined by the mean free path in the vapor in the superleak. If the mean free path is very short compared with the size of the vapor spaces then the sound will propagate isothermally. This is the case for third sound on a flat substrate like CaF (Fraser) with helium vapor above it. In this case the temperature swings in the wave are shorted out by the vapor and the propagation is isothermal.

If the mean free path is long compared to the vapor spaces the propagation is adiabatic. This is the case for third sound between to parallel substrates separated

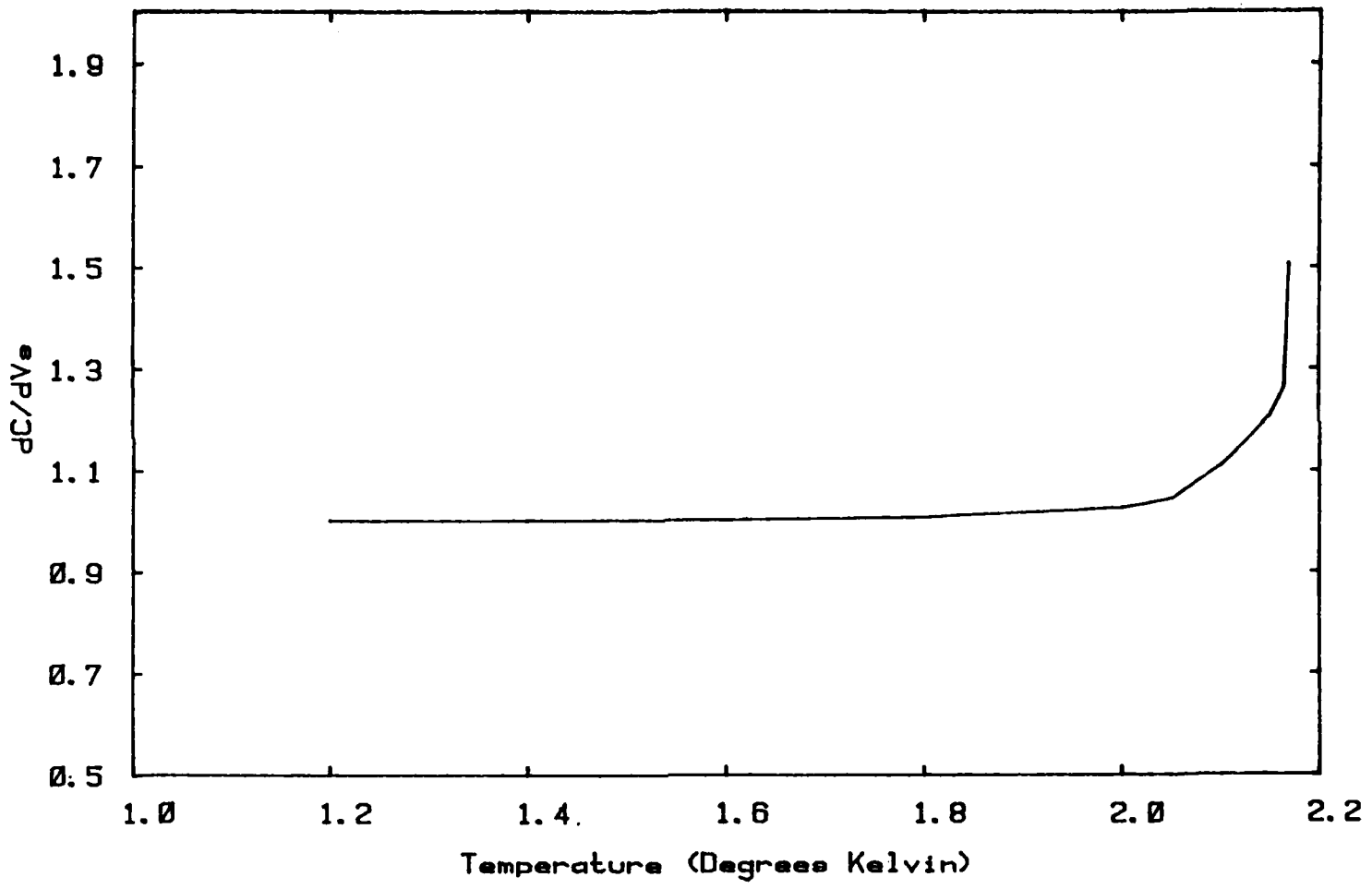

Figure II.C.2 Doppler Shift Coefficient, $\frac{dc}{dv_s}$.

by less than the mean free path. In this case the temperature swings are not shorted out by the vapor as the thermal conductivity is very low. Figure II.C.3 shows the mean free path for a filling fraction of 0.5 as a function of temperature. The mean free path is equal to or greater than the size of the vapor spaces (1 micron or less see section II.D) for temperatures of 1.2 degrees Kelvin and below for all filling fractions. This is the region in which most of the current work is done. It is also true for higher temperatures and lower filling fractions.

The other factor to consider is the thermal conductivity of the superleak itself. The diffusive thermal wavelength is on the order of several millimeters. This is much longer than the dimensions of the powder grains (1 micron) or the vapor spaces whose size depends on the filling fraction (1 micron when f = 0 and 0 when f = 1). This means that the temperature swings in the wave are able to communicate through the superleak and are in phase with each other as they propagate around the cell.

The persistent current velocity Vn-Vs may now be obtained from the experimental splitting. Using the solution of the wave equation from II.C.2 and the doppler shift from II.C.4 equation II.C.6 results.

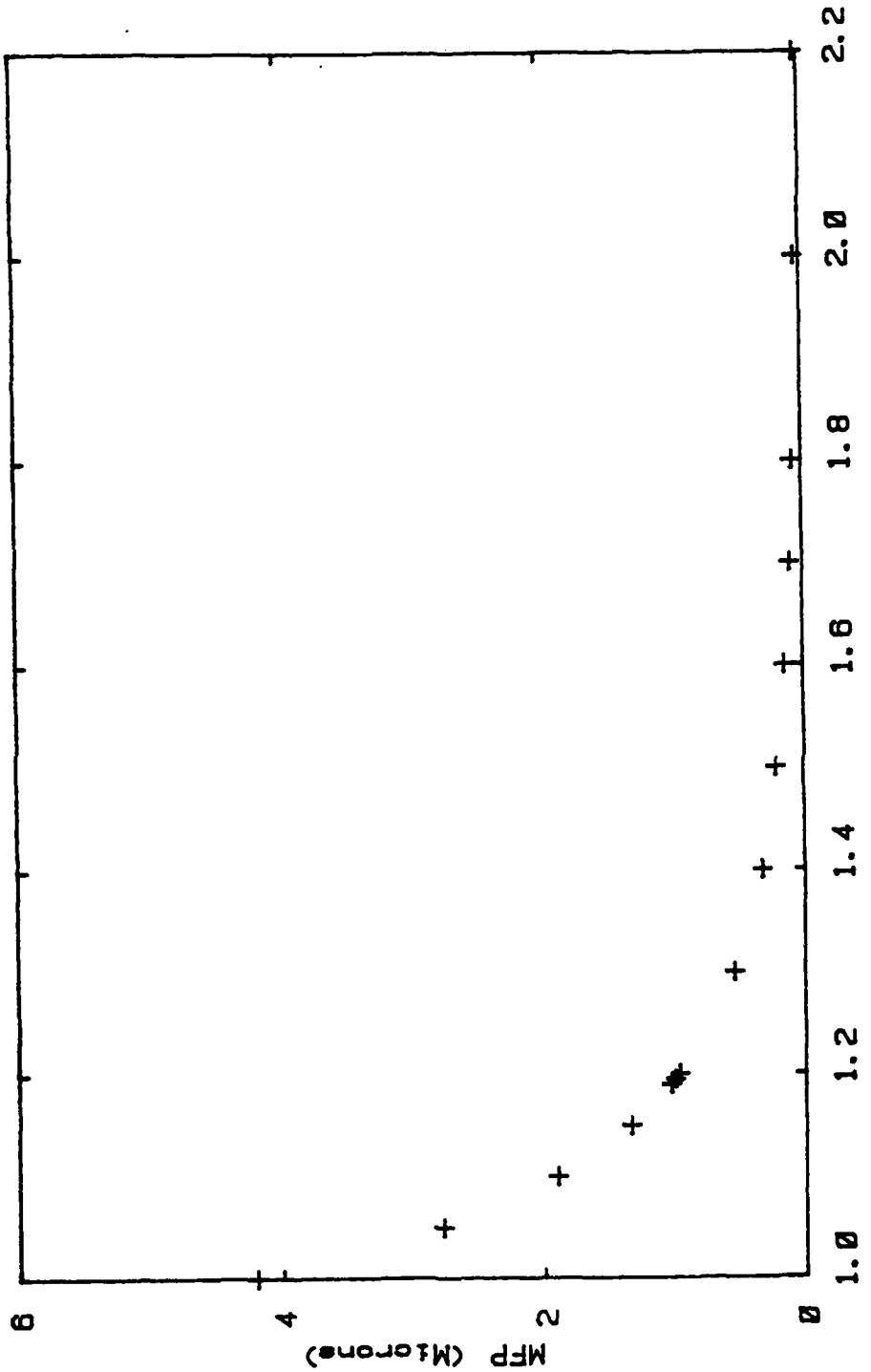

Figure II.C.3 Mean Free Path in He Gas at 95% S.V.P.

$$V_n - V_s = \frac{\Delta f}{m} \cdot \pi r \cdot \left(\frac{\partial C}{\partial V_s}\right)^{-1} \qquad \{II.C.6\}$$

In practice the resonance spectrum is taken on a FFT and the frequencies read directly off it (see section III). The spectrum may also be plotted on a XY plotter. A graph from the XY plotter is shown in figure II.C.4 in which there is no flow present (single resonance peaks). Figure II.C.5 shows an expanded view of the unsplit resonance peaks. Figure II.C.6 shows the spectrum again but with Vn-Vs different from zero. The splitting is clearly seen. Figure II.C.7 shows an expanded view of the splitting.

In figure II.C.8 the frequency splitting is plotted against frequency. It shows straight line behavior which indicates that the splitting is proportional to the mode number as in equation II.C.2. The fundamental is missing from figure II.C.8 as the peak was very noisy and an accurate measurement could not be made.

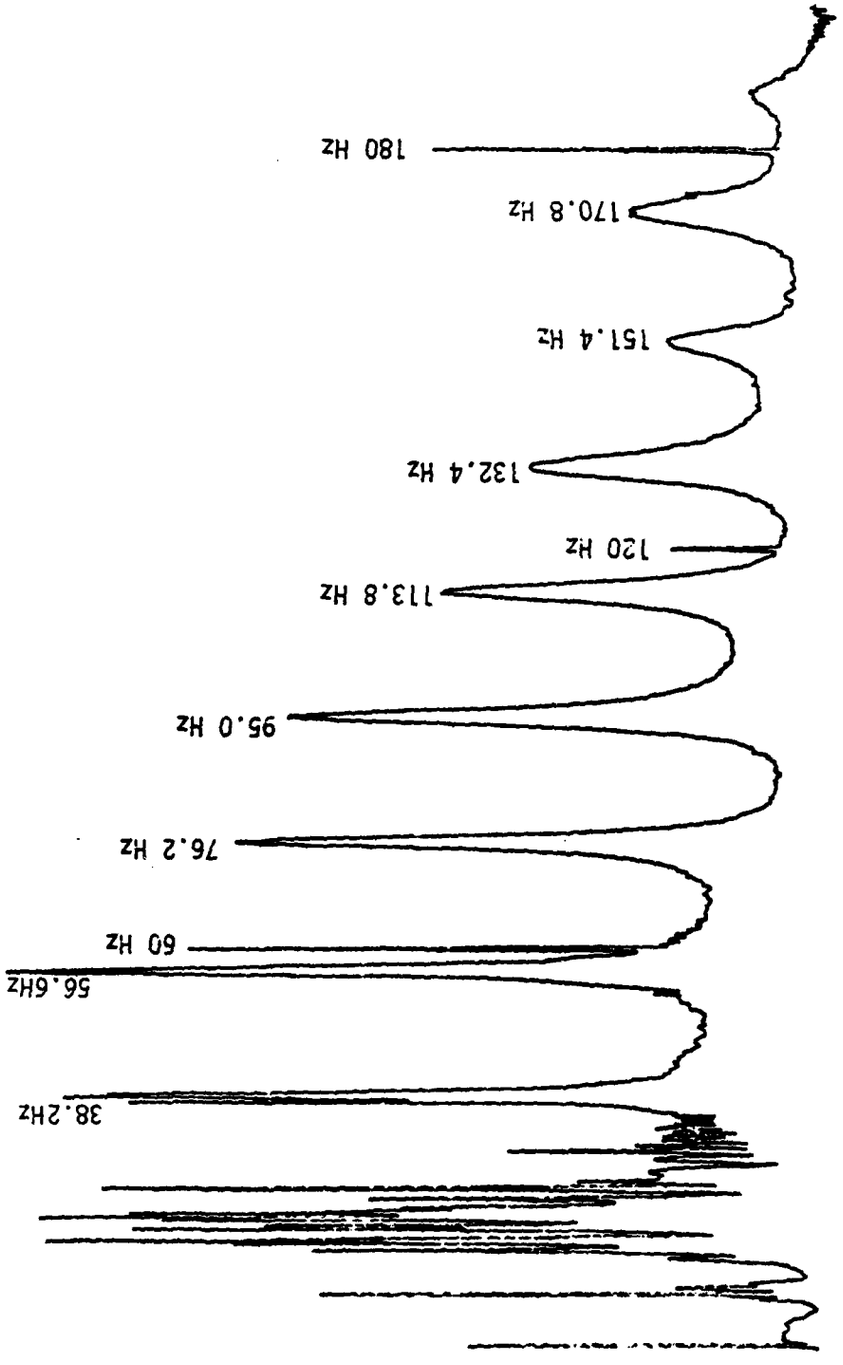

Figure II.C.4 Resonance Spectrum (No Splitting).

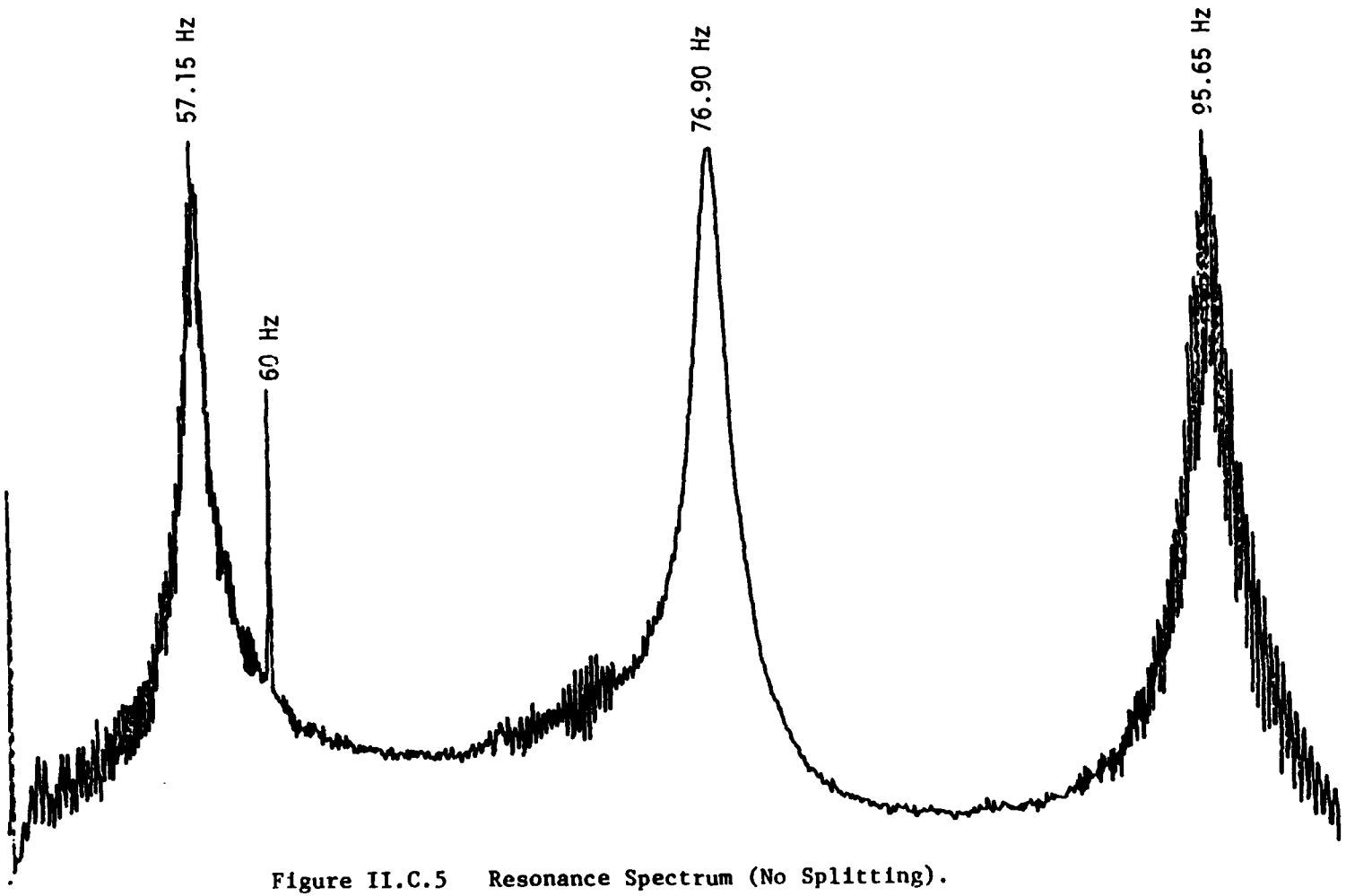

Figure II.C.5 Resonance Spectrum (No Splitting).

Figure II.C.6 Resonance Spectrum (Splitting).

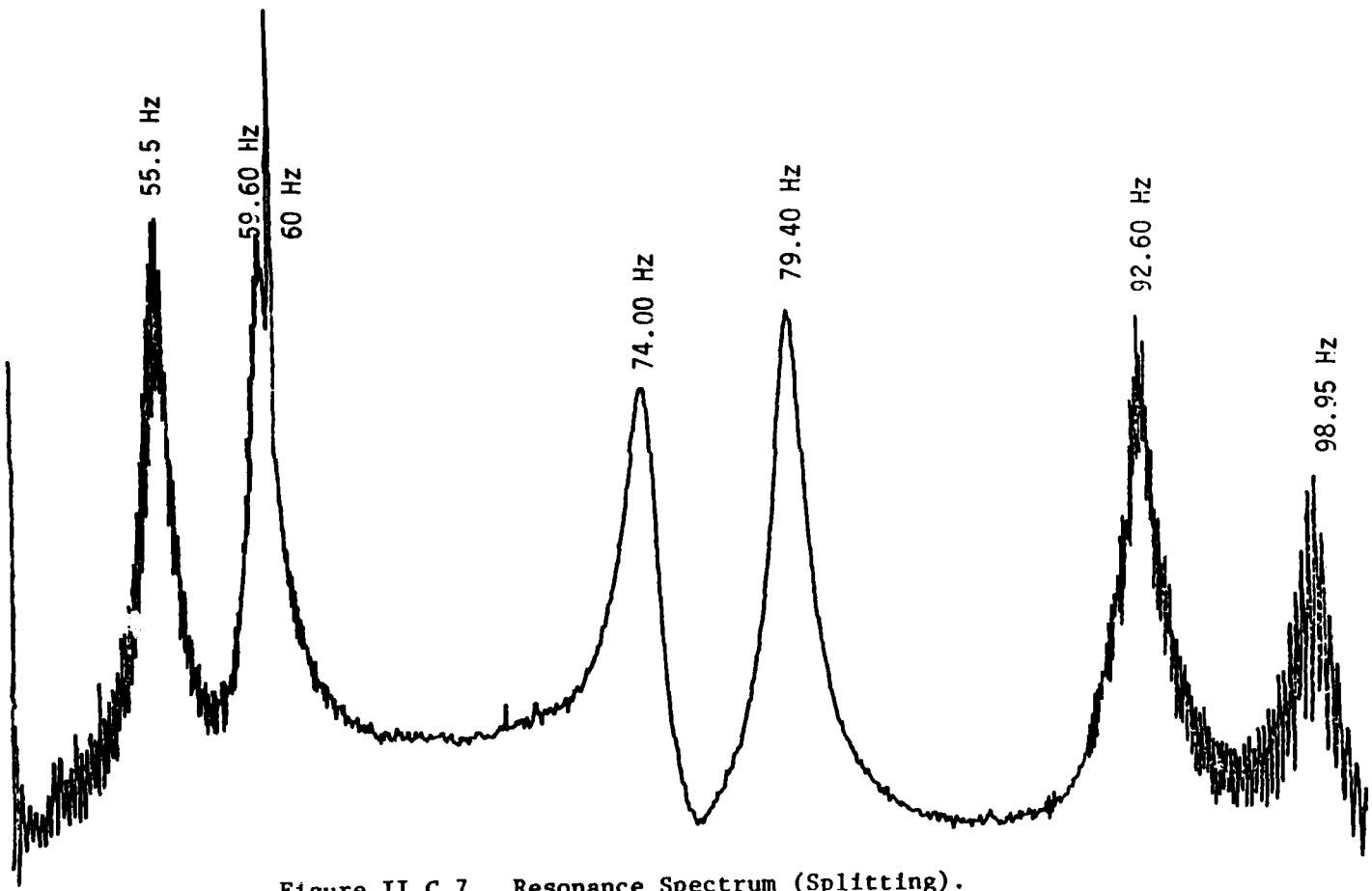

Figure II.C.7 Resonance Spectrum (Splitting).

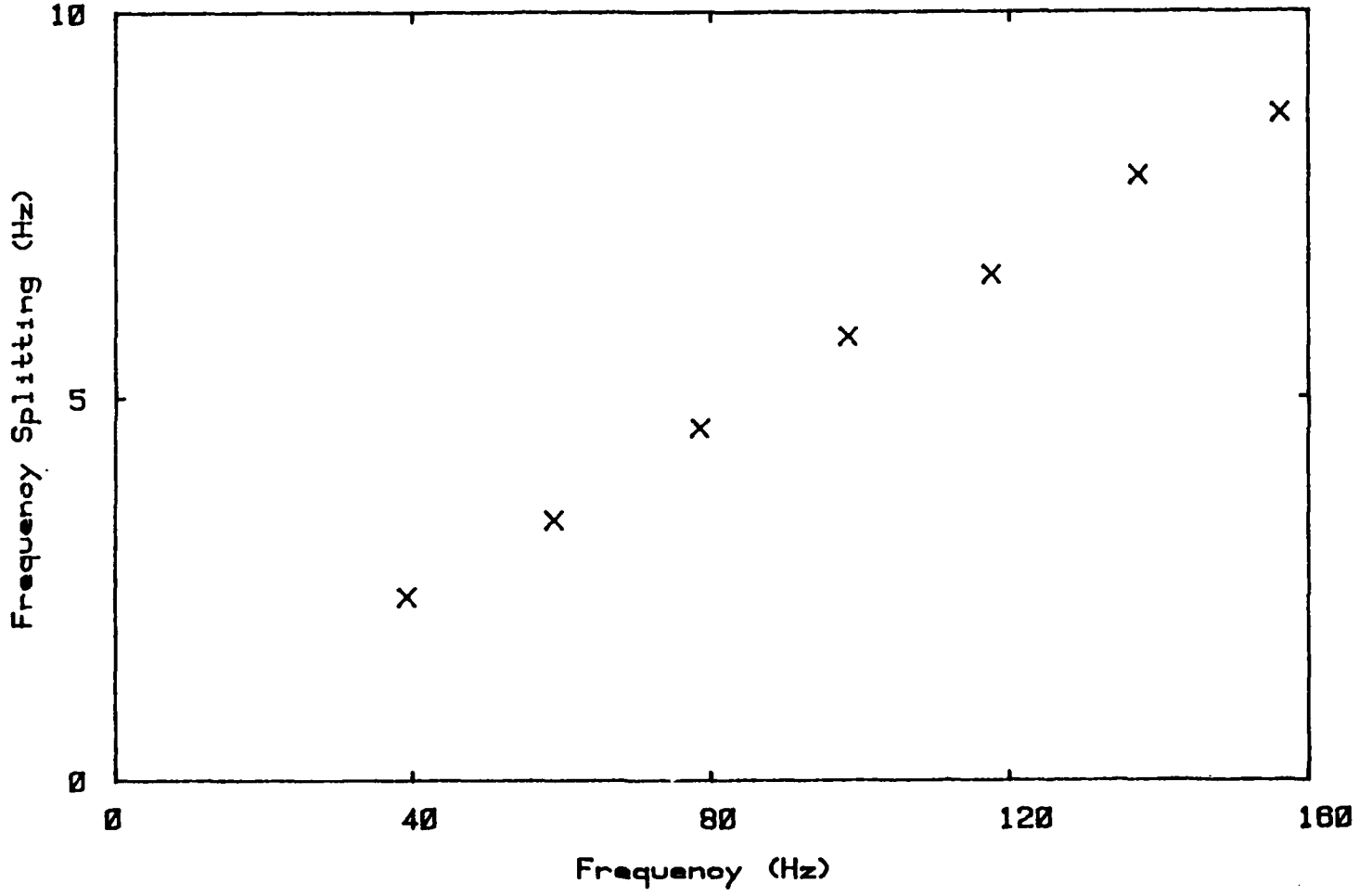

Figure II.C.8 Frequency Splitting versus Frequency

III EXPERIMENTAL APPARATUS

III.A INTRODUCTION

The experimental cell contains an annular resonator packed with a superleak of 1 micron alumina powder packed to 0.78 porosity. It is fitted with drive and pick-up transducers. The cell is mounted on a rotatable shaft in a standard cryogenic helium dewar system. The speed of rotation is controlled by a motor and power supply. The temperature is controlled by the pumping rate and a feedback heater in the helium bath and maybe regulated to 250 microdegrees while stationary and 1 millidegree while rotating. The acoustic signals are

sent and received from the cell via slip rings and are analysed on a FFT spectrum analyser. A complete and detailed description of the apparatus now follows.

III.B EXPERIMENTAL CELL

The cell is illustrated in figure III.B.1. It is made out of brass. Brass is an easy material to work, easy to solder to, and a good heat conductor. As shown in the figure the powder fills the lower two thirds of the annular channel. Figure III.B.2 is a dimensioned cross sectional schematic drawing of the cell. The transducers are imbedded in a lucite ring which serves both as a transducer mount and as filler to exclude any vapor above the powder which would lead to very large acoustic losses. The lucite ring is held firmly against the powder by small blocks of foam sandwiched between the top plate and the ring. A small channel (0.1 X 0.1 inch) was machined in the top of the ring to route the wires until they could be connected to the vacuum feedthrus. It may be that this vapor space limits the Q of the system through attenuation in the helium gas.

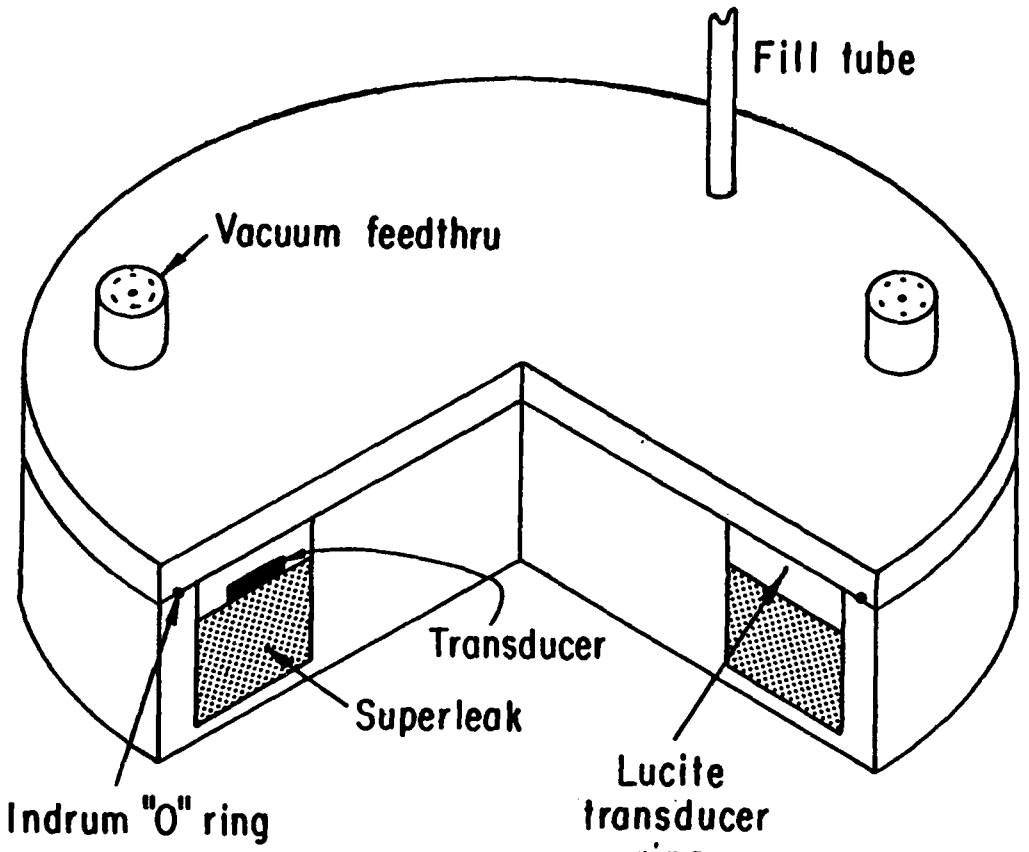

Figure III.B.1 Cell (Cut--away View)

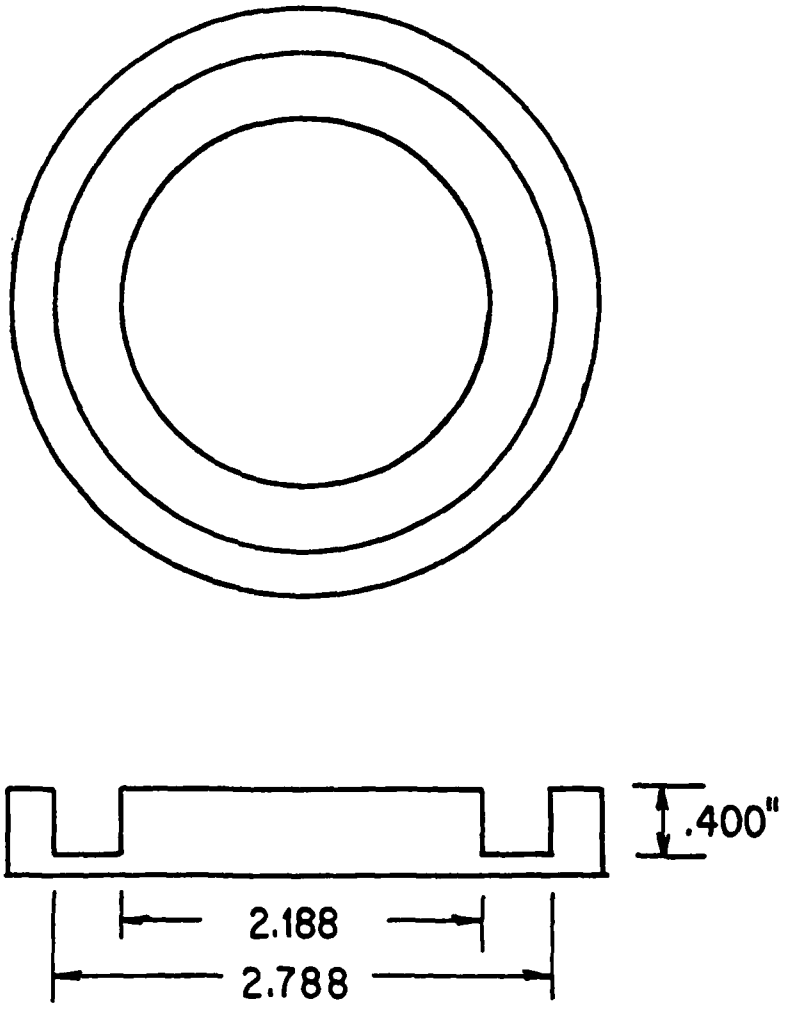

Figure III.B.2 Cell (Dimensioned Schematic).

The annular channel in the cell is packed (75 percent porosity) with 1 micron aluminum oxide polishing powder (Linde 1 micron Powder, Union Carbide Corporation, Linde Division, 1500 Polco Street, Indianapolis, Ind. 46224). The tool used to pack the powder is shown in figure III.B.3. It was machined out of stainless steel for both strength and ease of maintainance. To pack the cell with powder the bottom of the cell is mounted in the packing tool as shown in the figure. Then about a quarter of the powder is put in the cell and the ram placed on top. It is then lightly pressed in a hydraulic press. The ram is pulled out and another quarter of the powder is added and the cell is pressed again. This process is repeated until all the powder has been added. On the final pressing the press is brought up to the full desired pressure. The whole packing tool assembly is then carefully taken apart to avoid cracking the now compressed powder. Once the cell is separated from the packing tool it is mounted on a lathe. It is aligned with a dial indicator to run true (+0.001 inches) . The powder surface is then machined away to remove the high density region near the surface and to make room for the lucite transducer ring.

The desired porosity of the packed powder must be determined before the powder is weighed out for packing.

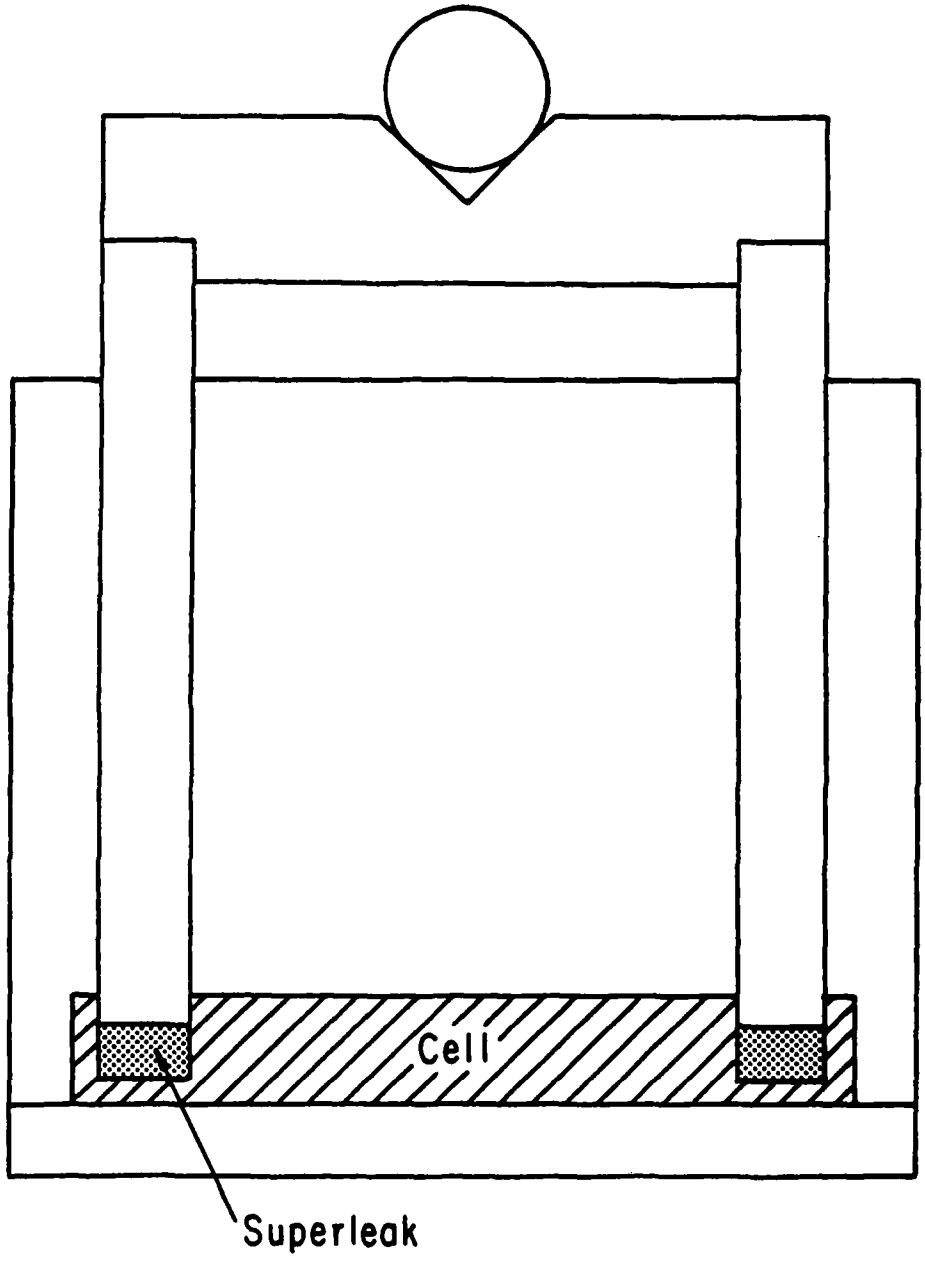

Figure III.B.3 Superleak Packing Tool.

The porosity is defined as the ratio of the open volume to the total volume the powder occupies, as given in equation III.B.1.

$$P = \frac{V_{TOTAL} - V_{POWDER}}{V_{TOTAL}} \qquad \{III.B.1\}$$

In the lab this is obtained through weighing the powder and measuring the volume it will occupy. Once the cell is packed, the volume is remeasured and the total weight of the cell is checked. The porosity is then given in terms of measured quanities in equation III.B.2.

$$P = \left[V_{TOTAL} - \frac{\text{MASS POWDER}}{\text{DENSITY POWDER}} \right] [V_{TOTAL}]^{-1} \qquad \{III.B.2\}$$

Where the density of the aluminum oxide powder is 3.97 grams/cc.

The cell's top surface and the cell top plate are throughly cleaned with TCE. An indium "O" ring is now made from carefully washed (TCE) indium wire (0.047 inch diameter). The "O" ring is now fitted. The top plate and cell are now bolted to the flange at the bottom of the main probe tube. The fill line from the probe tube is then soldered in place. The completed probe is now helium leak checked with a Veeco leak dectector (Veeco Model 17AB).

III.C PROBE WIRING

The transducer wires are brought out of the cell through two vacuum feedthrus (Hermetic Seal Corp.); one on each side of the cell, separated by an electrostatic shield. The feedthrus are each wired to a miniature Amphenol connector (Amphenol 221 series strip connector). The connector is plugged into its matching socket, mounted on the shield. This allows the cell to be dismounted for service. The wires from the main probe tube are attached to the mounted connectors. There are eight miniature hard coax cables (Uniform Tubes UT-85SS) and four twisted pairs which run from the sockets up to the epoxy feedthru at the top of the probe. The coax cables, the twisted pairs, and the gas fill tube are all held in place by teflon washers spaced about ten inches apart in the main probe tube. The

twisted pairs are terminated with miniature Amphenol plugs, while the eight hard coax cables are terminated with Microdot coaxial plugs (Microdot S-50 series). The plugs are rigidly attached on the probe on round fiberglass disks mounted to the gas tube. This was done in order to allow complete disassembly of the probe without unsoldering any wires and to allow the main probe tube to be removed from the slip rings and bearings. Some of the wires from the slip rings are terminated in matching Microdot coax plugs and attached to the mounted sockets while the others are terminated with the Amphenol plugs and matched to the twisted pairs. The slip rings have two sets of BNC connectors mounted on opposite sides. One set is for the drive signals and the other is used for the pickup and temperature control signals. The electronics are then attached to the slip rings with standard 50 ohm coaxial cable terminated with BNC plugs.

III.D ELECTRONICS

The electronics for this experiment are naturally divided into four groups. They are transducers, drive side electronics, pickup side electronics, and peripheral devices. There are four transducers mounted in the experimental cell, two pickups and two drivers. The pickups are made from 200 ohm carbon resistors (Allen Bradley 1/8 Watt), chosen for their large temperature coefficient at low temperatures (0.2 ohms/microdegree at 1.2 degrees Kelvin). Each resistor is ground flat along one side by sanding against a piece of sandpaper held flat against a sheet of glass. This is to expose the carbon, to increase the contact area with the helium, and to reduce their thermal mass. The factory leads are clipped short and thin copper wires are soldered to the resistors. Heat shrink tubing is added and the resistors are ready for mounting in the lucite transducer ring.

Four rectangular holes are milled into the face of the ring to accept the two pick-up transducers and the two drive transducers. Four holes are then drilled all

the way through the ring to pass the transducer leads through. On the opposite face of the ring, a groove is milled all the way around to run the lead wires in until they can be fed to the vacuum feedthrus.

The drive transducers are wound out of resistance wire which has no observable temperature coefficient. The wire is wrapped around the flat end of a toothpick to present as much surface area to the helium as possible. The back side of the drivers are dabbed with glue to prevent the wire from unwinding. The leads are clipped short and copper wire is soldered in place to confine the heating to the transducer itself.

The four transducers are now mounted in the lucite ring. Their leads are passed through the holes provided for this and they are expoxied in place. Once cured, then ring is checked for flatness and sanded if needed. The transducer ring is now complete and wired to the fedthrus in the cell top plate.

The electronics are shown in a block diagram in figure III.D.1. The rotating constant current supply provides the bias current to the pick-up transducers. The signal voltage is generated across the pickup transducer when its temperature is changed by the sound wave passing by. This is shown in equation III.D.1 where dV is the signal voltage, Io the bias current, dT

III.D.1 Electronics Diagram

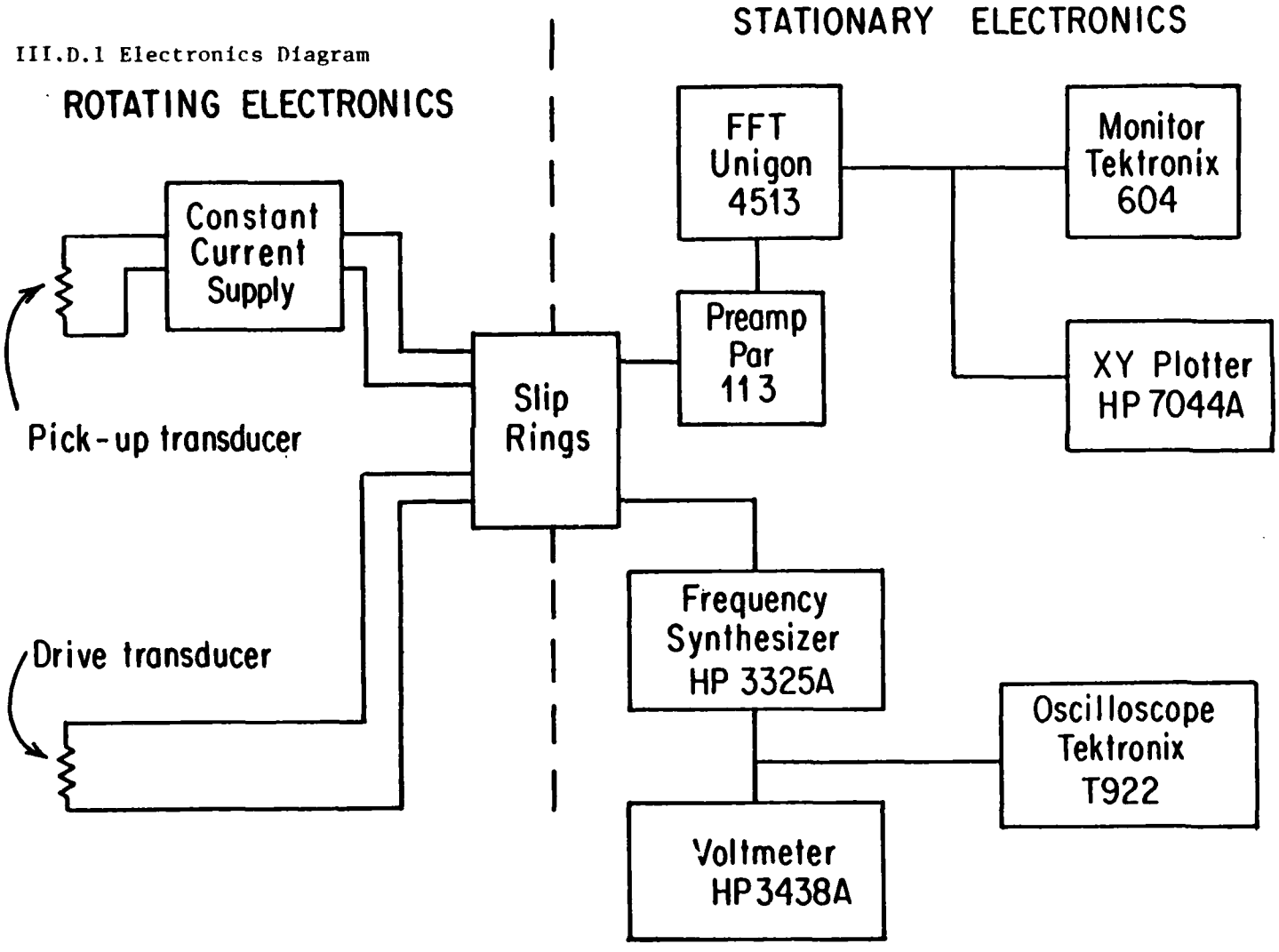

the temperature swing and dR/dT the temperature coefficient of the pickup.

$$dV = Io(dR/dT)dT \qquad \{III.D.1\}$$

The signal voltage dV, is then fed out of the rotating frame through slip rings (Fabricast, Inc., 9835 E. Alpaca St., So El Monte, Ca.) to a high impedance amplifier (Princeton Applied Research Model 113).

In this configuration only the voltage need be passed through the slip rings. If the current supply were mounted in the laboratory frame the current would be passed through the slip rings and generate considerable ohmic noise. Since the input impedance of the amplifier is about 100 megohms almost no current flows in the slip rings and very little noise is generated in them.

The amplifier has high and low pass filters which are set to their appropriate values in order to limit unwanted noise. The signal is then fed to the FFT real time spectrum analyzer (Unigon Real Time Spectrum Analyzer Model 4513). The FFT was chosen for its very narrow bandwidth at low frequencies. At ten hertz it may be set as narrow as 0.025 hertz. The FFT then displays the signals on the Tektronix Monitor (Model 604). The movable cursor is be used to read off both

frequency and amplitudes from the monitor display. The output may also be fed to the XY Chart Recorder (Hewlett Packard 7044A) so a hardcopy may be retained.

The drive side electronics are kept as separate from the detection circuits as possible. This seems to have paid off as there is very little pick up or crosstalk. The drive electronics are shown in figure III.D.1. A frequency synthesizer (Hewlett Packard Model 3325A) is used to generate the drive signal. The frequency range is set to match the range of the FFT. In practice the synthesizer is set to sweep about a ten hertz wider range than the FFT. This prevents undesirable edge effects in the output of the FFT. The amplitude, DC offset, and sweep time are set on the frequency synthesizer. The DC offset is set so the whole sine wave is between zero and its peak voltage. This insures that the Joule heating at the drive transducer has the same frequency as the sine wave, since the heating is proportional to the current squared. The drive signal is then fed through the slip rings into the rotating frame and down a twisted pair to a drive transducer in the cell. The drive signal is monitored by a Tektronix oscilloscope (Model T922) for proper DC offset and wave form. A digital multimeter (Hewlett Packard Model 3438A) is used to monitor the drive voltage.

The speed of rotation of the probe is measured with an optical switch (HEI Model OS 591S Optical Switch) and frequency counter. A disk with one hundred equally spaced holes drilled around its perimeter is mounted in the mechanical drive circuit. As the disk revolves the light beam from the optical switch is interupted at a rate dependent on the speed of rotation. The optical switch outputs a square wave from these interruptions in the light beam. The square wave is fed to a frequency counter (General Radio Model 1911). From the frequency displayed by the counter the rotational speed of the probe is calculated. The signal is also fed to the Tektronix scope described in the drive side electronics section so the light beam may be properly aligned with the perforated disk (equal on and off time).

III.E ROTATING PROBE

The basic design of the probe is shown in figure III.E.1. Figure III.E.4 is a photo of the probe on its work rack. Figure III.E.5 is a photograph of the probe in the dewar. The probe consists of the experimental cell rigidly supported by a rotatable, stainless steel tube. The tube is supported above the dewar by two sets of self-aligning ball bearings (FAG Model 1207K) contained in a modular housing. The tubing consists of two pieces, the inner one being the full length while the second is used to increase the wall thickness above the helium for added mechanical strength while keeping heat conductivity to the bath to a minimum. The tube passes through a quick disconnect fitting with a "O" ring in the dewar top plate. The compression on the "O" ring is set by adjusting the fitting and then locking it

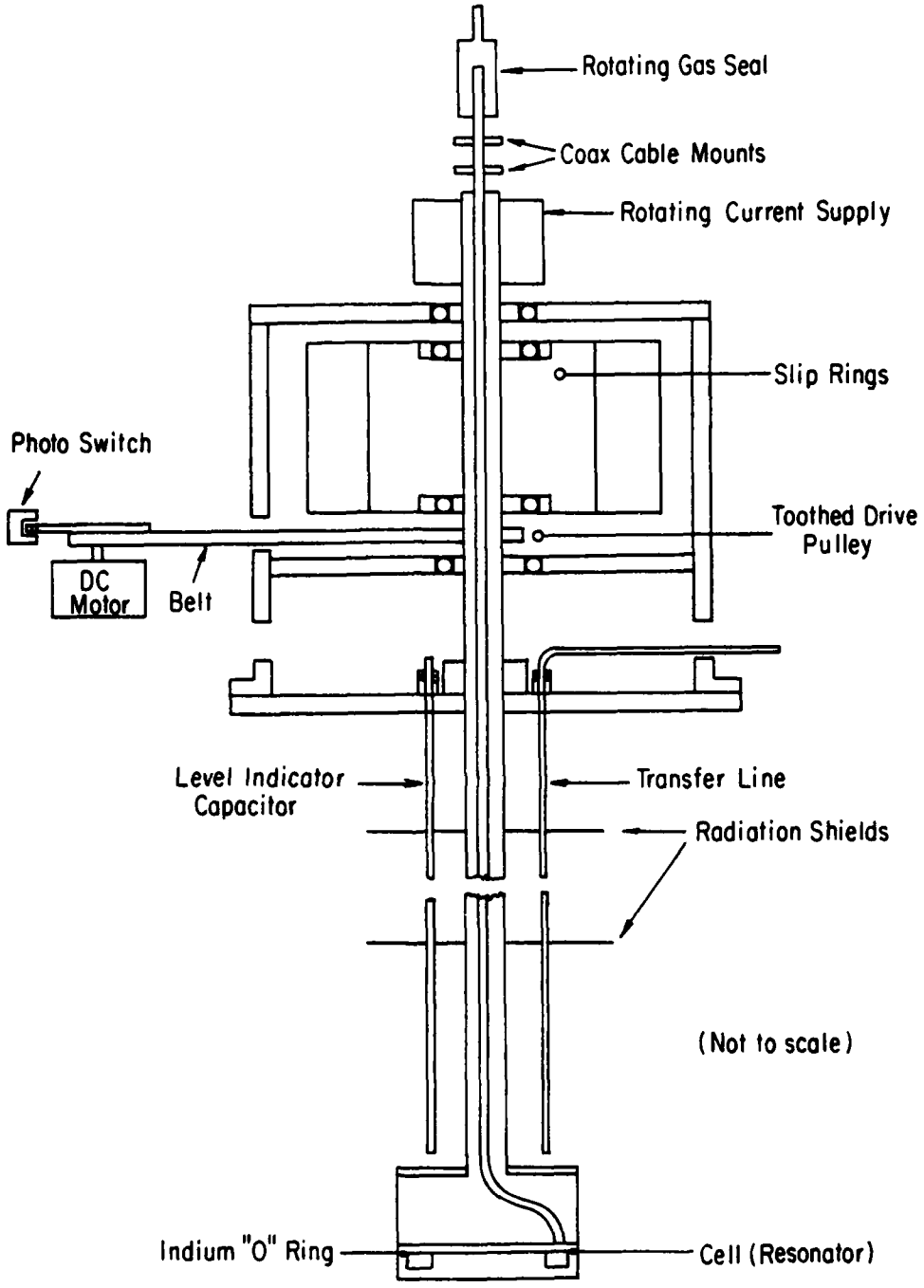

Figure III.E.1 Rotating Probe Drawing

in place. This forms the rotating seal betwee. the helium vapor (1mm) and the air in the lab (760mm).

On the upper end of the probe another type of gas seal was used. It is shown in figure III.E.2. This is for the helium gas system used to add gas to the cell. A 1/4 inch tube runs up the center of the mechanical support tube from the cell to the top where it is soldered to a very smooth (better than 32 microinchs surface roughness) brass sleeve. The sleeve runs in two Delrin (E. I. duPont de Nemours & Co.,Inc.) bearings supported by the outside housing. Between the bearings are two "O" rings fitted into carefully machined "O" ring grooves. Between the "O" rings a pumping port was provided although it was never needed, as there was no detectable leakage past the "O" rings.

The probe is driven by a DC motor controlled by a regulated power supply (Hewlett Packard Model 6274B). It is belted to the probe with toothed timing belts (UniRoyal PowerGrip Series XL037). The motor speed was stepped down via an intermediate pulley and then belted to the probe shaft where another toothed pully was mounted. As described in section III.C, a perforated disk was fixed to the intermediate stage so that the speed of rotation could be measured. The overall gear ratio was 13.5 to 1. The speed of rotation could be

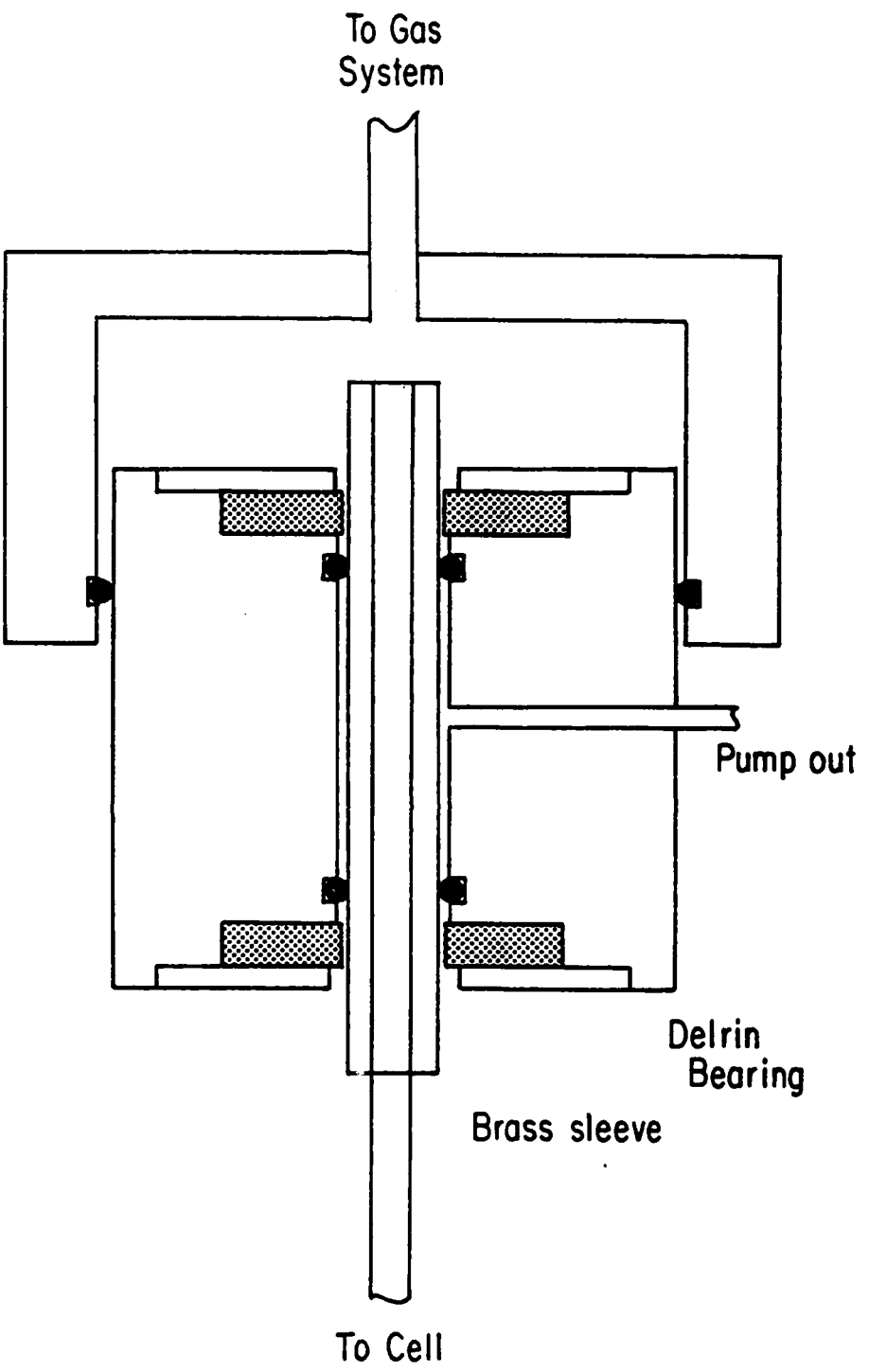

Figure III:E.2 Rotating Gas Seal.

held constant to within 0.01 revolutions per second while rotating measurements were being taken at speeds over 0.3 revolutions per second.

A system separate from the dewar system was used to control the filling fraction in the experimental cell. The helium gas system is shown in block diagram form in figure III.E.3. It consists of a combined one liter reference volume and cold trap. A one liter stainless steel can is held inside a small nitrogen dewar. A small amount of the molecular sieve, Zeolite, was put in the bottom as a cold trap to keep the helium gas pure. In use the reference volume was filled from a commercial gas bottle and the small dewar is filled with liquid nitrogen. It is then allowed to cool down completely before any gas is transfered into the cell. The presssure in the reference volume is monitored on a 0 to 800mm pressure gauge (Wallace and Tiernan Model FA 145). The gas is connected to the cell through copper tubing and the rotating gas seal described in section III.D. Several other connections are made to this system. Both a mechanical vacuum pump and a diffusion pump are plumbed into the system. Also a thermocouple pressure gauge (CVC GTC- 100) and a Ion Gauge (Veeco Model RG 2A). Tubing was also run to one side of the MKS differential pressure gauge so it could be run against the diffusion pump for absolute pressure measurement or

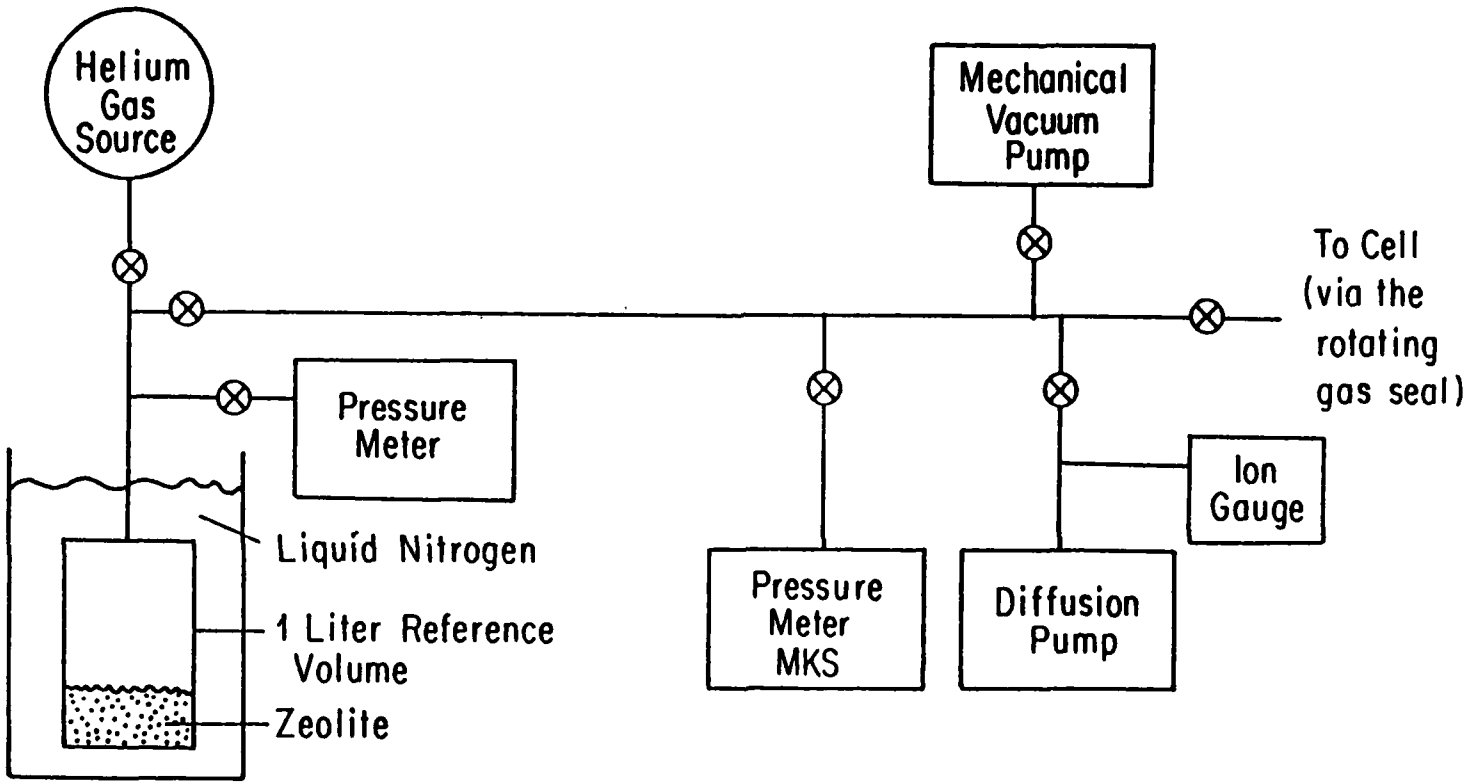

Figure III.E.3 Helium Gas System

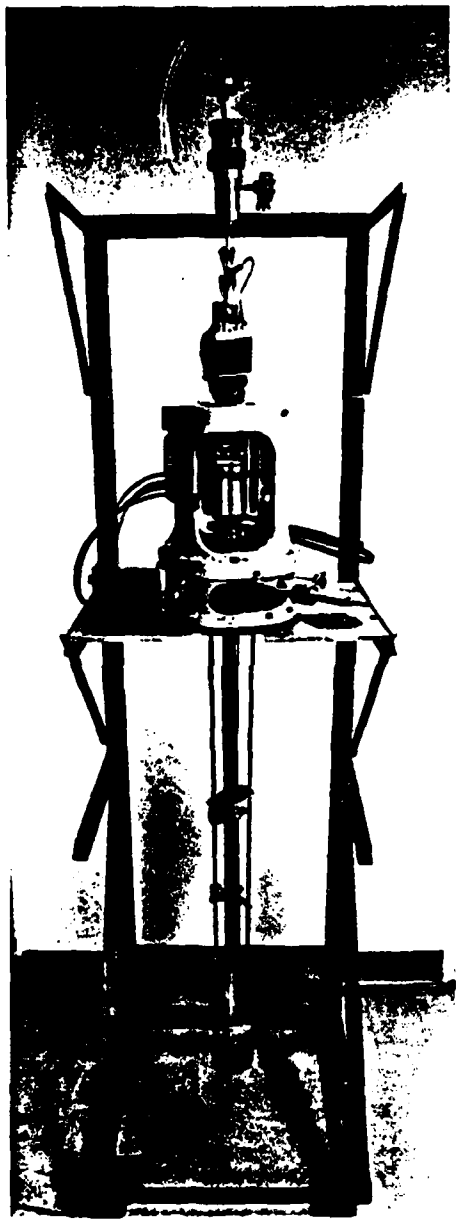

Figure III.E.4 Probe on Work Rack

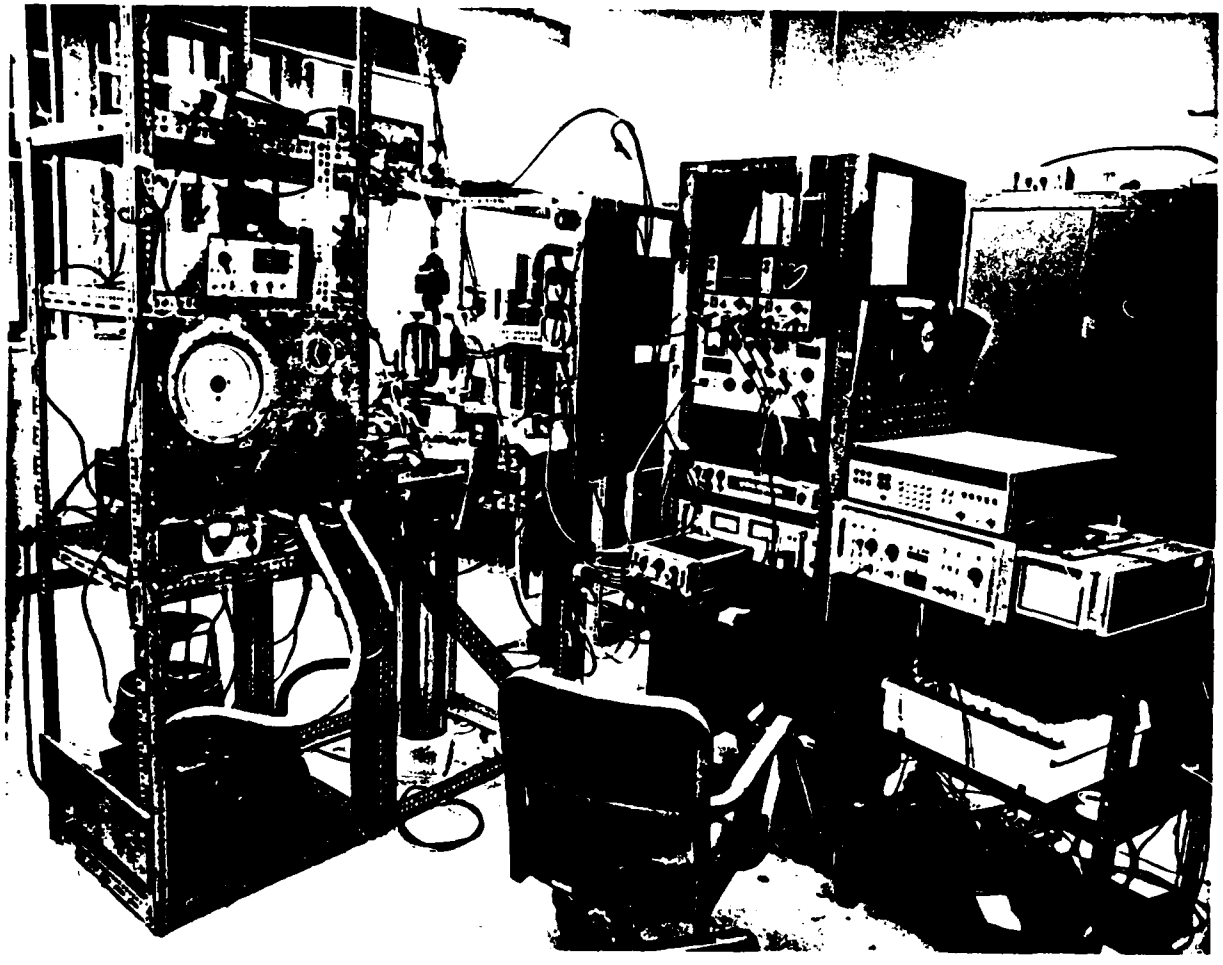

Figure III.E.5 Apparatus Overview

valved through to the cell to measure Po-P.

III.F DEWAR AND TEMPERATURE CONTROL

A stainless steel dewar system was chosen for this experiment to reduce the risks in case of an accident while rotating. It consists of a four inch internal diameter by 29 inch long inner dewar surounded by another dewar to hold liquid nitrogen. The inner dewar is mounted to a four inch copper tee. The top of the tee being fixed to the dewar top plate while the side was connected to the four inch copper vacuum line. The helium was cooled by pumping on its vapor by a mechanical pump (Stokes Model 212H-10 140CFM). A minimum temperature of 1.22 degrees Kelvin could be reached in this manner.

The level of the liquid helium in the dewar was monitored electronically, with an oscillator (Leonard)

and frequency counter. A long coaxial capacitor was fitted parallel to the main probe tube. It was fed through the top plate with a quarter inch quick disconnect and sealed with a hermetically sealed BNC connector. The dielectric for the capacitor is the helium, as the liquid level is reduced the capacitance goes down and increases the resonance frequency of the oscillator. This was continuously monitored on a frequency counter (Fluke Model 1910A).

The temperature of the bath was controlled by adjusting the pumping rate through a four inch main valve and two auxilary needle valves and heating feedback provided by a resistance bridge temperature controller (UCLA Physics Electronics Shop PO 97). A carbon resistor (Allen Bradley 200 ohms 1/8 Watt) was used as the thermometer in the bath and a wire wound 50 Ohm resistor was used as the heater. All temperature control wiring goes through the slip rings. The temperature could be held to 250 microdegrees while stationary and to 0.001 degrees Kelvin while rotating. The temperature was monitored by measuring the vapor pressure of the bath with a differential pressure meter (MKS Baratron Model 170M-6C and 170M-27E). This provided a readout to 0.1 microns. The pressures were converted to temperature using the 1958 Helium Four Scale of Temperature (NBS Monograph 10).

IV. EXPERIMENTS AND PROCEDURES

IV.A INTRODUCTION

The start up procedure to begin any given run is the same. The cell is pumped out to several microns and valved off. The evacuated inner dewar is filled with helium gas and the outer dewar is filled with liquid nitrogen (77.4 degrees Kelvin). After the probe has cooled down, liquid helium is transferred via a stainless steel vacuum insulated transfer tube. The dewar is then evaporatively cooled by pumping away on the helium gas in the dewar. The reference volume of helium gas for the cell is also cooled with liquid nitrogen. The filling fraction is then decided upon and the correct amount of gas is transferred into the cell

from the reference volume, the amount being monitored on the reference volume pressure gauge.

The type of experimental run must be chosen before the temperature drops below the lambda point (2.17 degrees Kelvin) and the normal liquid helium (He I) becomes superfluid (He II). If the run is to be started from rest then the temperature must be lowered and regulated at the desired operating temperature. There are several different types of runs started this way. They are 1) Sound Speed versus Filling at Fixed Temperature, 2) Po-P versus Filling at Fixed Temperature, 3) Measurements made in the Landau Region (Potential Flow) and 4) Hysteresis Curves with $\omega_i = 0.0$.

If the run is to be started with the cell in rotation, the initial speed of rotation is chosen and set by adjusting the regulated power supply and monitoring the frequency counter displaying the speed of rotation. The dewar is then cooled below the lambda point and regulated at the desired operating point. The types of experiments done in this way are 1) Hysteresis Curves with ω_i different from zero, 2) Decay Measurements of the Persistent Current, and 3) Critical Velocity Measurements.

IV.B SOUND SPEED VERSUS FILLING FRACTION

The most fundamental data for the experiment are those of the velocity of sound as a function of the filling fraction and temperature (see section II). The run is started as described in the introduction with the cell at rest. The temperature is fixed and a small amount of helium gas is added. The resonance spectrum is then recorded as well as the filling fraction. This process is then repeated until the cell is full. From the fundamental frequency the speed may be calculated from equation II.B.7. The experimental results are shown in figures IV.B.1 through IV.B.6 for temperatures from 1.216 (the lowest temperature we could reach) to 1.678 degrees Kelvin. They show the observed sound speed plotted against the filling fraction f for a given temperature. A composite graph is shown in figure

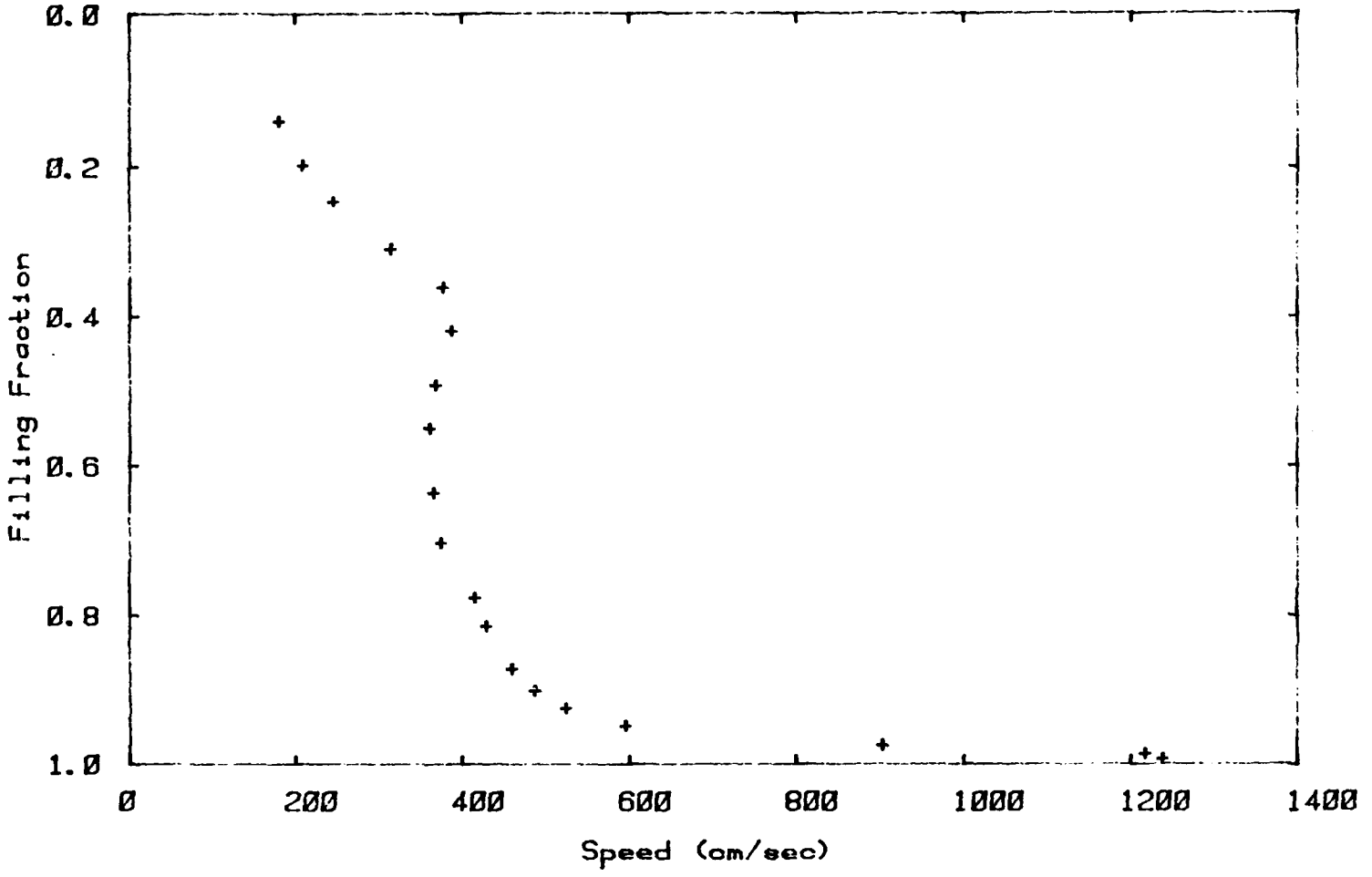

Figure IV.B.1 Sound Speed versus Filling Fraction T = 1.216°K.

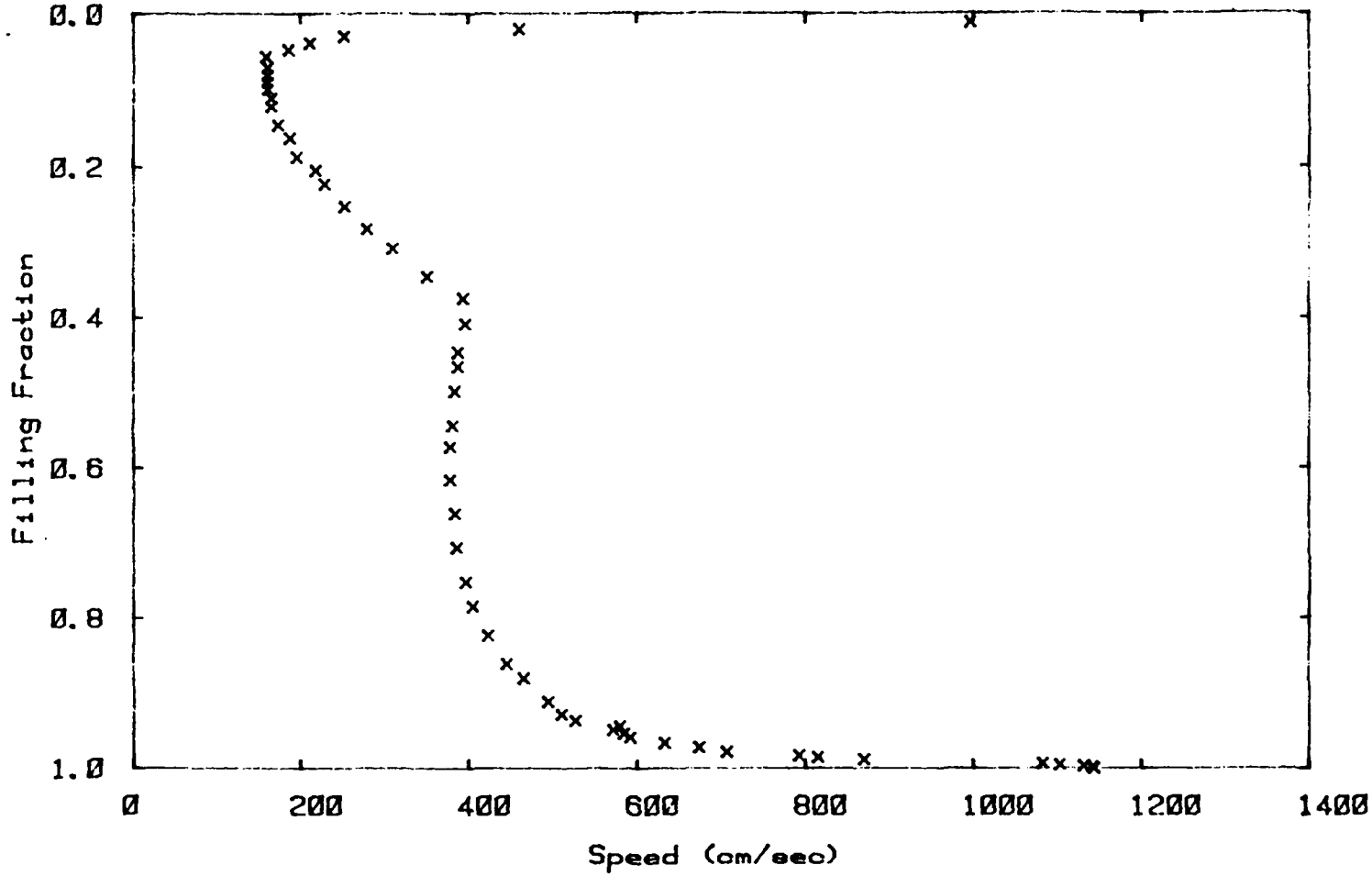

Figure IV.B.2 Sound Speed versus Filling Fraction T = 1.283°K.

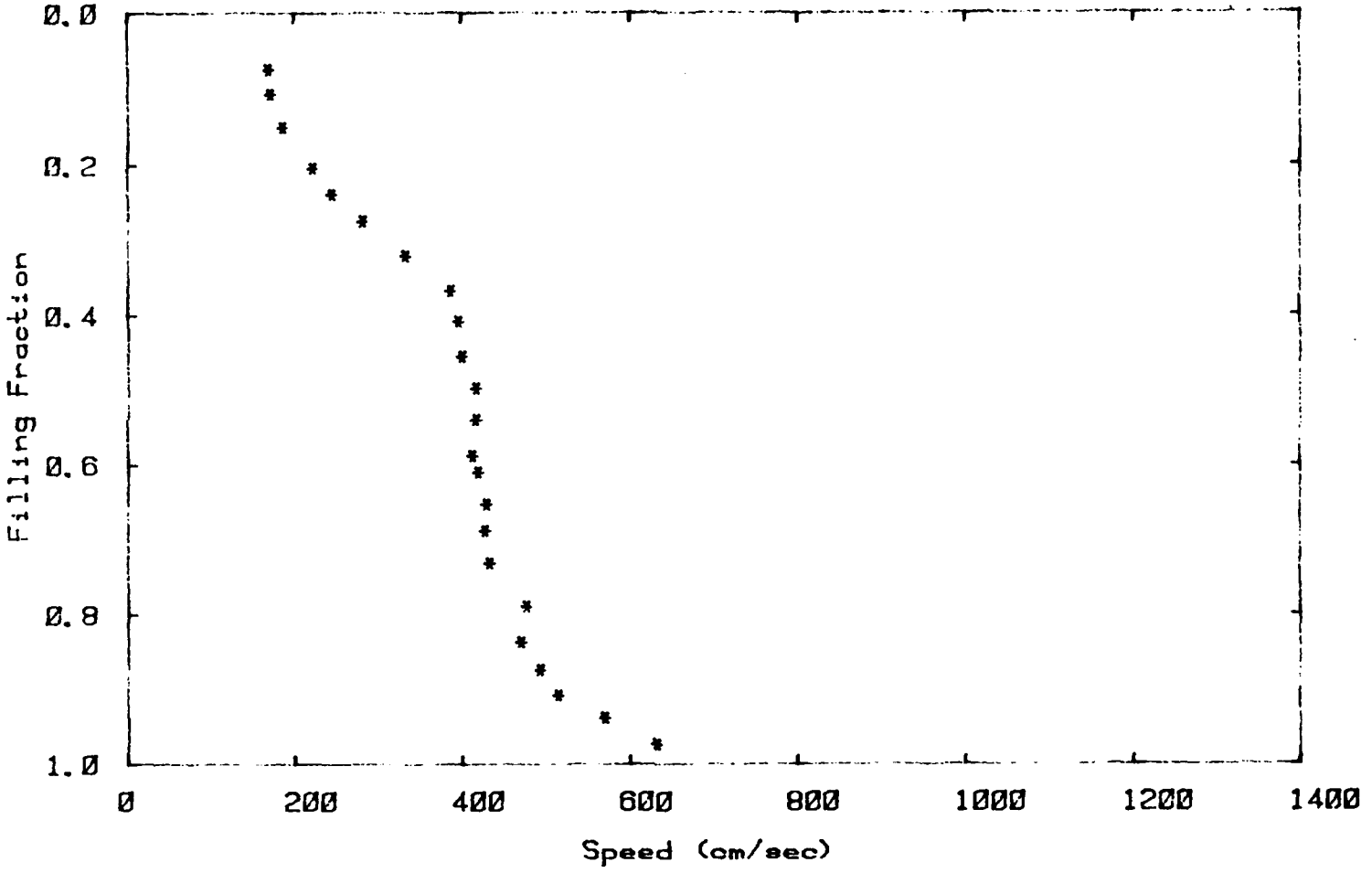

Figure IV.B.3 Sound Speed versus Filling Fraction T = 1.380°K.

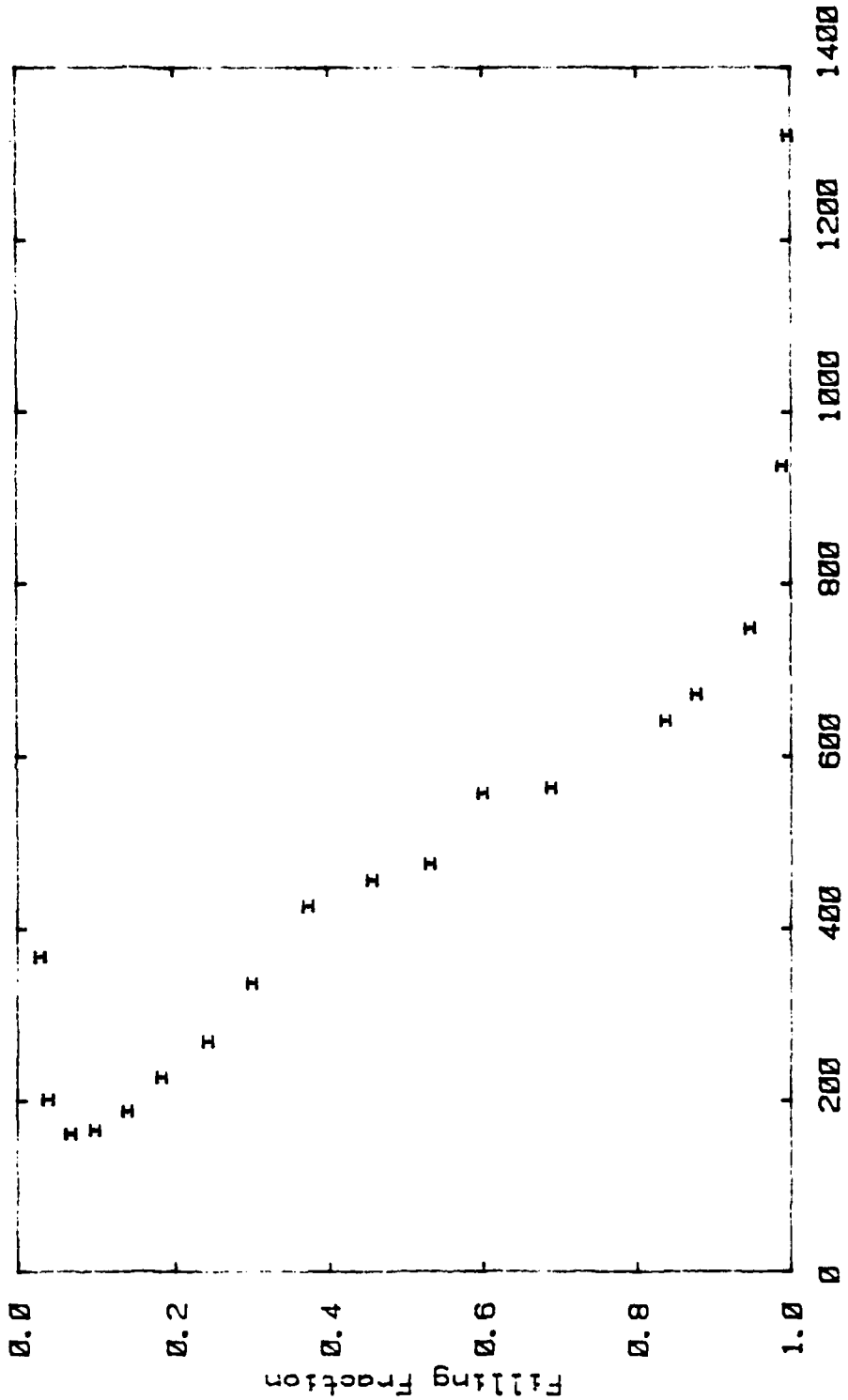

Figure IV.B.4 Sound Speed versus Filling Fraction T = 1.481°K.

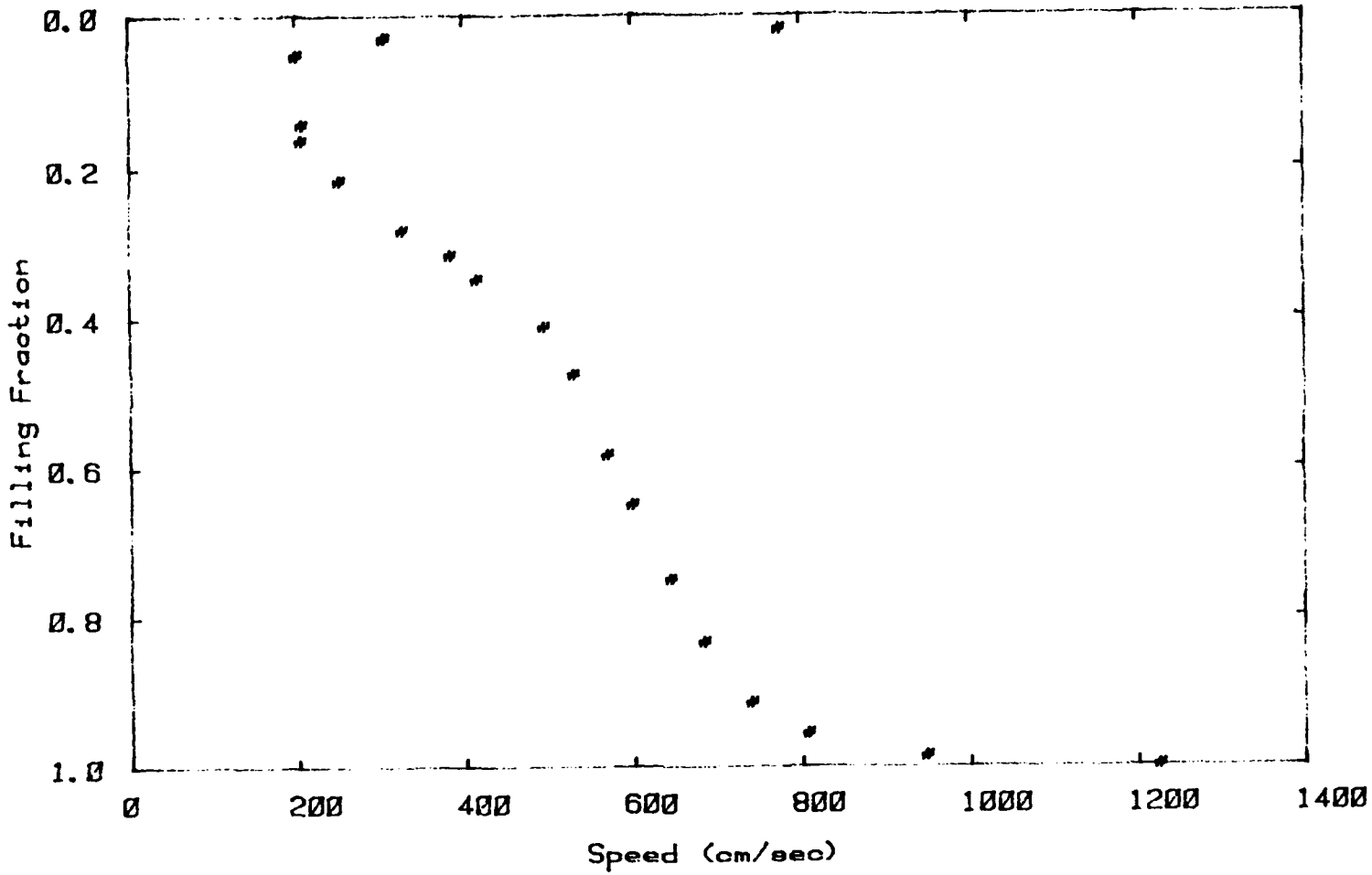

Figure IV.B.5 Sound Speed versus Filling Fraction T = 1.574°K.

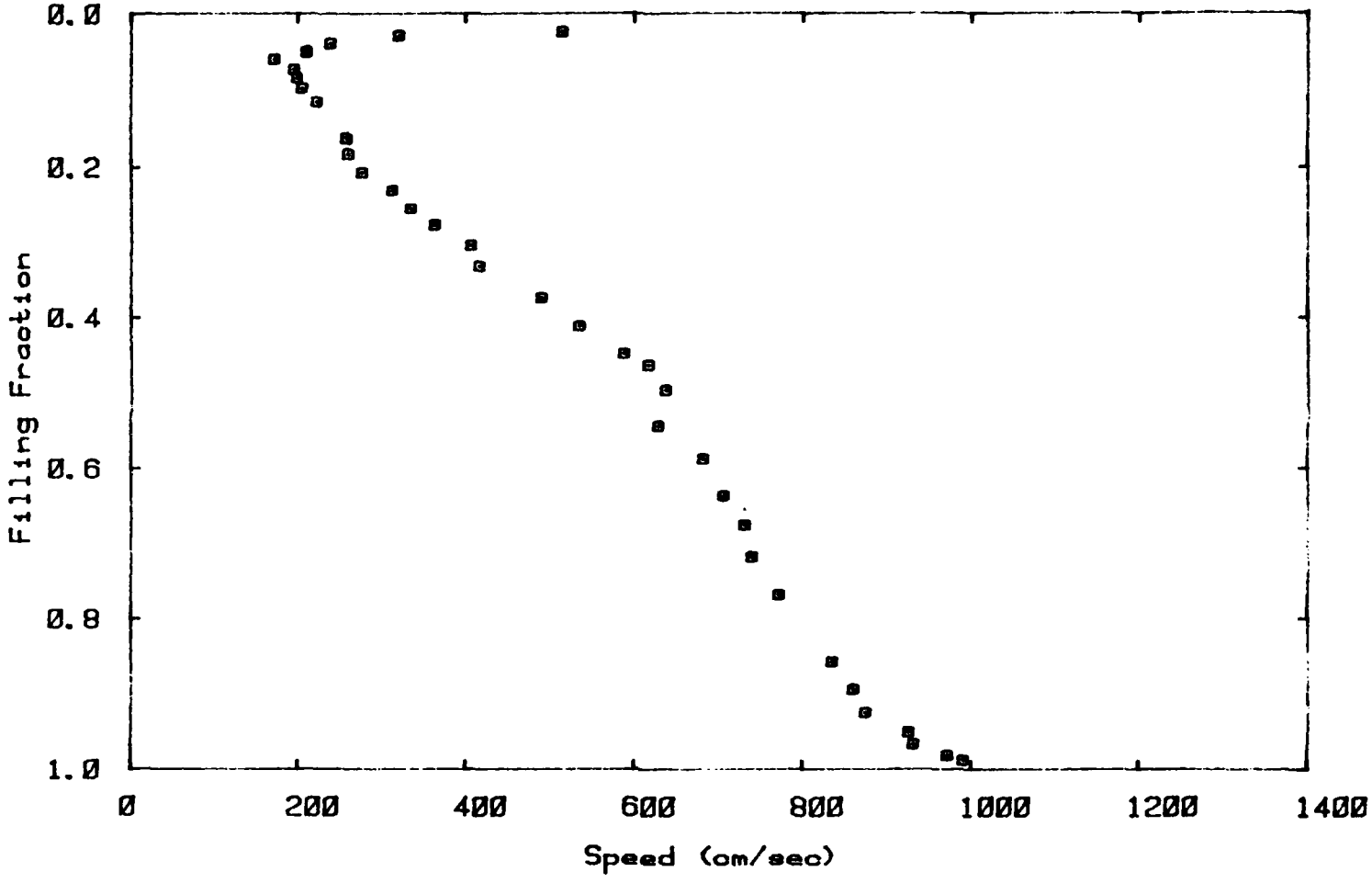

Figure IV.B.6 Sound Speed versus Filling Fraction T = 1.678°K.

IV.B.7 which shows the results from the various temperatures superimposed. These results agree closely with our earlier work shown in figure II.B.3. The basic description of these curves is found in section II.B.

The Q was determined for a resonance peak by measuring the center frequency and dividing it by the full width at half the maximum power. The Q is shown as a function of temperature in figure IV.B.8. The Q increases with decreasing temperature, at 1.25 degrees Kelvin it is about 100. Since a higher Q provides better resolution most of the experimental data was taken around 1.25 degrees Kelvin.

The increasing losses with increasing temperature are believed to be due primarily to the presence of increasing amounts of helium vapor. There are two places where the vapor interacts with the wave. The first is in the vapor pockets distributed throughout the superleak which are formed from only partially filling the cell with helium. The second is the open volume of the cell above the superleak. This volume has been filled mostly by the lucite transducer ring. There is still however some vapor present which can dissipate the energy of the propagating wave. Other loss mechanisms must also be present. Heat conduction to the powder and to the cell walls also account for some losses. Also,

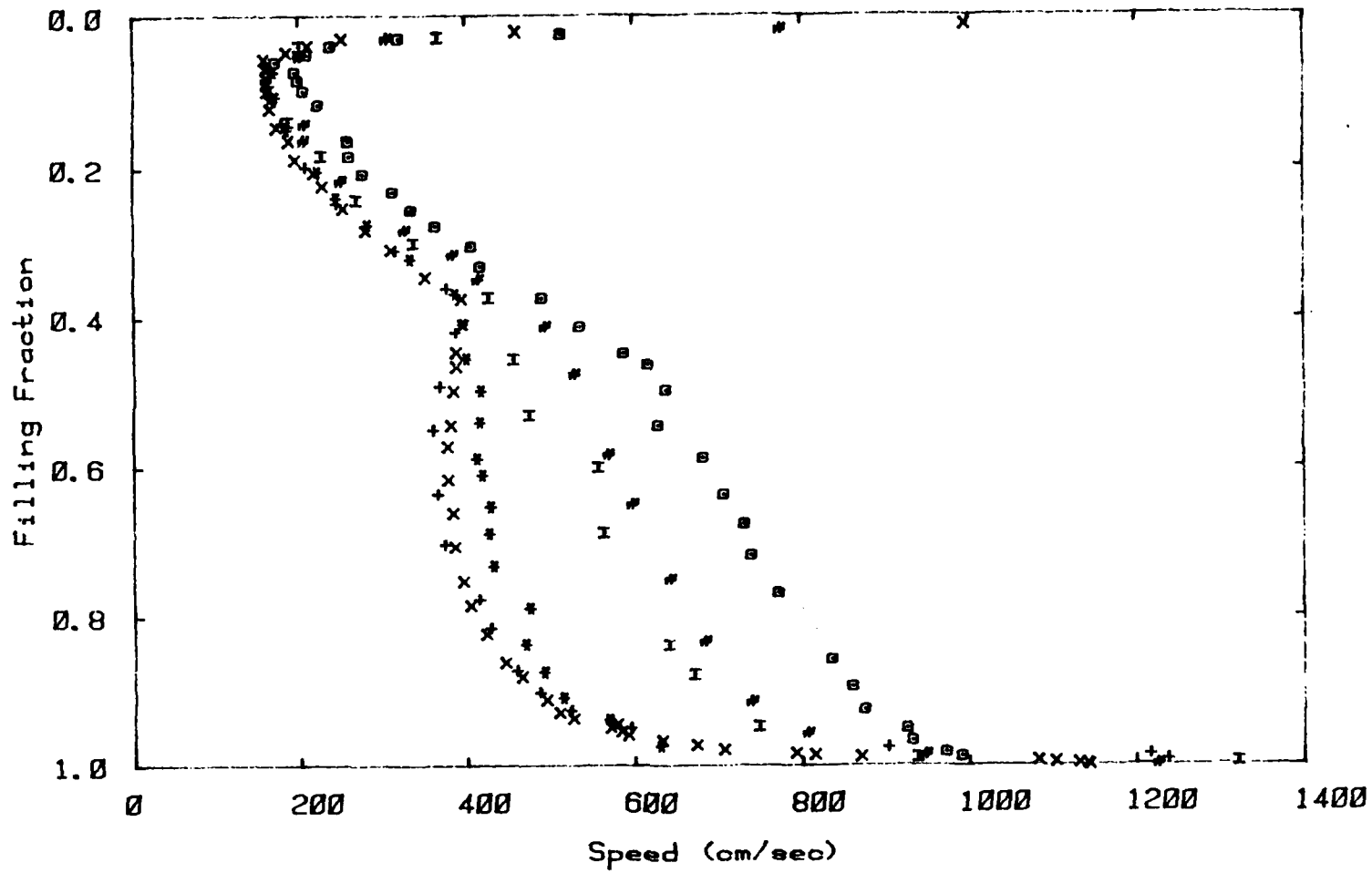

Figure IV.B.7 Composite Sound Speed versus Filling Fraction

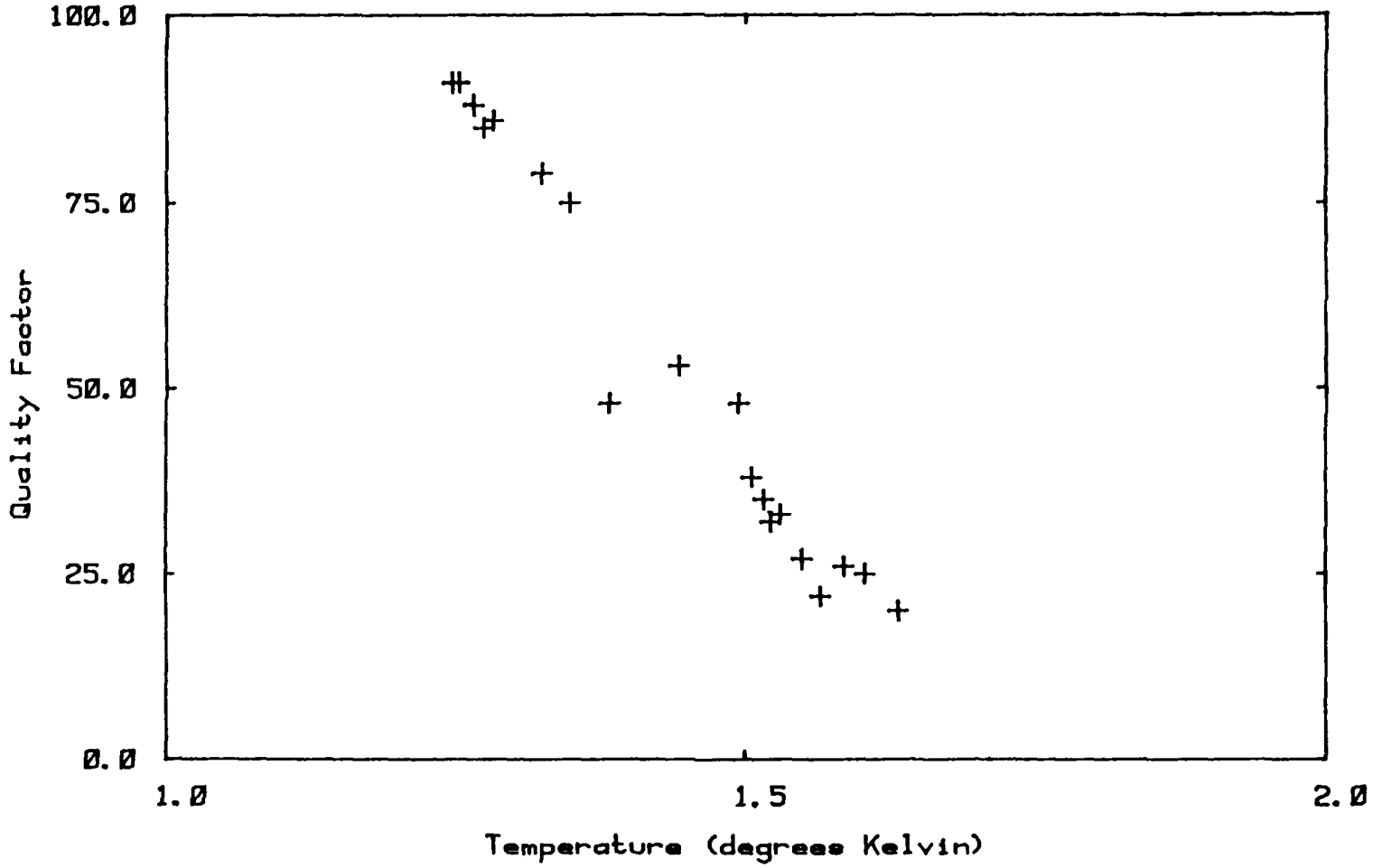

Figure IV.B.8 Q versus Temperature.

if the normalfluid component becomes unlocked from the superleak there will be viscous losses.

IV.C SCATTERING CORRECTION - EXPERIMENTAL

A complete description of the sound speed must take into account the scattering correction or the acoustic index of refraction n. The scattering correction n is the ratio of the speed of sound propagation in the absence of any scattering to the experimentally observed velocity. The scatttering correction can, in the simplest examples, be seen as a change in the effective bulk modulus and density, as would be the case for sound propagation in a porous medium filled with air. There are several good references on the problem of classical acoustic scattering including Lord Rayleigh (Rayleigh).

Shapiro and Rudnick (Shapiro) found that the empirical scattering correction n for a filled superleak of porosity P is given by equation IV.C.1.

$$n^2 = 2-P \qquad \{IV.C.1\}$$

Equation IV.C.1 gives agreement to several percent for the porosities which have been investigated (0.45 to 0.90). A theorectical model has been worked out by Johnson and Sen (Sen) which calculates the scattering correction for the filled superleak. Their model will be discussed in section IV.D.

The scattering correction in a superleak partially filled with helium II was first investigated here at UCLA in 1979 (Williams 79 and also Rosenbaum et al). From the basic velocity measurements shown in figures IV.B.1 and II.B.3 the scattering correction *n* is extracted as follows.

Equation II.B.1 which gives the velocity of the mode is modified to become equation IV.C.2 which corrects the speed of sound for the scattering correction n.

$$n^2C^2 = C_3^2 + C_\sigma^2 + C_5^2 \qquad \{IV.C.2\}$$

The observed sound speed decreases with decreasing temperature until about 0.8 degrees Kelvin. This is due to the velocity fifth sound dominating the sum decreasing with temperature. The ve...

AD-A123 522 PERSISTENT CURRENTS IN A ROTATING SUPERLEAK PARTIALLY FILLED WITH SUPERFLUID HELIUM(U) CALIFORNIA UNIV LOS ANGELES DEPT OF PHYSICS J S MARCUS DEC 82 TR-41 2/3

UNCLASSIFIED N00014-75-C-0246 F/G 20/4 NL

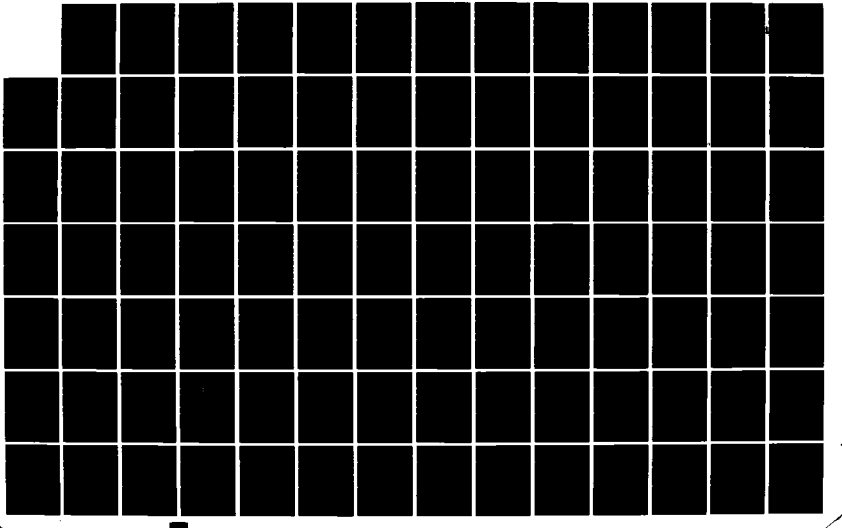

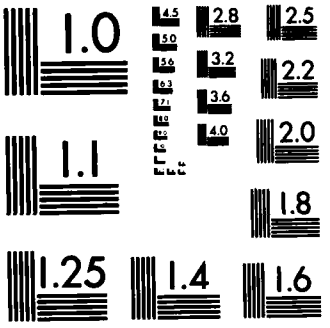

sound wave is proportional to T to the fourth and rapidly decreases with decreasing temperature. This can be seen by writing the velocity of fifth sound squared as $\frac{\rho_s}{\rho} \frac{T_s^4}{C_p}$ and looking at the temperature dependence.

Below 0.8 degrees Kelvin the velocity of third sound approaches a constant value as a function of temperature as the superfluid fraction approaches one.

$$C_3^2 = \frac{\langle \rho_s \rangle}{\rho} \frac{\partial \mu}{\partial d} d \qquad \{IV.C.3\}$$

$$C_5^2 = \frac{\rho_n}{\rho} C_2^2 = \frac{\rho_s}{\rho} \frac{T_s^2}{C_p} \qquad \{IV.C.4\}$$

At 0.8 degrees Kelvin and lower the contribution from fifth sound is vanishingly small. The observed velocity is dominated by the temperature independent velocity of the third sound contribution and the lack of a surface tension contribution. This leads to an observed temperature independent velocity Co which depends only on the filling fraction for a given cell (given porosity). This can easily be seen in figure II.B.3.

The scattering correction n may now be written as a function of the experimentally observed speed C, the temperature independent speed Co, and the velocity of fifth sound.

$$n^2 = C_5^2 \left[C^2 - \frac{\rho_s}{\rho} C_o^2 \right]^{-1} \qquad \{IV.C.5\}$$

Equation IV.C.5 is now solved for the scattering correction n as a function of the filling fraction f.

The results of this procedure are shown in figure IV.C.1 for filling fractions of 0.3 to 0.8 (the arrow shows the value of n calculated from (2-P) derived from fourth sound measurements). Here the index of refraction n is plotted against the filling fraction f. This data is taken from Williams et al. The resulting values of the scattering correction n are a strong function of the filling fraction and are temperature independent. One set of data had a small amount (2% molar concentration) of the isotope helium three added. It was found that the scattering correction was unchanged.

The strong dependence of the scattering correction on filling fraction is to be expected. The tortuosity (see section IV.D) of the helium in the superleak is dependent solely on the filling fraction for a given cell. Since the scattering correction is in a sense a measure of the tortuosity, the dependence of the scattering correction is reflected in its dependence on filling fraction and not temperature. The relationship between the tortuosity and the scattering correction will be treated more fully after the rest of the experimental results are presented in section IV.D.

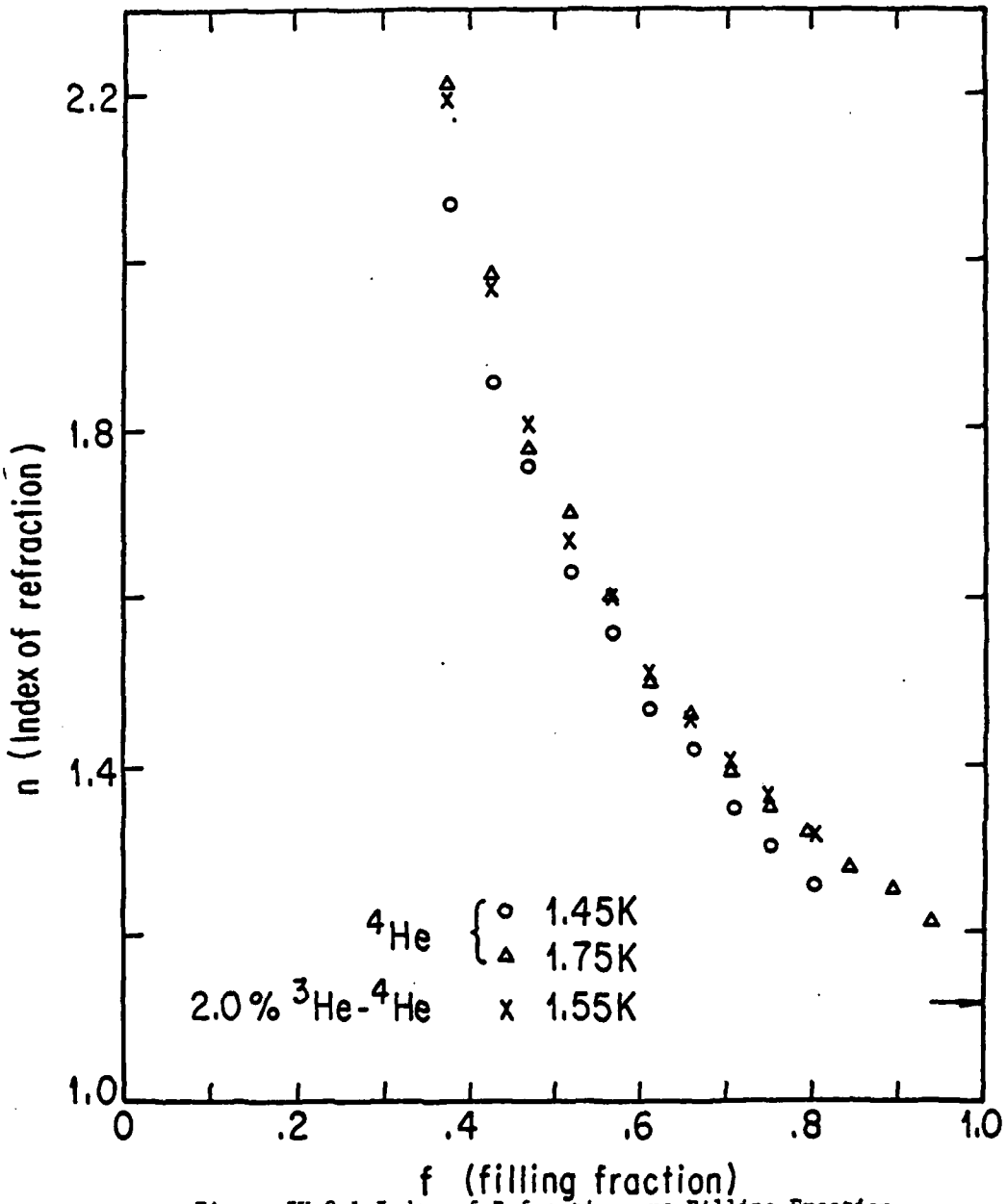

Figure IV.C.1 Index of Refraction vrs Filling Fraction
(Williams et al.)

The analysis of the data from the present work is slightly different from that of Williams et al. Since temperatures below 1.2 degrees Kelvin are not experimentally accessible the temperature independent velocity Co cannot be directly measured. The scattering correction may be found, however, by taking equation IV.C.5 at two temperatures and fixed filling fraction. The value of Co is eliminated between the two equations and the scattering correction n is then obtained for the given filling fraction f. This is then repeated for the available range (this is limited by the resolution of the sound speed as differences must be taken between numbers approaching the same value near f = 0.3) of filling fractions and the scattering correction n is obtained as a function of the filling fraction f. The individual results from a given filling fraction and all temperature combinations are then averaged for each filling fraction.

The results from this calculation are shown in figure IV.C.2. The scattering correction n is plotted against the filling fraction f. These results are in close agreement with the earlier work just discussed and shown in figure IV.C.1.

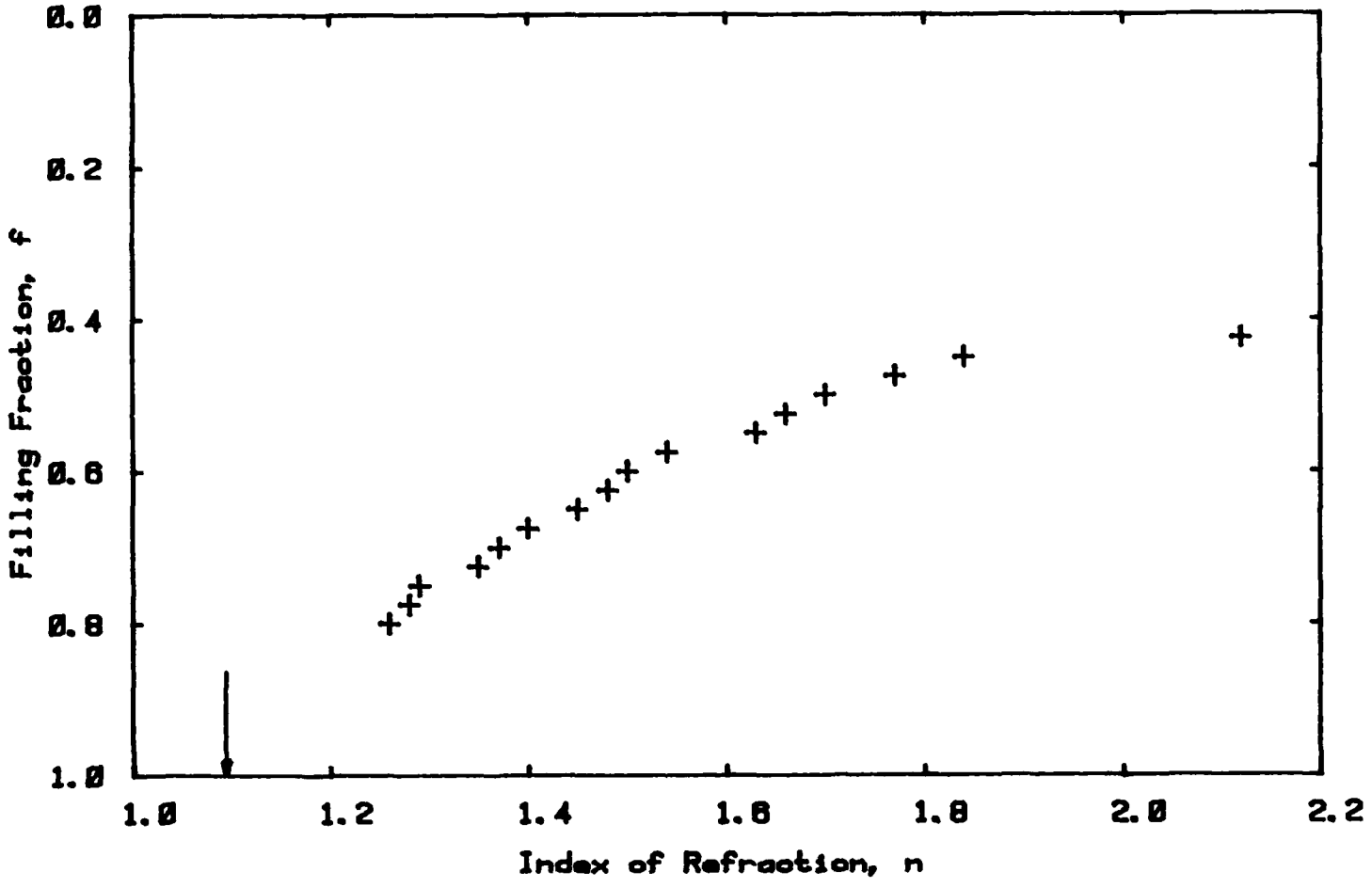

Figure IV.C.2 Index of Refraction, n vrs Filling Fraction, f

IV.D SCATTERING CORRECTION - THEORY

This section presents a functional form for calculating the scattering correction for the surface wave which propagates in a superleak partially filled with helium. This work has been done with the help of Steve Baker and Gary Williams here at UCLA (Baker). By way of introduction the model of Johnson and Sen (Sen) is presented for the scattering correction in a completely filled superleak in which fourth sound propagates. Also the empirical results of Rudnick and Shapiro for the filled superleak (Shapiro) are reviewed in comparison with the results of Johnson and Sen.

It is well known that experimental fourth sound velocity data must be corrected for the effects of multiple scattering of the wave by the grains of powder that comprise the superleak (Shapiro) if it is to be compared with the predictions of the two fluid theory.

This correction is made by introducing the scattering correction n which is empirically found to be temperature independent. For packed powder superleaks Shapiro and Rudnick (Shapiro) have found that the data can be corrected with a precision of a few percent by the empirical equation IV.C.1.

Based on a self-similar calculation for the acoustic index of refraction n of a random collection of like obstacles of all sizes, Johnson and Sen (Sen) have suggested the form:

$$n^2 = P^{-\beta} \qquad \{IV.D.1\}$$

The exponent beta is indicative of the detailed microscopic geometry of the obstacles (porous media) that scatter the sound wave. Beta has a very physical meaning in terms of Kelvin drag. It is the Kelvin drag coefficent. It is defined as the fraction of displaced incompressible fluid which is brought into motion when a body is accelerated in the fluid. For example if a sphere is accelerated to a velocity u it will impart a momentum to the fluid equal to one half (beta = 0.5) the displaced mass of fluid times u. For infinitely long cylinders (or long, slender, needle-like ellipsoids) oriented perpendicularly to the direction of wave propagation beta is equal to 1.0. For randomly oriented needle-like obstacles beta is 0.666.

By empirically choosing beta approximately equal to 2/3, the self-similar expression describes the fourth sound velocity correction about as well as the empirical expression over the experimental range of porosity (0.45 to 0.90).

The theory of Johnson and Sen is meant to apply only to media completely filled with fluid. There are advantages in studying the index of refraction in the partially filled superleak which are not available in the completely filled cell. Since the experimental index of refraction is a strong function of filling fraction a large range of values for n (factor of 3) is obtained from a single cell as a function of filling fraction. This means that the porosity and the microscopic substructure remains unchanged for a large range of measurements of the scattering correction.

Experimental sound velocity data for the surface wave that propagates in a partially filled superleak must be corrected by the index of refraction n as is the case for fourth sound in a helium filled superleak. The experimentally derived correction was introduced in section IV.C. The surface wave which propagates in a partially filled superleak is very different from the fourth sound wave which propagates in the filled

superleak. There are tiny (about 0.75 micron) vapor pockets distributed throughout our superleak as well as the powder grains which scatter the wave. The vapor pockets are an additional phase which is not present in the fourth sound cells. Both the powder grains and the vapor pockets act as scattering centers from which the wave is scattered. The index of refraction is easily varied by changing the filling fraction f. In fourth sound f = 1 and this type of change cannot be made. To change the index of refraction in fourth sound the microscopic geometry would have to be changed.

The data to calculate the index of refraction from each temperature (figures IV.C.1 and IV.C.2) was fit on an HP-67 calculator to the form of equation IV.D.4.

$$n = af^{-b} \qquad \{IV.D.4\}$$

This was done using the least squares curve fitting program supplied by HP. The resulting fits are shown as solid lines in figures IV.D.1 through IV.D.5 (the arrow indicates the value of n from (2-P) derived from fourth sound measurements). Each plot shows log n plotted against -log f. The first curve IV.D.1 is from our data. The data in Rosenbaum et al was used in obtaining figures IV.D.2 through IV.D.5. Figure IV.D.6 is a table of the coefficients obtained from the fitting procedure for the various data sets. In discussing the problem

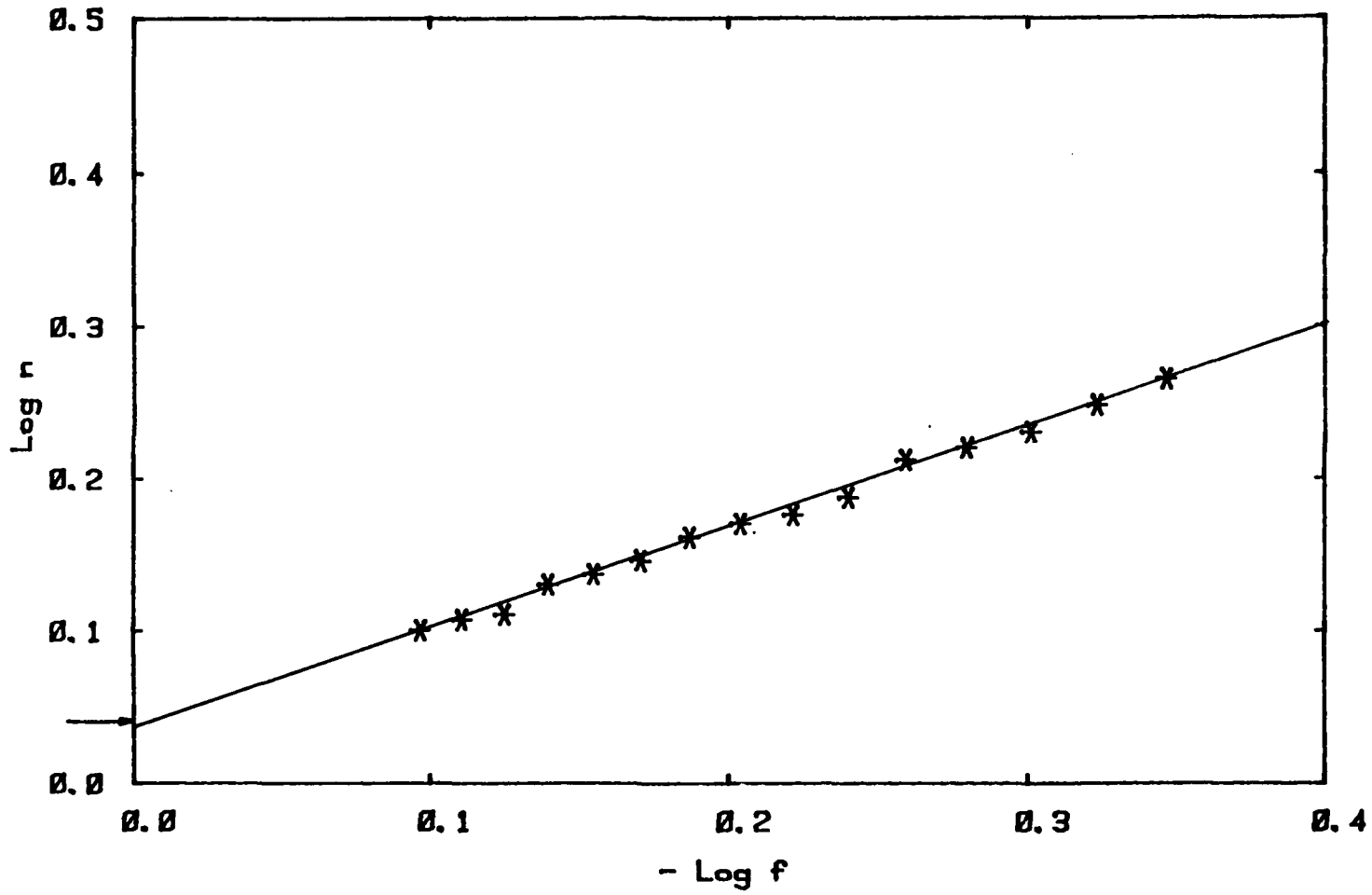

Figure IV.D.1 Log n versus -Log f.

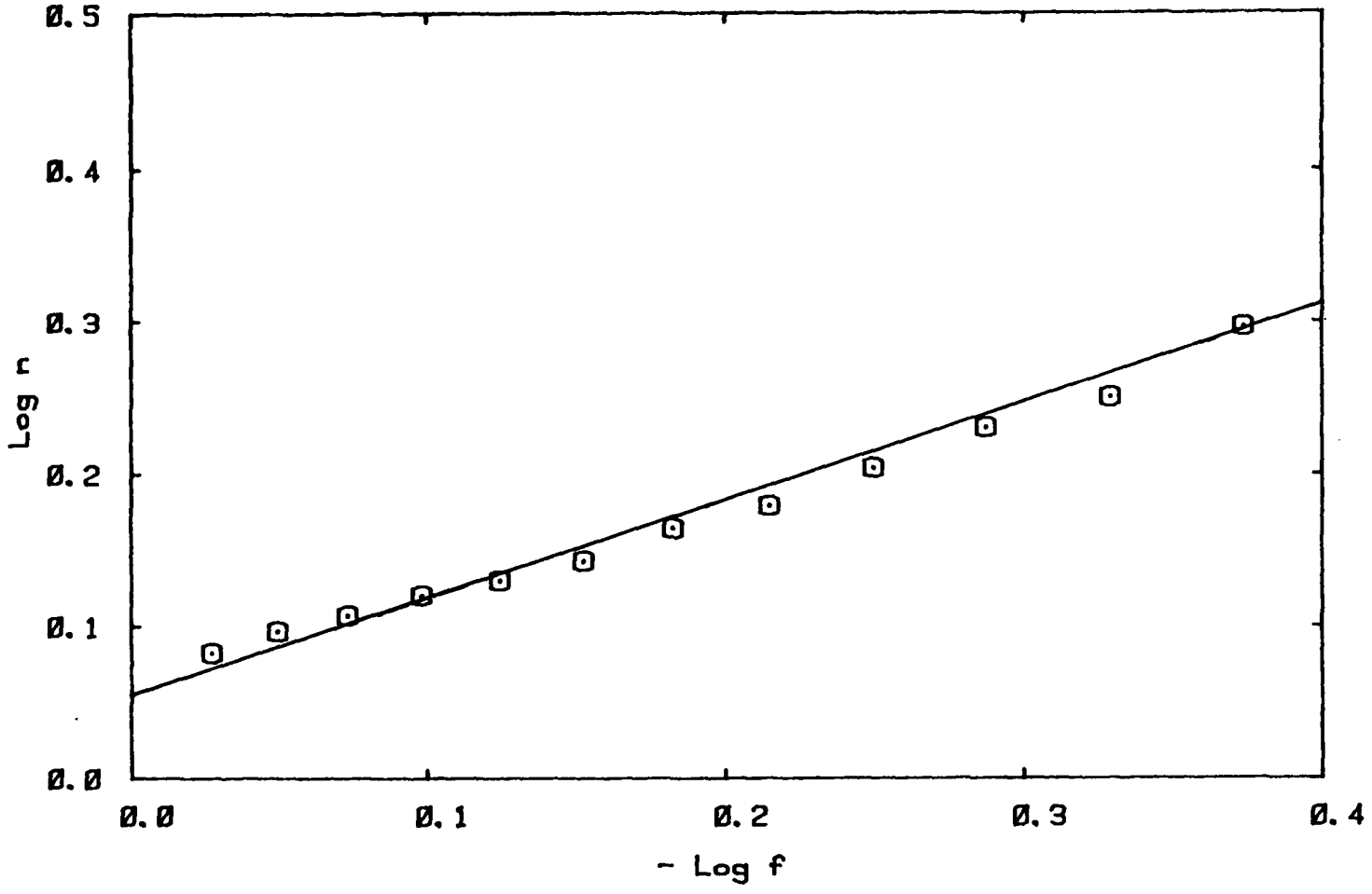

Figure IV.D.2 Log n versus -Log f T = 1.75°K (Williams et al.)

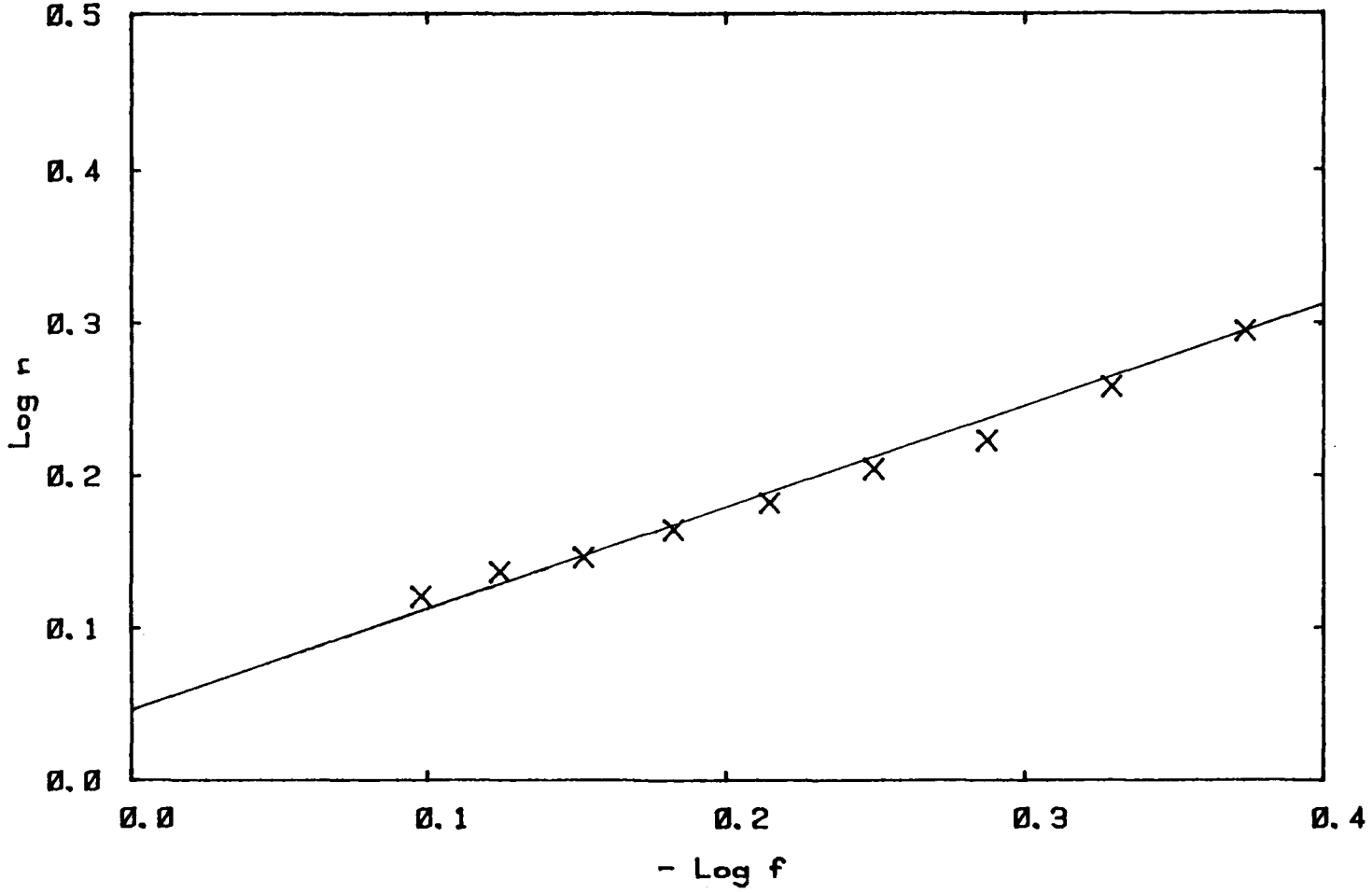

Figure IV.D.3 Log n versus -Log f T = 1.55°K 2% He^3 (Williams et al.)

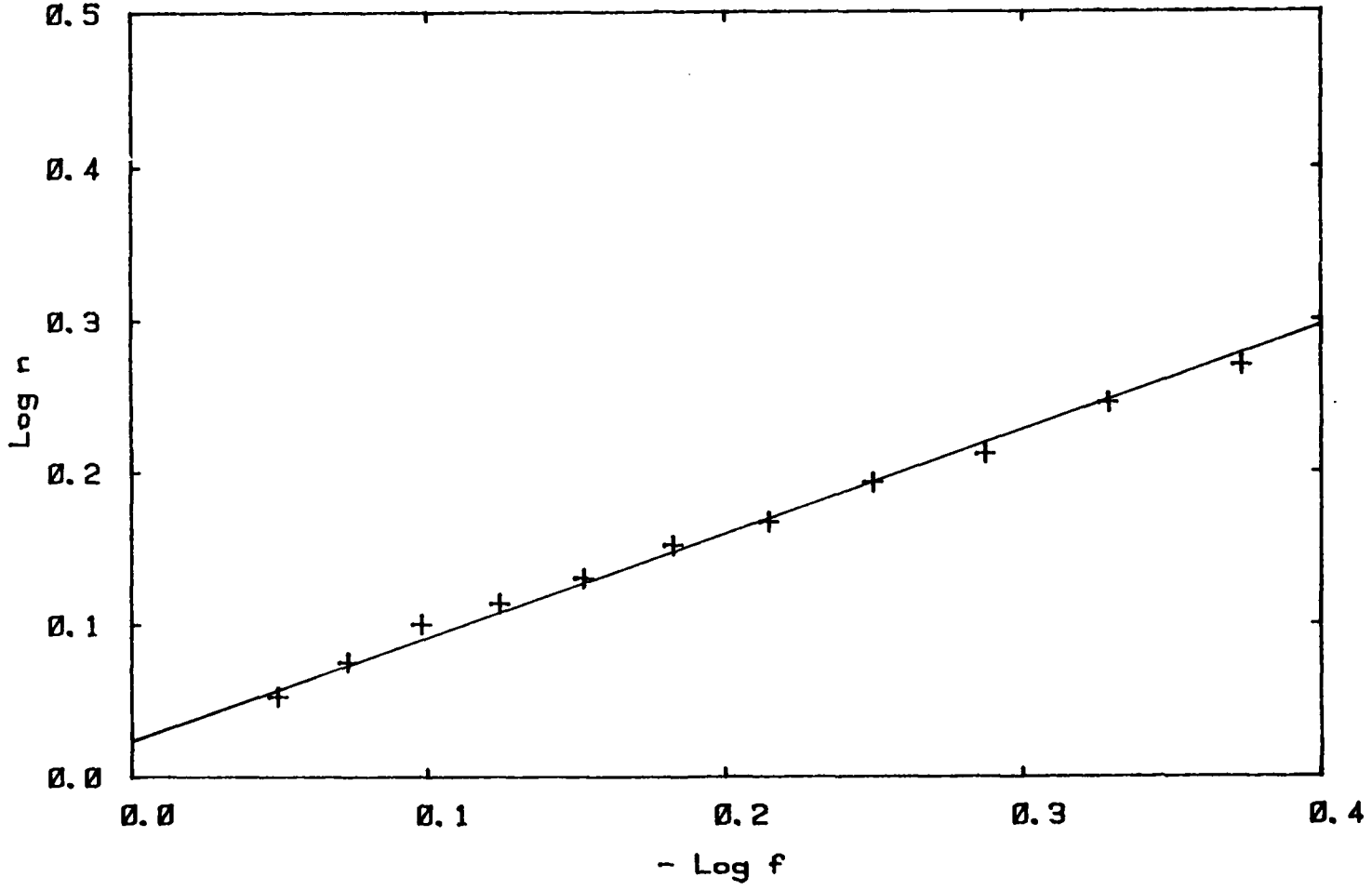

Figure IV.D.4 Log n versus -Log f T = 1.45°K (Williams et al.)

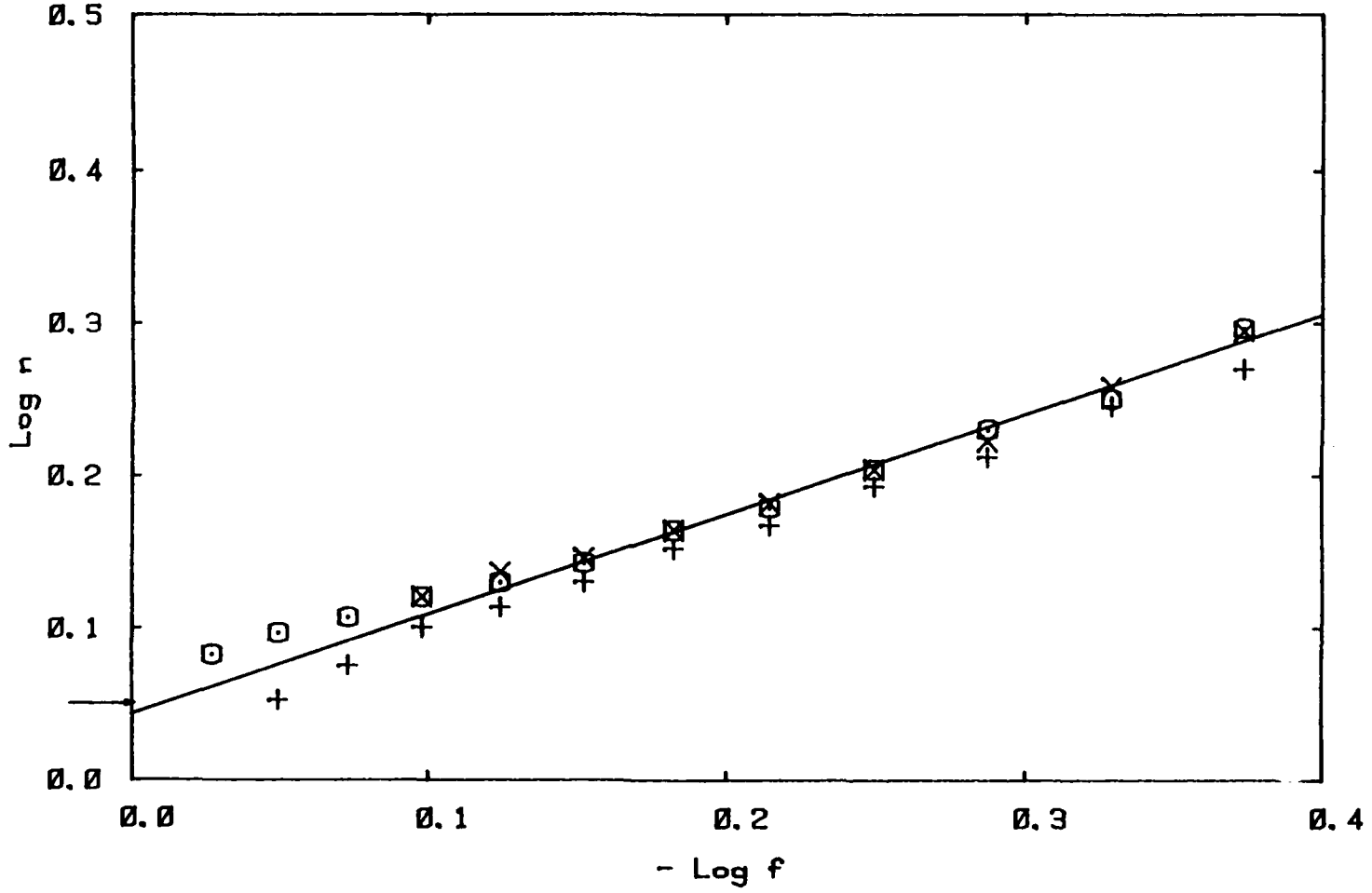

Figure IV.D.5 Composite Log n versus -Log f (Williams et al.)

TABLE IV.D.6

SUMMMARY TABLE OF SCATTERING CORRECTION FITS
TO EQUATION IV.D.4

DATA	a	b
Present Work	1.083	0.659
1.45 degrees Kelvin *	1.066	0.662
1.75 degrees Kelvin *	1.137	0.628
1.55 degrees Kelvin * 2% Helium 3	1.113	0.660
Average of *	1.107	0.647

FIGURE IV.D.7 SUMMARY OF FITS TO EQUATION IV.D.5

DATA	BETA 1	BETA 2
1.45 degrees Kelvin *	0.554	1.318
1.75 degrees Kelvin *	0.893	1.324
1.55 degrees Kelvin * 2% Helium 3	0.893	1.256
Average	0.707	1.294

* Taken from Williams et al

Johnson suggested to Professor Rudnick that the form of equation IV.D.5 might be the appropriate choice with which to model the results.

$$n^2 = f^{-\beta_2} \cdot p^{-\beta_1} \qquad \{IV.D.5\}$$

Equation IV.D.5 has the feature that it treats the vapor pockets and powder particles as independent scattering centers. That is, it recognizes the difference in the specific geometries and compressibilites of the vapor pockets and the powder particles. This in fact must be the case if one tries to visualize the shapes of the vapor spaces in comparison with the powder grains. In the the limit as the filling fraction f approaches 1.0 (fourth sound limit) equation IV.D.5 reduces to the familiar self-similar result suggested for fourth sound by Johnson and Sen and the empirical results of Shapiro and Rudnick. This also corresponds to the experimental observation that in the same limit the scattering correction tends to the value recognized for fourth sound.

Recasting our fit (equation IV.D.4) in terms of equation IV.D.5 using the porosity P, beta one, beta two, and the filling fraction f, the fit of the data in figure IV.D.5 is physically well described by equation IV.D.5. Figure IV.D.7 shows a table which summarizes the coefficients from the various fits.

The physical understanding of these results is not difficult. In the limit of the filling fraction approaching 1.0 (filled) the scattering correction squared approaches the empirical value of (2-P) from fourth sound measurements. The value from equation IV.C.1 (n = 1.118) is only 1% different from the partially filled case (n = 1.107) in the limit of complete filling. The value of n from (2-P) is shown by an arrow on figures IV.C.1, IV.C.2 and IV.D.1.

The exponent (beta one) accompanying the porosity P in equation IV.D.5, 0.707, from the fit of the data from figure IV.D.5 is a representative value for fourth sound. This supports the earlier claim that in the limit of complete filling the results yield the accepted fourth sound values of refraction. The exponent (beta two) characterizing filling fraction, 1.294, suggests that the underlying geometry of the vapor pockets is much more tortuous than the underlying geometry of the powder grains as high values of beta are associated with high degrees of tortuosity. The fact that beta two is roughly twice beta one suggests that the vapor pockets are very different from the powder grains.

From the fit to our data using equation IV.D.4 and using the value of 0.707 for beta one from table IV.D.7,

equation IV.D.5 can be used to calculate the porosity. The porosity calculated is 0.798, which is very reasonable. The scattering correction n can be calculated from (2-P) and this value gives n = 1.096. This is very close (1.2%) to the extrapolation of the fit to our data in figure IV.D.1.

The problem that still remains is to model the scattering correction at low filling fractions. For very low filling fraction our model gives much greater values than comparing the third sound results of Rudnick and Fraser (Fraser) to our work. From this comparison the scattering correction is determined to be approximately 3.75. It is my opinion that the nature of the scattering changes somewhere below a filling fraction of 0.3 and a different model will be needed there. It is not realistic to expect our model to cover the complete range of filling fractions although it does well for filling fractions from 0.3 up to nearly 1.0.

The region between filling fractions of about 0.05 and 0.3 is still an open question. It at this time not possible to extract the scattering correction from the experimental data nor or there any comparable experiments as is the case for the thin film region mentioned above. It is easy to believe that this will be a transition region in which the index of refraction

will roll over to intersect its axis at about 4.

The resulting fits from equation IV.D.5 are quite encouraging. In the limit of complete filling the well known value from fourth sound work is regained. In the region of low filling more work is needed. It would seem that more work in this area would yield much new knowledge of scattering which is finding many applications in the recent publications. Also the theoretical derivation of equation IV.D.5 still needs to be worked out in detail.

IV.E PERSISTENT CURRENTS - LANDAU REGION

There are two types of flow which may make up a persistent current. One is potential flow and the other is the flow resulting from vortices trapped in the superleak. The Landau region is composed only of potential flow and obeys the Landau restriction that Vs be curl free. The types of flow present at a given time depends on the way in which the cell was prepared.

To study the Landau region the cell is cooled down at rest below the lambda point and then brought into rotation. As the cell begins to rotate the normalfluid component is held tightly to the rotating superleak by viscosity. The superfluid component has no viscosity and is not forced to rotate with the superleak through viscous interaction. If there were no superleak the

normalfluid component would be brought into motion from the viscous interaction with the walls. The superfluid component would remain at rest. Since the annular channel is filled with the superleak its effect must be accounted for. The powder particles which make up the superleak reversibly drag on the superfluid. The drag is Kelvin drag and it does not depend on viscosity. The rotating powder grains impart some momentum to the fluid when they are accelerated. For a sphere brought into motion in an ideal incompressible non-viscous fluid the momentum is equal to one half of the mass of the displaced fluid multiplied by the velocity of the sphere. Hence the velocity of the superfluid is less than the normalfluid (Vn) and their ratio Vs/Vn is a measure of the Kelvin drag. The velocity of the normalfluid component (ω_n or Vn) is always equal to the velocity of the superleak (velocity of rotation). The velocity of the superfluid component (ω_s or Vs) is not directly related to the rotational speed of the superleak.

To take experimental data the system is prepared at rest as described in section IV.A. The resonance spectrum is then recorded. The cell is rotated slowly from rest and held at a constant angular velocity. The splitting of the resonance peaks (frequency doublets) and the rotational speed are recorded. The speed of

rotation is increased a little more and the new splitting and the rotational speed are recorded. The results from this type of measurement are shown in figure IV.E.1. The graph shows the splitting of the frequency doublets divided by their mode number plotted against Wn the speed of rotation. The slope, s, of the linear portion beginning at the oirigin of this graph gives a measure of the Kelvin drag as previously discussed (Vs/Vn or ω_s/ω_n). The value of ω_s/ω_n is given by equation IV.E.1 in terms of the slope s from the Landau region (potential flow only). See appendix 1 for a derivation of IV.E.1.

$$\frac{\omega_s}{\omega_n} = 1 - \pi \cdot s \qquad \{IV.E.1\}$$

That is when the graph has zero slope the superfluid component moves with the normal fluid component (Wn = Ws). When the slope, s, is equal to (dC/dVs)/pi the superfluid velocity Ws is zero. Since dC/dVs is about 1.0 this occurs for a slope of 0.318 (1/pi = 0.318). Then the superfluid component is at rest and Wn - Ws = Wn. Figure IV.F.13 shows the results from five runs in which the frequency splitting divided by mode number is plotted against the rotational speed $\omega_i - \omega_n$ (ω_i is the initial speed of rotation see IV.F). The ratio Ws/Wn is 0.276 with a standard deviation of 0.042. The various ratios of ω_s/ω_n are shown tabulated in table IV.E.2 for

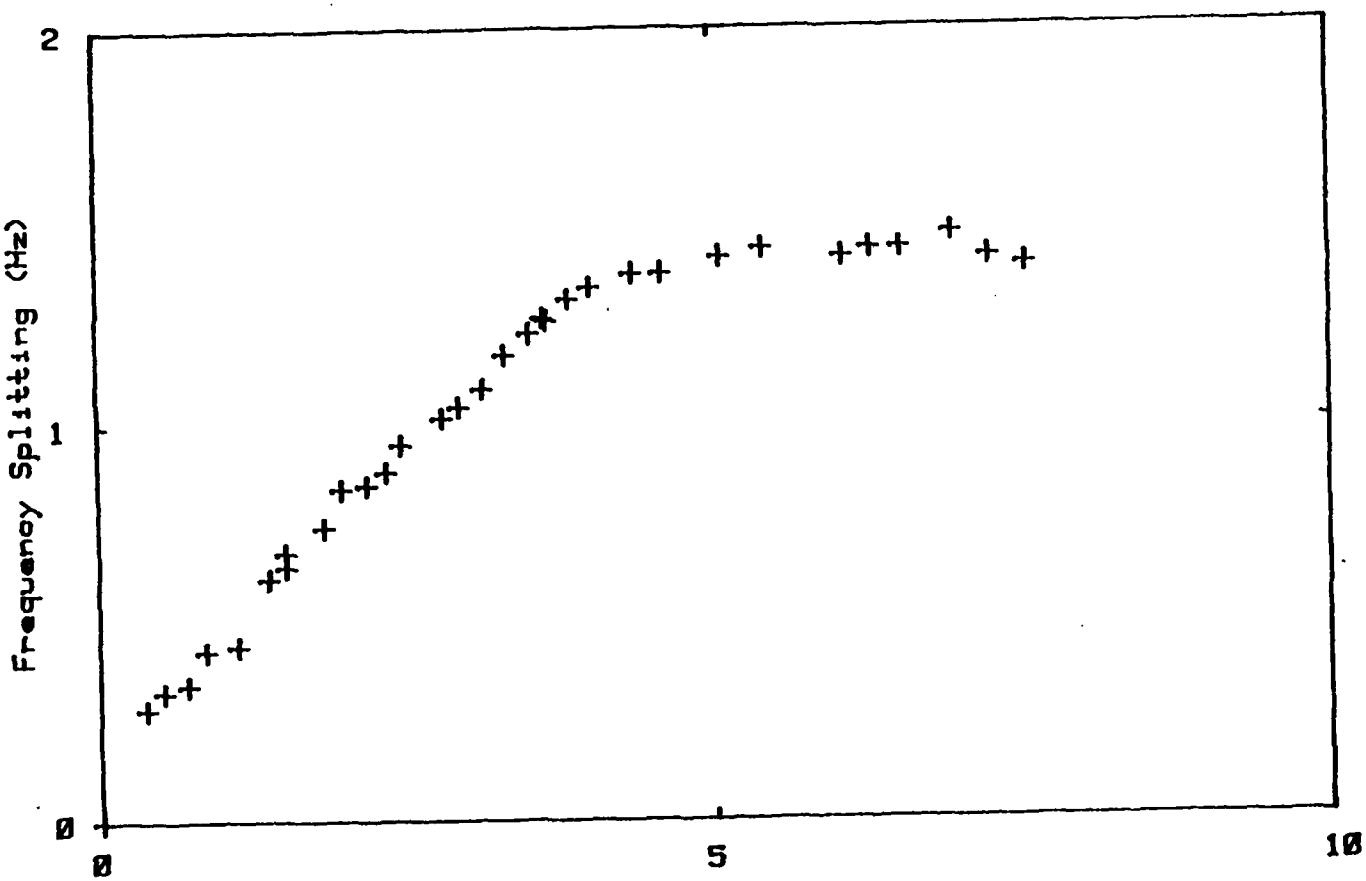

Speed of Rotation, ω_n (rad/sec)

Figure IV.E.1 Landau Region.

TABLE IV.E.2

SUMMARY OF THE KELVIN DRAG ω_s/ω_n FROM THE LANDAU REGION

FILLING FRACTION, f = 0.500 AND TEMPERATURE = 1.294 DEGREES KELVIN
FOR VARIOUS INITAL ROTATIONAL SPEEDS ω_i

ω_i (rads/sec)	ω_s/ω_n
0.0	0.262
1.451	0.319
1.571	0.321
3.142	0.208
4.712	0.268
4.763	0.279
AVERAGE	0.276 ± 0.042

DATA FOR VARIOUS FILLING FRACTIONS AND TEMPERATURES

FILLING FRACTION	TEMPERATURE (Kelvin)	ω_s/ω_n
0.800	1.29	0.042
0.703	1.28	0.106
0.599	1.37	0.205
0.500	1.49	0.250
0.335	1.27	0.532
0.225	1.29	0.752
0.145	1.28	0.844

various runs. The top section shows the ratio ω_s/ω_n as a function of various intial velocities ω_i (the next section discusses the state prepared with ω_i different from zero). The lower half of table IV.E.2 shows the ratio ω_s/ω_n for various filling fractions. The ratio gets smaller for higher filling fractions, this means relatively less of the superfluid component is brought into rotation the higher the filling fraction. Figure IV.E.3 shows Ws/Wn plotted against the filling fraction. It is interesting to note that a linear fit to the data results in a value of 0.99 for f = 0.0.

In the next figure IV.E.4, points are taken as described above but the the probe is slowed or brought to rest. Then it is again brought up to speed and the data again recorded. The graph is labled numerically, in chronological order. The probe is at rest at point 0 on the graph. It is brought into rotation and the Landau region is traced out, points 2 and 3. Points 4 and 5 show the reversible return to the origin. The probe is again rotated and point 6 shows this. As it is slowed the splitting does not go away and the splitting is shown at point 7 when it is again at rest. Past point 6 the Landau region is exceeded and vortices are created. Once this occurs the flow is no longer reversible.

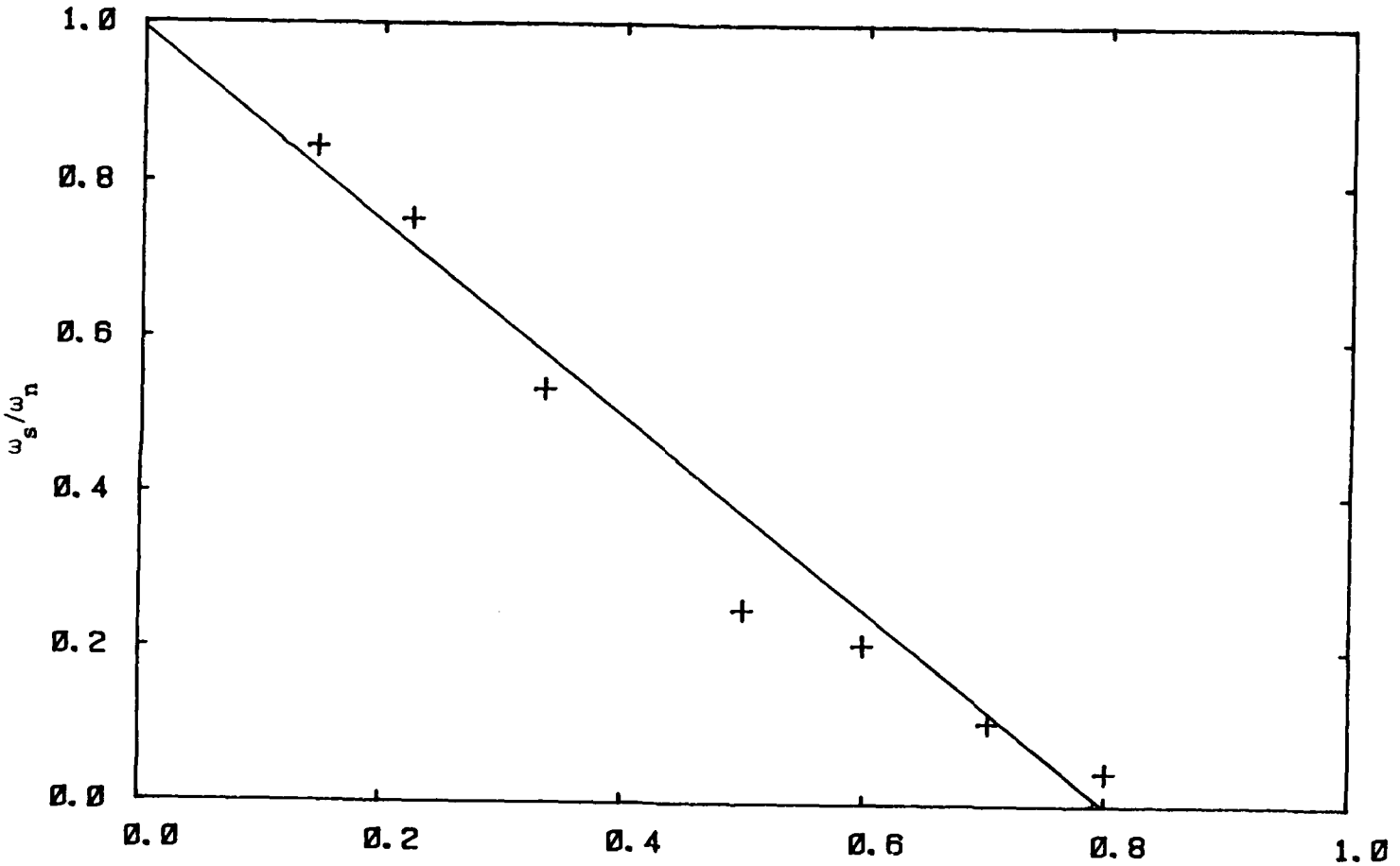

Figure IV.E.3 ω_s/ω_n versus Filling Fraction.

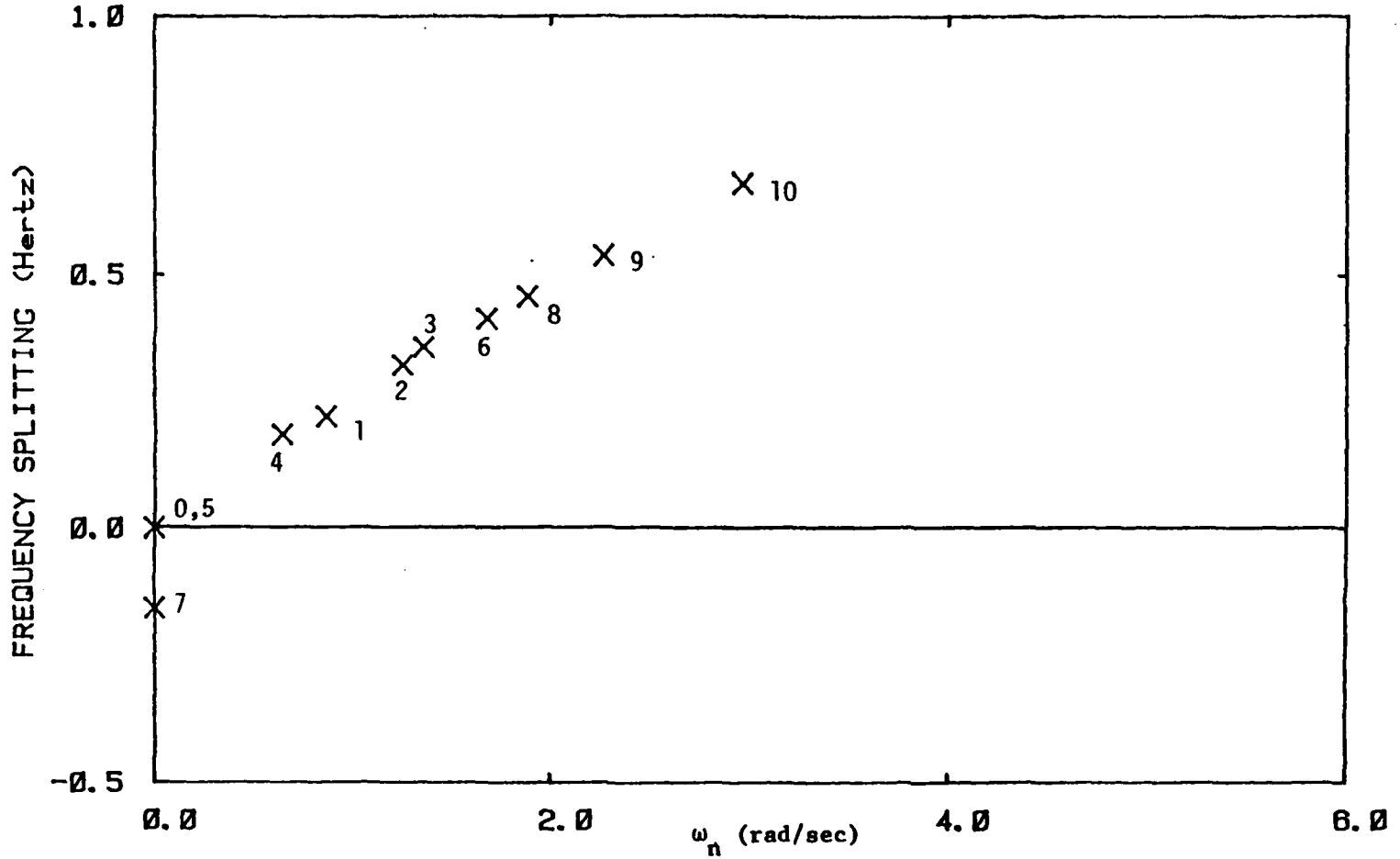

Figure IV.E.4 Labeled Landau Region.

The next figure IV.E.5 shows the abrupt deviation from the Landau region when omega cee one is exceeded. Omega cee one is defined as the first critical velocity and it marks the upper end of the Landau region. It shows the difference in frequency from the experimental data points to a line extended through the Landau region plotted against the speed of roation ω_1. This abrupt behavior is due to the creation of vortices at rotational speeds greater than omega cee one. The vortices are believed to be pinned to the powder grains and remain in the system as long as it remains superfluid. A more detailed explanation follows in section IV.F

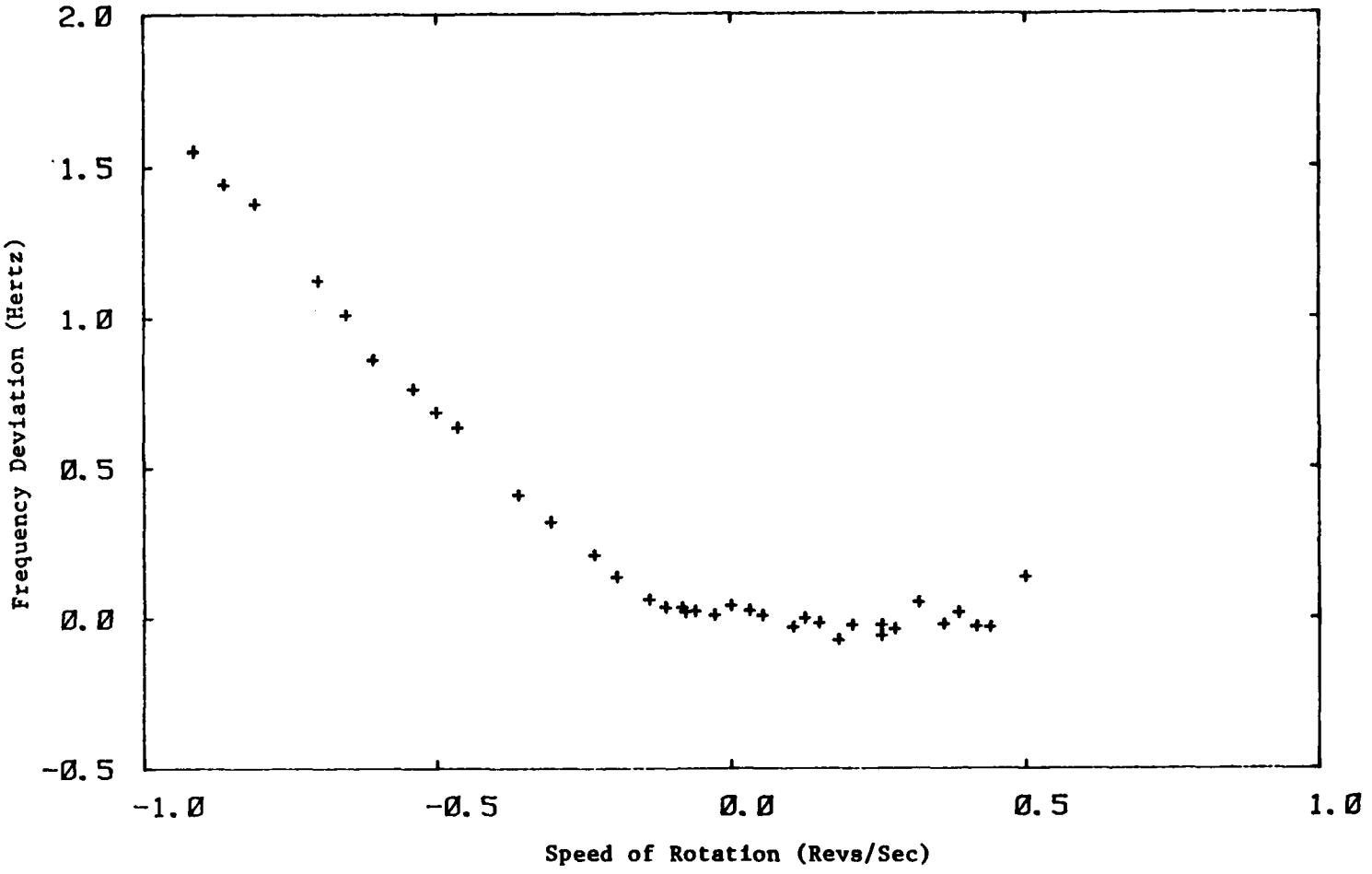

Figure IV.E.5 Deviation from Extended Landau Region
ω_i = 0.5, T = 1.28°K, f= 0.703

IV.F PERSISTENT CURRENTS - VORTEX STATES

As introduced in the previous section IV.E there are two types of superfluid flow which may make up a persistent current. Potential flow and flow from vortices. In this section persistent current made of both potential flow and vortices will be examined. There are two ways in which vortices may be introduced into the system. The first is to begin the experiment at rest and rotate at speeds greater than omega cee one. This produces both potential flow and vortices. The second is to cool down through the lambda point with the cell rotating. This produces only vortices with no potential flow (and no splitting unless the speed is changed). When the temperature equals T-lambda the critical velocity omega cee one vanishes. At this point there is a condensation of vorticity at the cores of the

quantized vortex lines. These quantized vortex lines closely mimic the solid body rotation of the rotating helium above the lambda point.

Once vortices enter the system they are very strongly pinned to the powder. This leads to strong hysterectic behavior. This was seen in section IV.E when omega cee one was exceeded. In this section the complete hysteresis curve will be presented and explained.

To study these phenomena and generate a plot of the frequency splitting versus rotation, the cell is prepared as per section IV.A. The first group of experiments are started at rest, as described in section IV.E. The acoustic spectrum is first recorded with the cell at rest. Then, as in the studies of the Landau region, the probe is slowly rotated and the spectrum is again recorded. The speed of the probe is gradually increased in stages and the splitting recorded at each point as a function of the speed of rotation. The speed is usually increased until no further splitting is observed or a little further. At the point at which the splitting first reaches its maximum value the persistent current is said to be saturated. The speed of rotation at which this occurs is called omega sigma. The probe is then slowed in stages and the splitting again

recorded at each point. The probe is finally brought to rest and there is finite splitting.

The polarity of the motor is now reversed and the probe is brought into rotation in the opposite direction. The splitting is again recorded as a function of the speed of rotation. Maximum splitting is again reached and the probe is slowed and brought to rest while taking data. Once again there is a finite persistent current at zero rotation and it is easily seen that the curve is highly hysteretic.

The experimental curves obtained in this way (started at rest $\omega_i = 0$) are shown in figures IV.F.1 through IV.F.5. They show the frequency splitting divided by mode number plotted against the speed of rotation Wn (radians per second). These five figures are all about 1.27 degrees Kelvin and are shown in decreasing order by filling fraction (0.800, 0.504, 0.335, 0.225, 0.145). It should be noted that the lower quality of IV.F.3, IV.F.4 and IV.F.5 were taken early in the research and both the technique and the temperature control were improved. The improvement can be seen in figure IV.F.1.

The superfluid velocity Ws can be found from the frequency splitting divided by mode number as shown in equation IV.F.1.

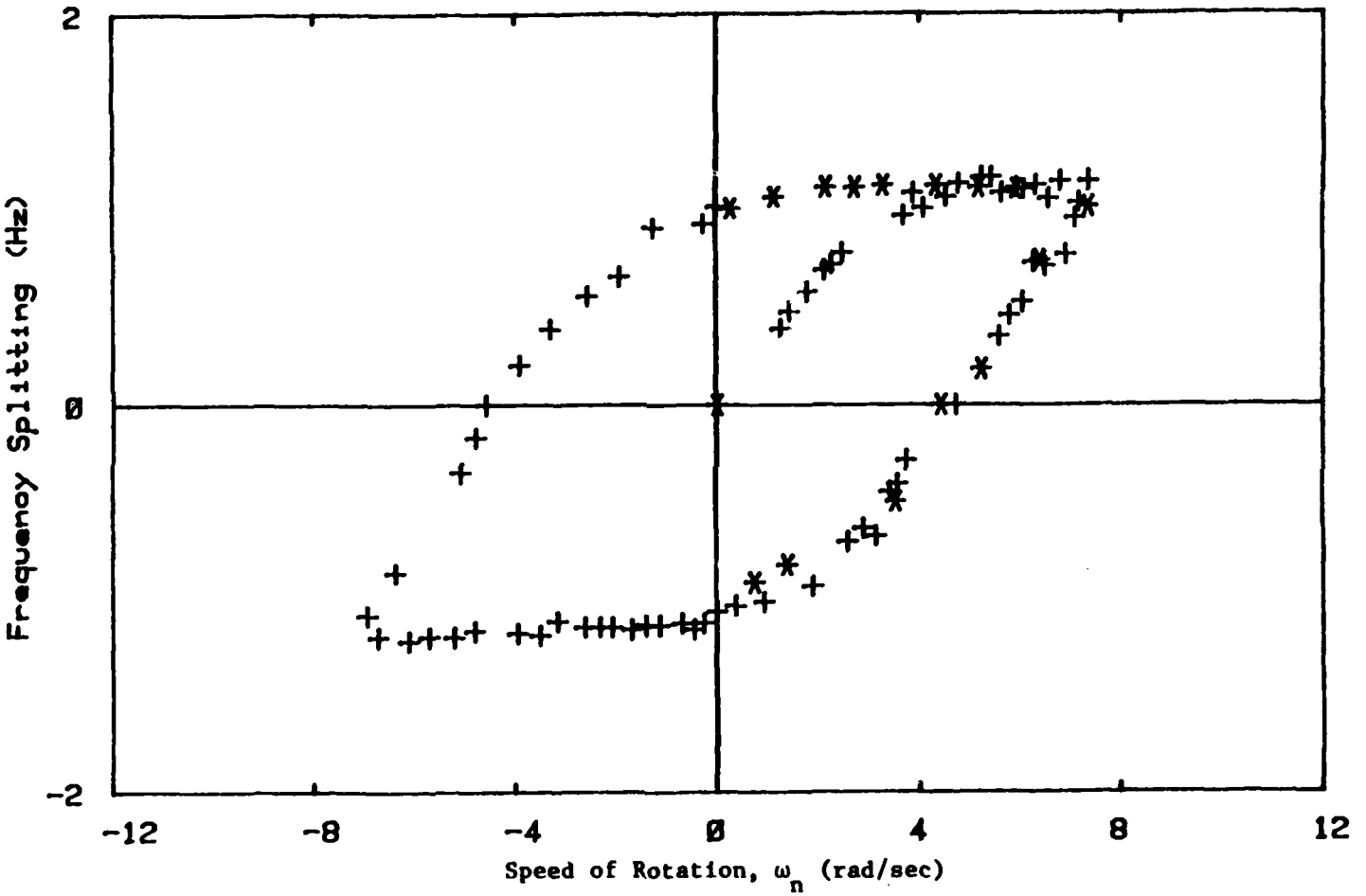

Figure IV.F.1 Hysteresis Curve ω_i = 0, T = 1.29°K, f = 0.800

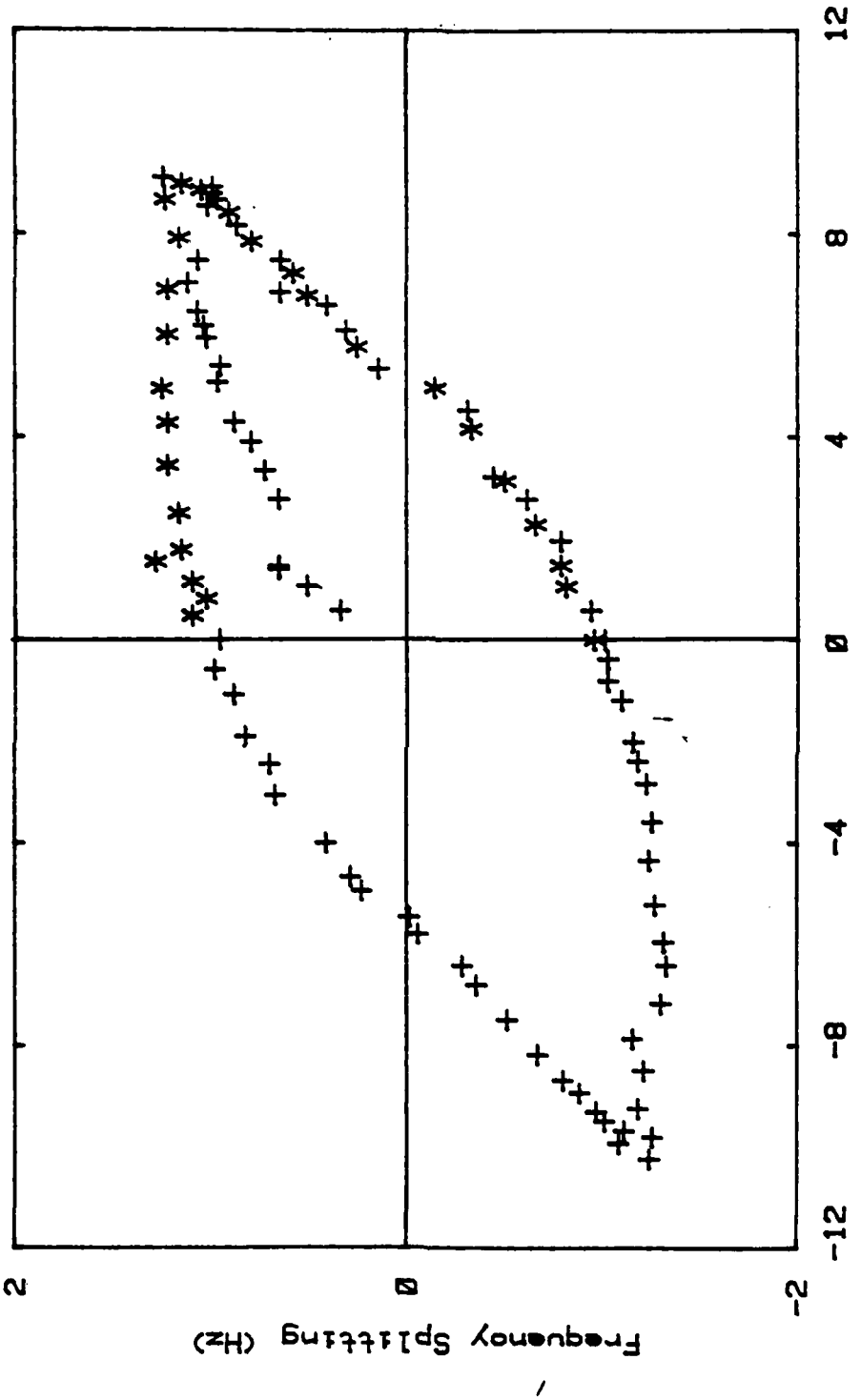

Figure IV.F.2 Hysteresis Curve $\omega_1 = 0$, T = 1.27°K, f = 0.504

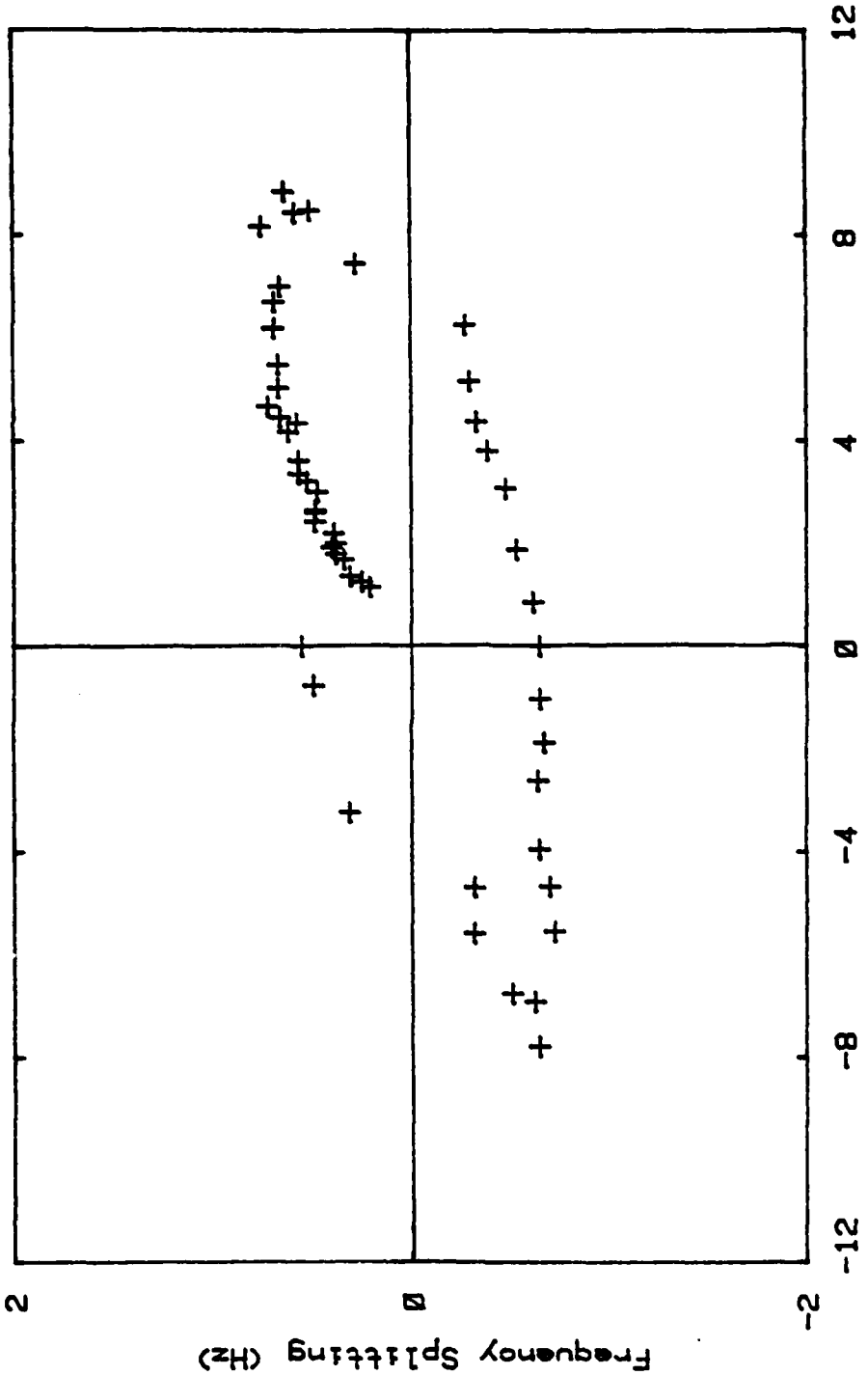

Figure IV.F.3 Hysteresis Curve $\omega_1 = 0$, T = 1.27°K, f = 0.335

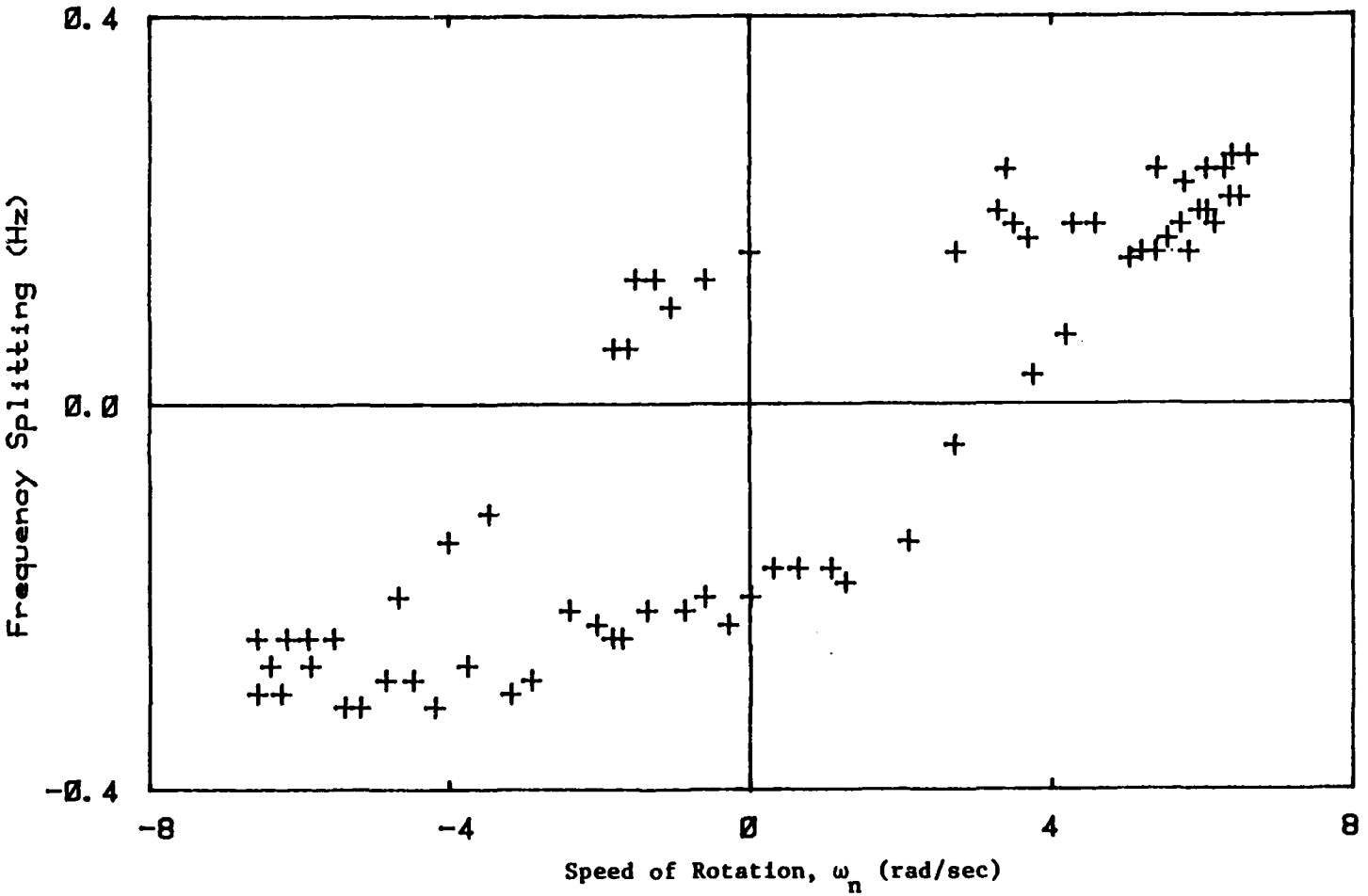

Figure IV.F.4 Hysteresis Curve ω_i = 0, T = 1.29°K, f = 0.225

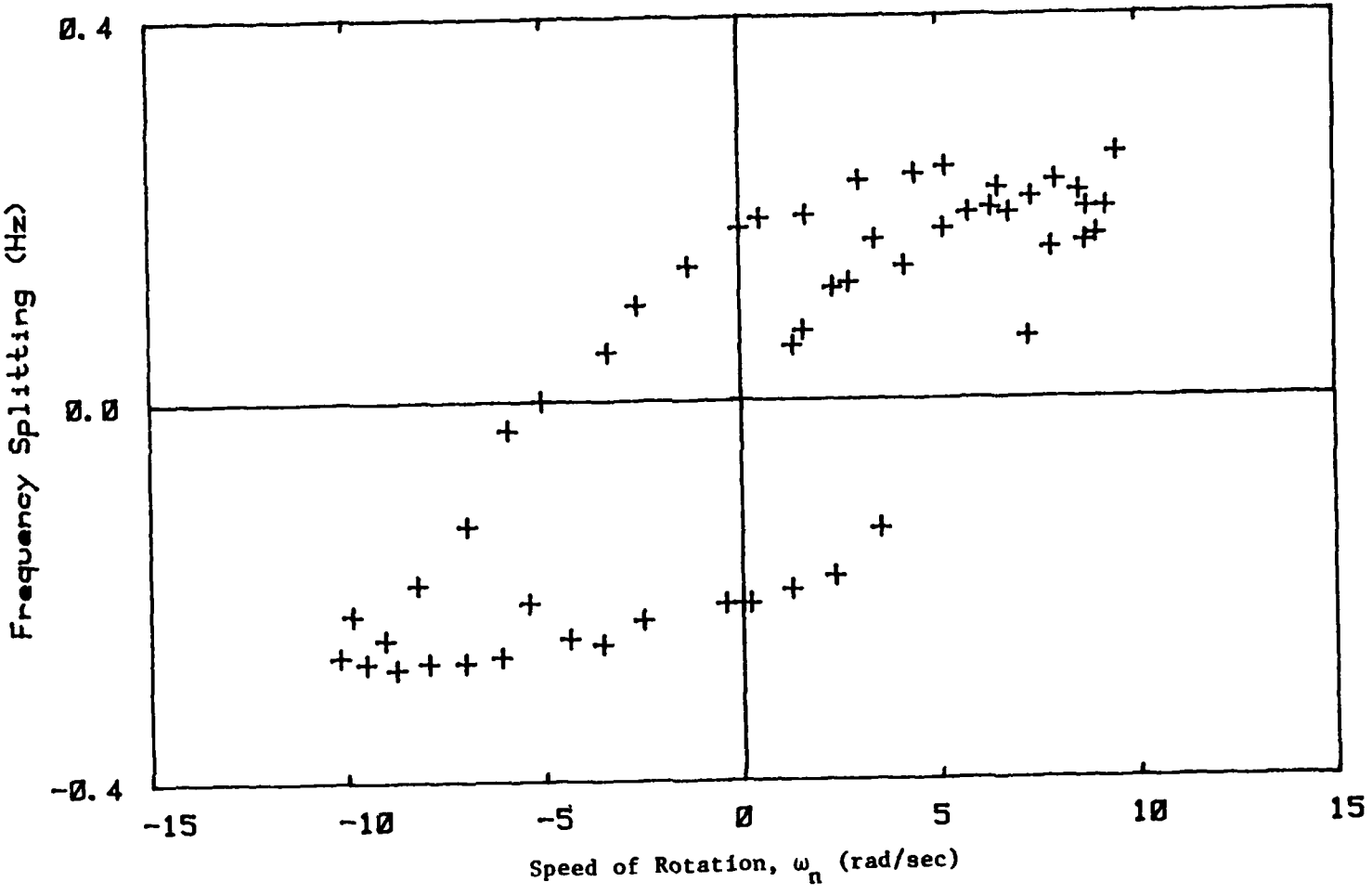

Figure IV.F.5 Hysteresis Curve $\omega_i = 0$, T = 1.28°K, f = 0.145

$$\omega_s - \omega_n = \pi\left(\frac{\Delta f}{m}\right) \qquad \{IV.F.1\}$$

The hysteresis curves which start with the helium at rest are understood as follows and may be followed by looking at figure IV.F.7 in which an idealized hysteresis curve is drawn and labled with letters. The cell and the helium start at rest (A). The cell is then brought into rotation. The normalfluid component is brought into rotation with the superleak to which it is viscously locked. The superfluid component is brought into motion by the Kelvin drag of the superleak on the helium. The beginning of each hysteresis curve is straight. This is the Landau region (A to B) which was discussed in section IV.E. The end of the Landau region occurs at a rotation speed of omega cee one. Above this speed vortices enter the system (B to C). A sharp transition from the Landau region into the region where vortices are present is observed. This was illustrated in figure IV.E.5 where the difference from the extended Landau region is shown plotted against speed of rotation.

As the speed of rotation is increased further the maximum value of Vn-Vs is soon reached (C). This point is called omega sigma. Rotation speeds faster than this

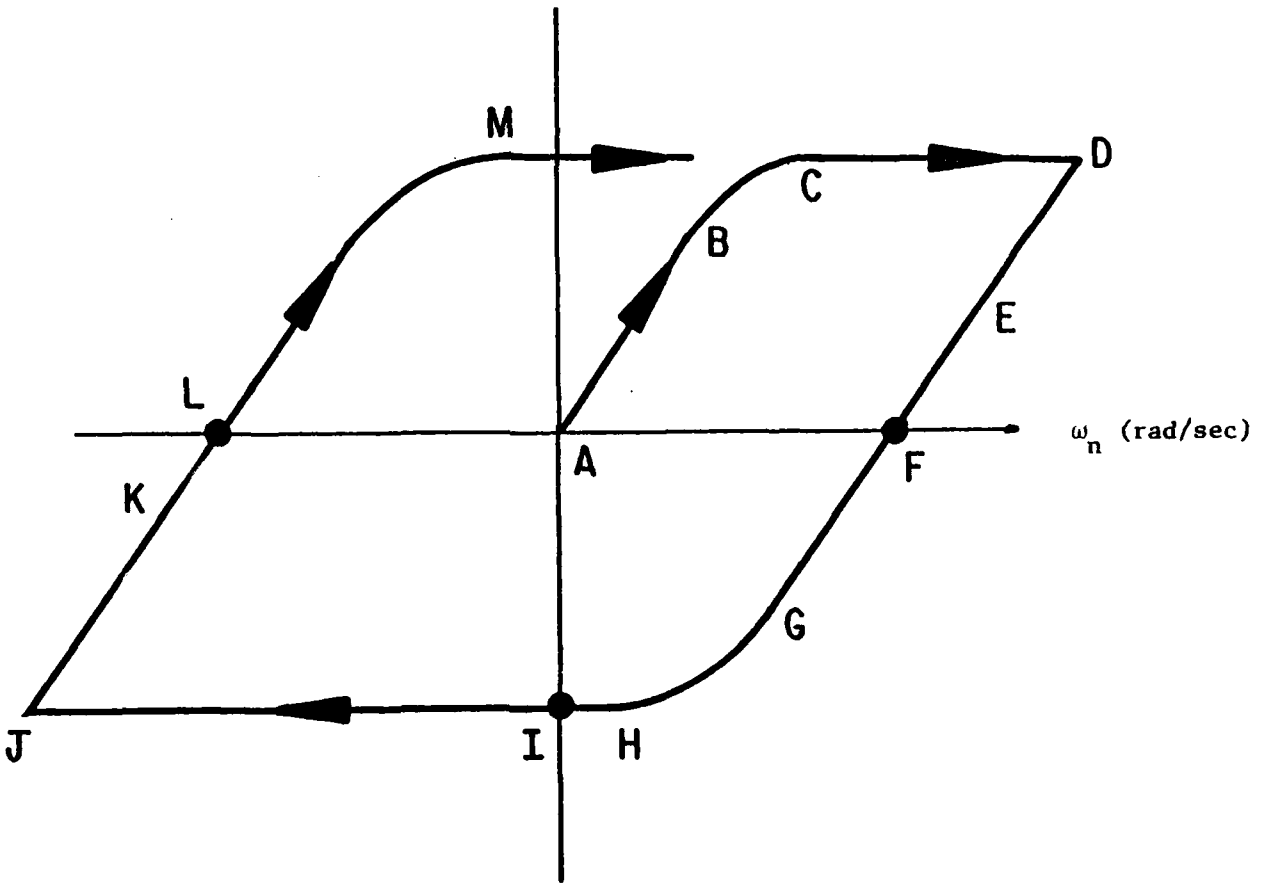

Figure IV.F.7 Idealized Hysteresis Curve

do not produce any further increase in the value of Vn-Vs. The speed of rotation is usually increased a little further to establish a straight line for the maximum value of Vn-Vs (D). The cell is now slowed a little (E). The Kelvin drag now removes the initial potential flow and creates it in the opposite sense. The slope in this region is the same as in the Landau region which confirms this interpretation. The persistent current velocity again decreases until it is zero (F). At this point the sum of the potential flow and both the clockwise and counterclockwise vortices sum to a total net flow of zero. As the speed of rotation is slowed further vortices and potential flow of the opposite sense are created (G) and the difference of Vn-Vs is increased further until it again saturates (H). When the cell comes to rest there is still a persistent current flowing inside (I).

The direction of rotation is reversed. The maximum value of the velocity difference increases further and then finally remains unchanged and the saturated constant value is further mapped out (J). The probe is then slowed and the velocity difference decreases with the slope of the Landau region (K). The persistent current velocity again decreases until it is zero (L). At this point the sum of the potential flow and both the clockwise and counterclockwise quantized vortices sum to

a total net flow of zero. The splitting increases as the saturated value of Vn-Vs is reached (M). The whole cycle may now be repeated with the exception of the original tracing out of the Landau region. This is because the quantized vortices introduced into the system are firmly pinned in the superleak. See section IV.G for the details of their decay.

The second method to introduce quantized vortices into the system is to rotate the cell above the lambda point and cool down while rotating, as described in section IV.A. As described earlier when the temperature drops below the lambda point the solid body rotation of the superfluid component of the helium is replaced by quantized vortices. The value of Vn-Vs is still zero as the vortex flow mimics solid body rotation and has the same velocity as the normalfluid component.

The experimental data is taken in the same manner as the previous case. The only difference is the cell has an initial rotational velocity Wi different from zero and contains many vortices which mimic solid body rotation. The speed of rotation is now changed and the new speed of rotation and frequency splitting are recorded. The rotational speed is either increased or decreased. If it is first decreased then the probe comes to rest and the direction of rotation reversed.

It is then sped up until the velocity difference Vn-Vs saturates. Usually the speed is increased further to give a good indication of the maximum persistent velocity. The cell is then slowed and brought to rest.

The results from this type of investigation are shown in figures IV.F.8 to IV.F.11 (ω_i different than 0). In these plots the frequency splitting divided by mode number is plotted against the speed of rotation in radians per second. In this series of graphs the speed is given as $\omega i-\omega n$ which is the difference in the speed of rotation ωn and the initial speed of rotation ω_i. This transformation makes them isomorphic to the curves (IV.F.1 thru IV.F.5) for which the cell started at rest and the splitting is plotted against ωn. Each graph is labeled with its temperature, filling fraction and its initial speed of roation ωi.

The explanation of these curves is then similar to the curves for which $\omega i = 0$. For the case in which the cell is slowed from ωi the description is as follows. When $\omega = \omega_i$, immediately after the dewar has been cooled to the operating temperature, the superleak contains enough vortices to mimic the solid body rotation of the helium above the lambda point. When the speed ωn is reduced, the powder grains exert Kelvin drag on the superfluid and impart some velocity to it. The

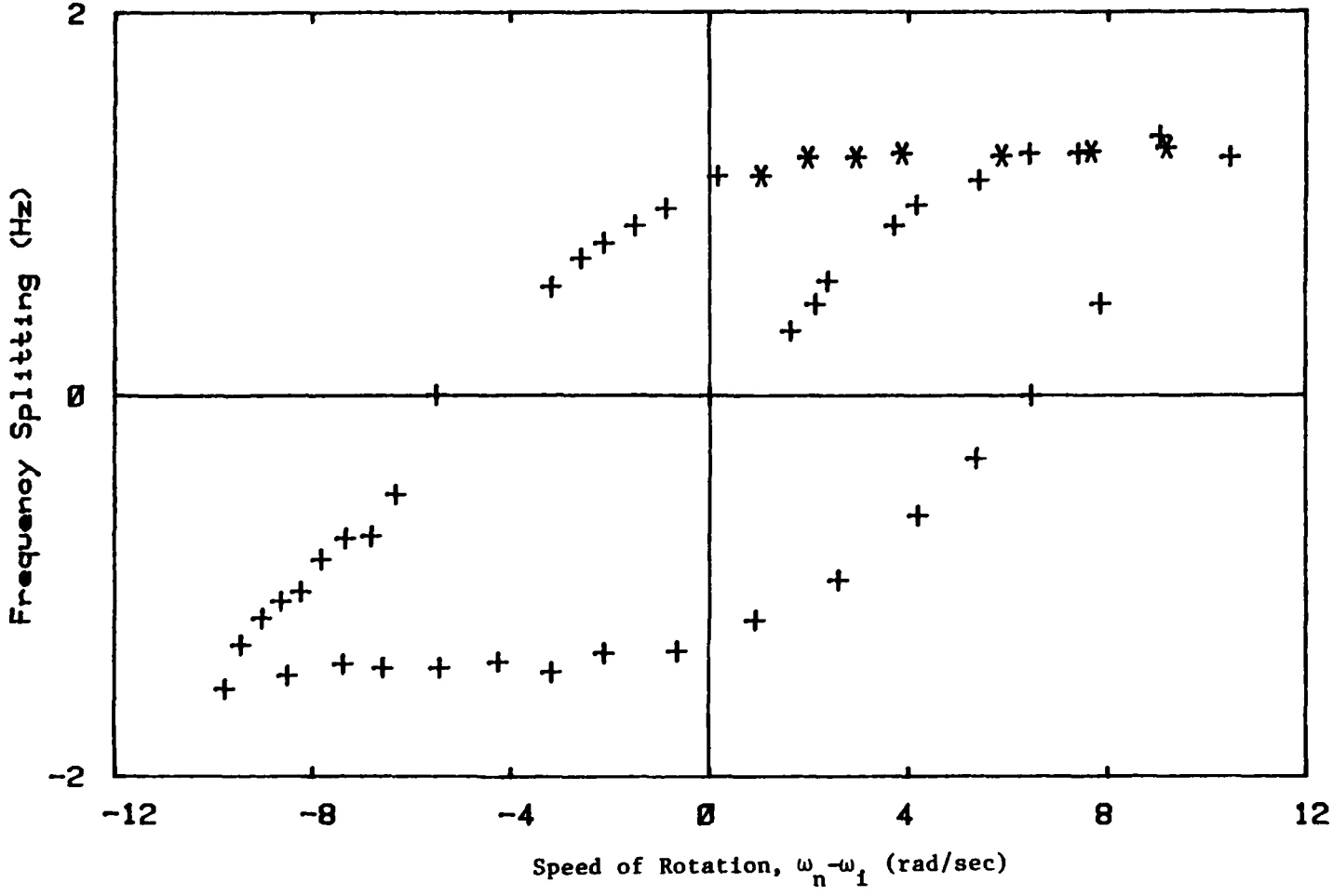

Figure IV.F.8 Hysteresis Curve, ω_i = 3.179, T = 1.37°K, f = 0.599

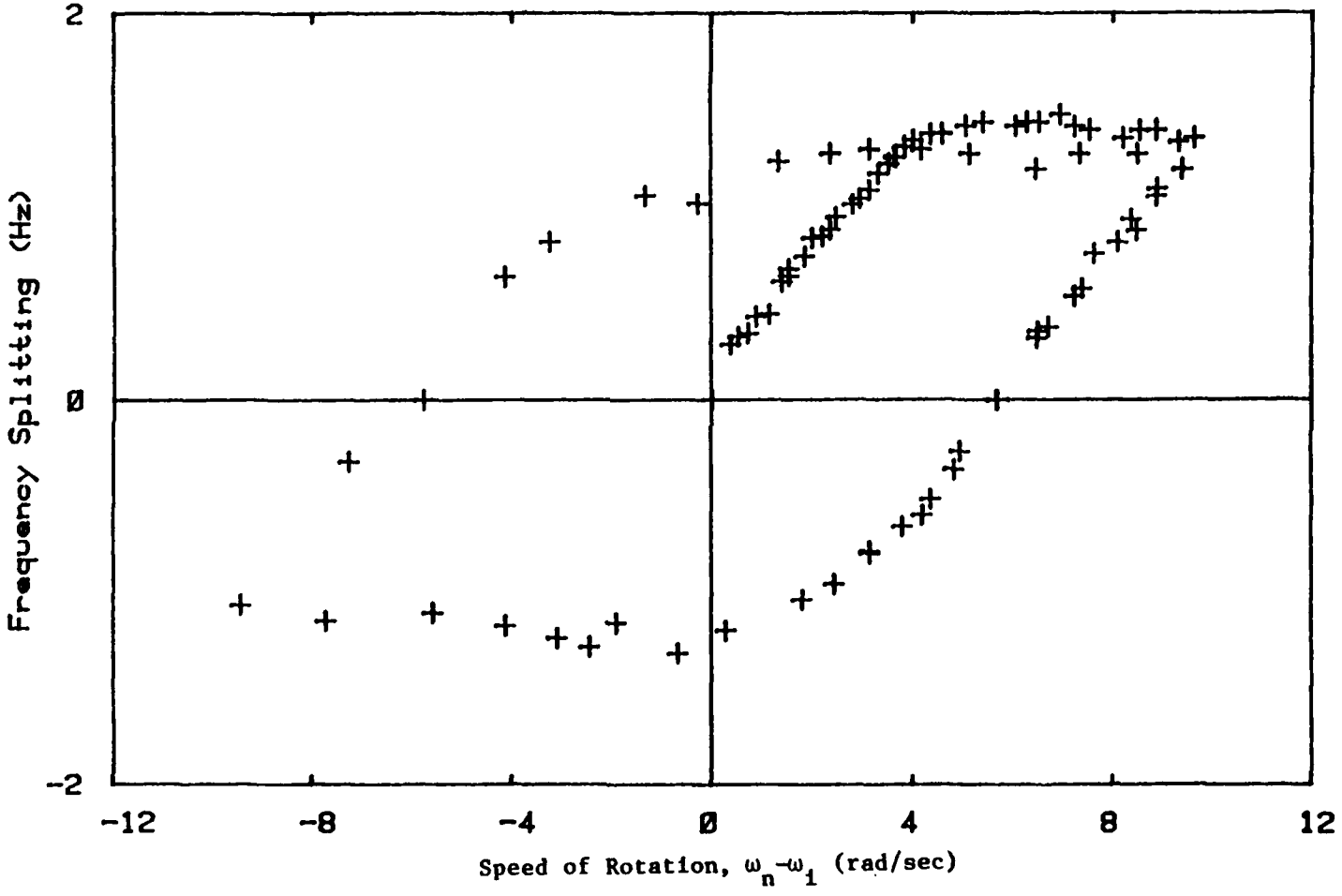

Figure IV.F.9 Hysteresis Curve, ω_i = 3.142, T = 1.28°K, f = 0.703

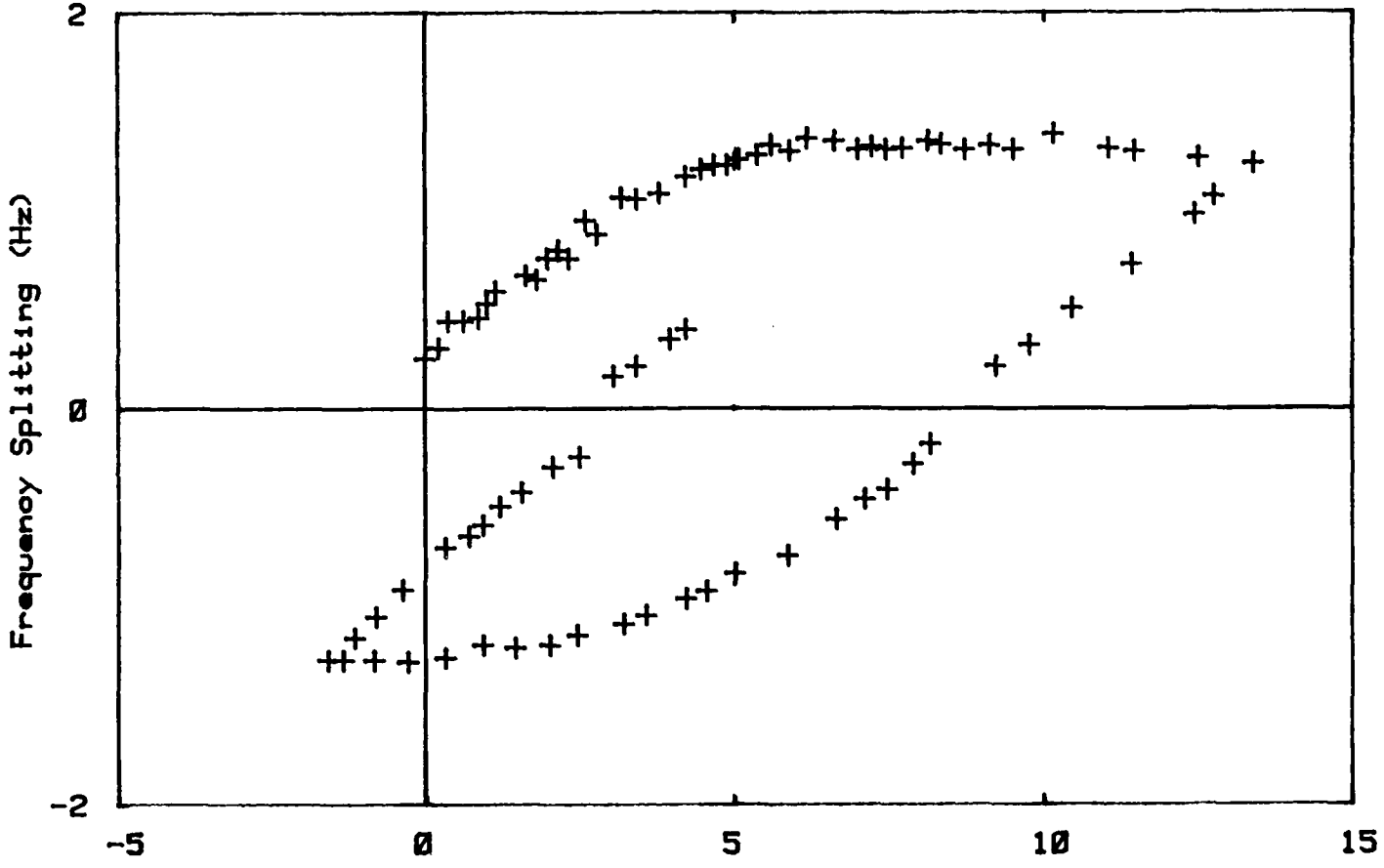

Figure IV.F.10 Hysteresis Curve ω_i = 3.142, $^1T = ^n$1.29K, f= 0.500

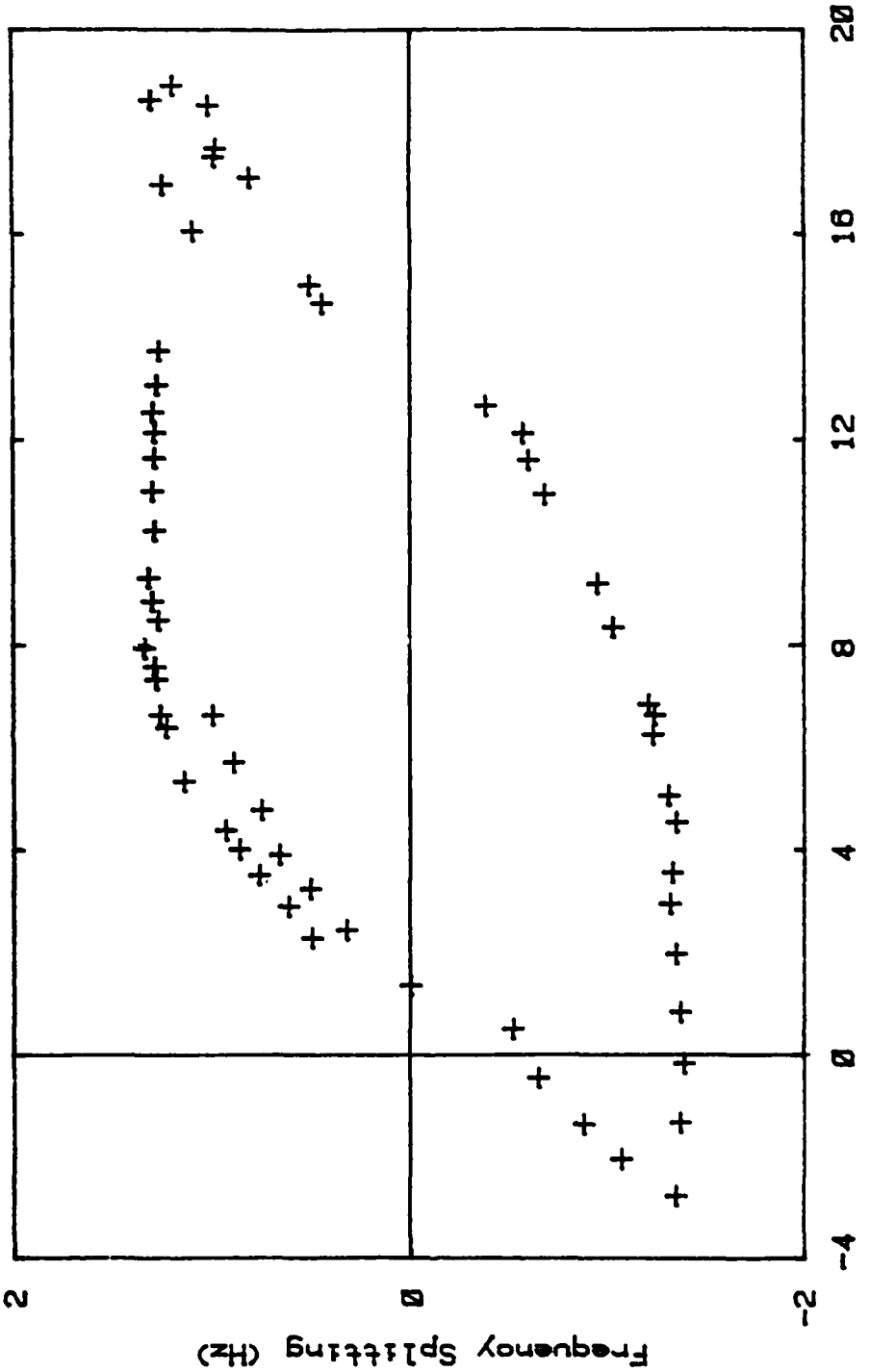

Figure IV.F.11 Hysteresis Curve ω_1 = 6.660, T = 1.35°K, f = 0.499

remaining difference $\omega n - \omega s$ is the persistent current velocity. This change is made with the same slope as the Landau region. As the speed is further reduced the saturated value of $\omega n - \omega s$ is achieved. This is true if $\omega i - \omega n$ is greater than omega sigma (omega sigma is defined to be the maximum value of $\omega n - \omega s$). When the probe comes to rest the value of $\omega n - \omega s$ is non zero. The direction of rotation is reversed and again the potential flow is removed by the Kelvin drag and introduced in the opposite sense.

The explanation of the curves produced when the inital speed of rotation is non zero is almost the same as the above case where $\omega i = 0$. The difference is that there are always vortices present and hence there is no true Landau region. However, the slope of the region where potential flow is introduced is the same independent of the number of vortices present. The value of omega sigma is also unchanged by the number of vortices present. This is dramaticaly illustrated in figure IV.F.13, which shows the results of five runs for values of ωi from 0.0 to 0.75. It also includes one set of points ($\omega i = 0.231$ rev/sec) for which the speed was initialy increased from i and was plotted as $\omega n - \omega i$ on the same axis.

Careful examination of the data shows that the line

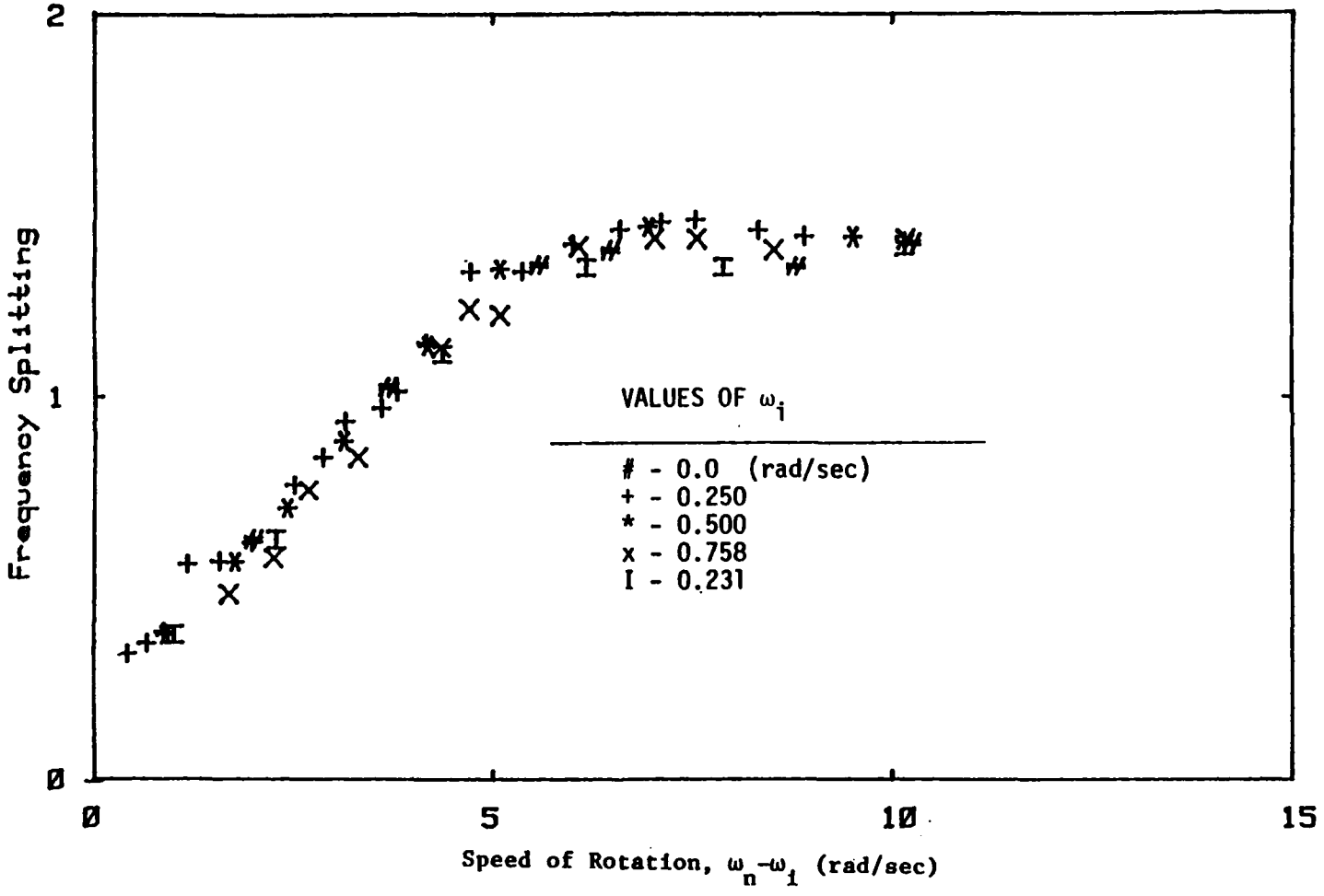

Figure IV.F.13 Universal Plot of Landau Region

formed by the points taken in the Landau region do not go through the orgin. This could be caused by several effects. The first attempt to explain this was to consider the case where there is a small persistent current present when the cell is first rotated. This would seem reasonable as this had often been seen in previous persistent current experiments (Kojima). This was ruled out as the offset is always positive and the probe may first be rotated either clockwise or counterclockwise. This would give offsets negative as well as positive.

The next explanation seems to fit the data well. It has been known for some time (Rudnick) that a slight geometeric irregularity (a point where sound reflection can occur) which couples the clockwise and counterclockwise sound waves lifts the degeneracy in an annular resonator. It causes the degenerate resonance frequencies to be split. If there were any irregularity in the superleak, such as, a slight porosity gradient, then such a splitting could occur. Assuming this to be the case and that the amount of geometric splitting is too small to be observed directly the following calculation may be made. Equation IV.F.2 describes the addition of geometric splitting and doppler shift splitting.

$$(\Delta f_{total})^2 = (\Delta f_{doppler\ shift})^2 + (\Delta f_{geometric})^2 \quad \{IV.F.2\}$$

The magnitude of the geometric splitting is chosen to put the origin of the Landau region at the origin of the graph.

It is found that a geometric splitting of 0.2 gives the best fit overall. From equation IV.F.2 it is clear that the offset will always be positive which agrees with our observations. The correction (0.2 = geometeric splitting) made to the data with equation IV.F.2 is just below the limit of direct observation. This corresponds to the observation that the peaks do not appear split until the cell is rotated and a persistent current is introduced.

Several sets of data were treated in this manner. The resulting curves are shown along with the original data in figures IV.F.14 through IV.F.16. The graphs show the frequency splitting divided by mode number plotted against the speed of rotation ($\omega i - \omega n$). The points are the original data while the solid line is the result of the correction from equation IV.F.2 to the data and a smooth line drawn through the resulting points for the Landau region. They to give results which are in very good agreement with the experimental

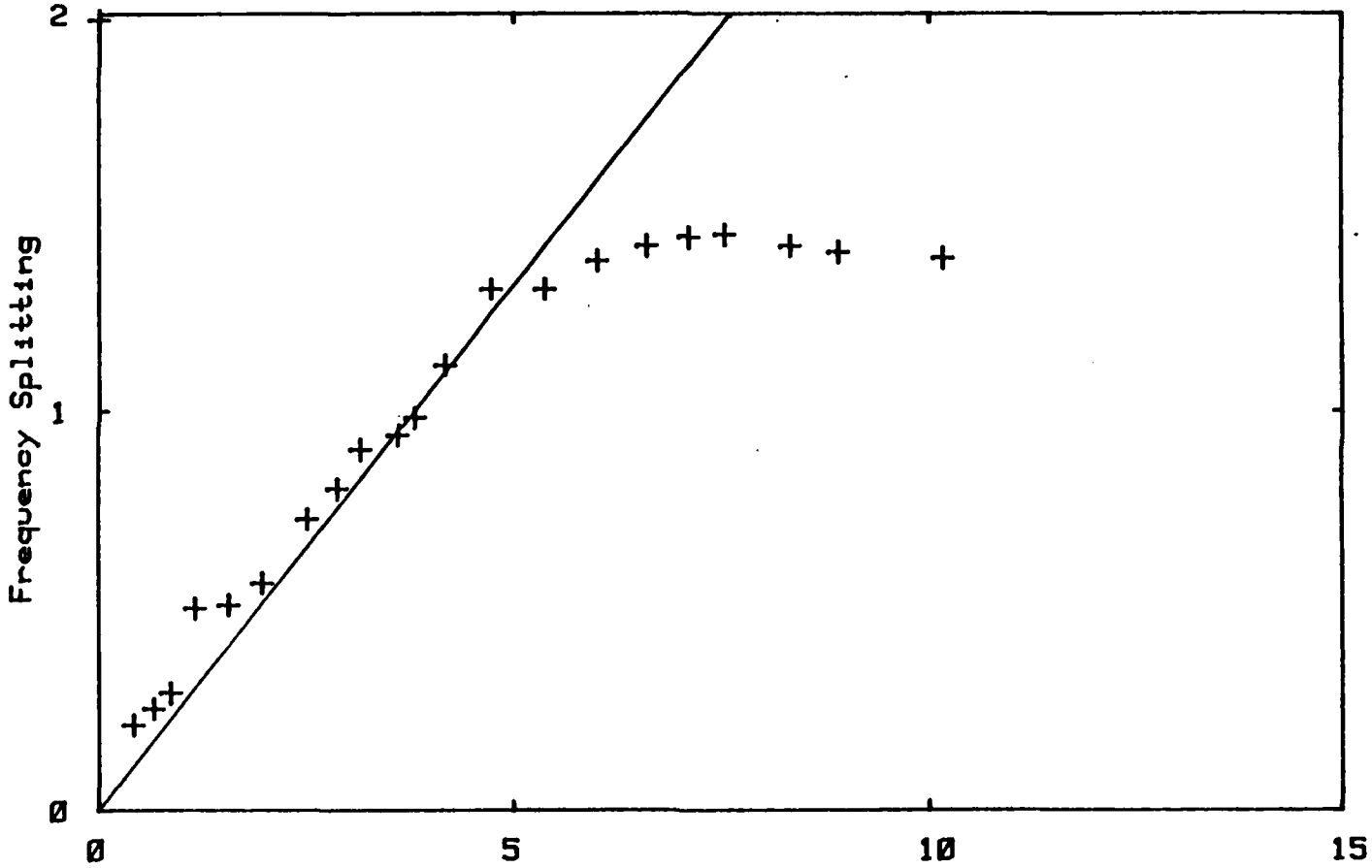

Figure IV.F.14 Landau Region Showing Fit of Equation IV.F.2
T = 1.29°K, f = 0.500, ω_1 = 1.57

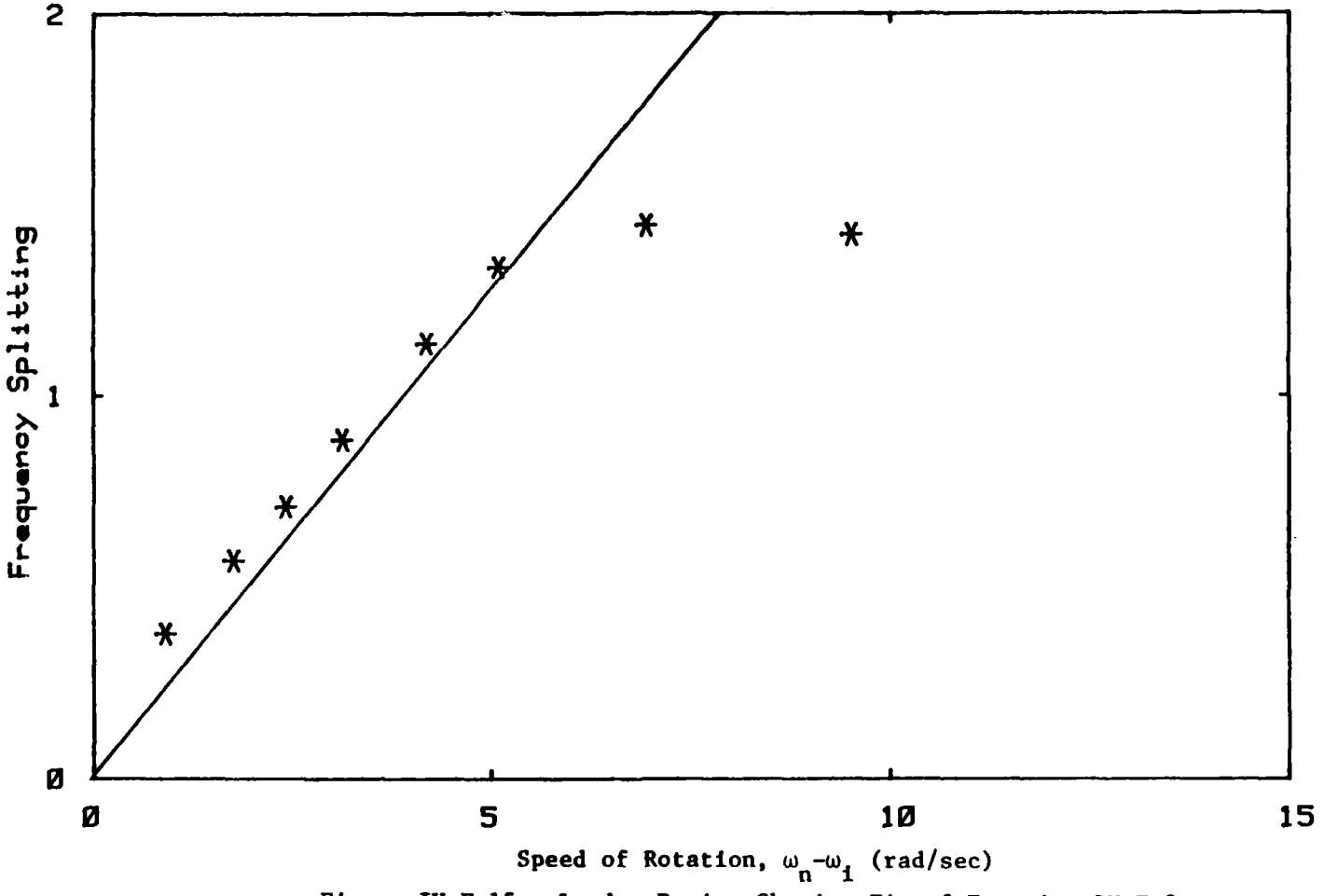

Figure IV.F.15 Landau Region Showing Fit of Equation IV.F.2
T = 1.29°K, f = 0.500, ω_i = 3.142

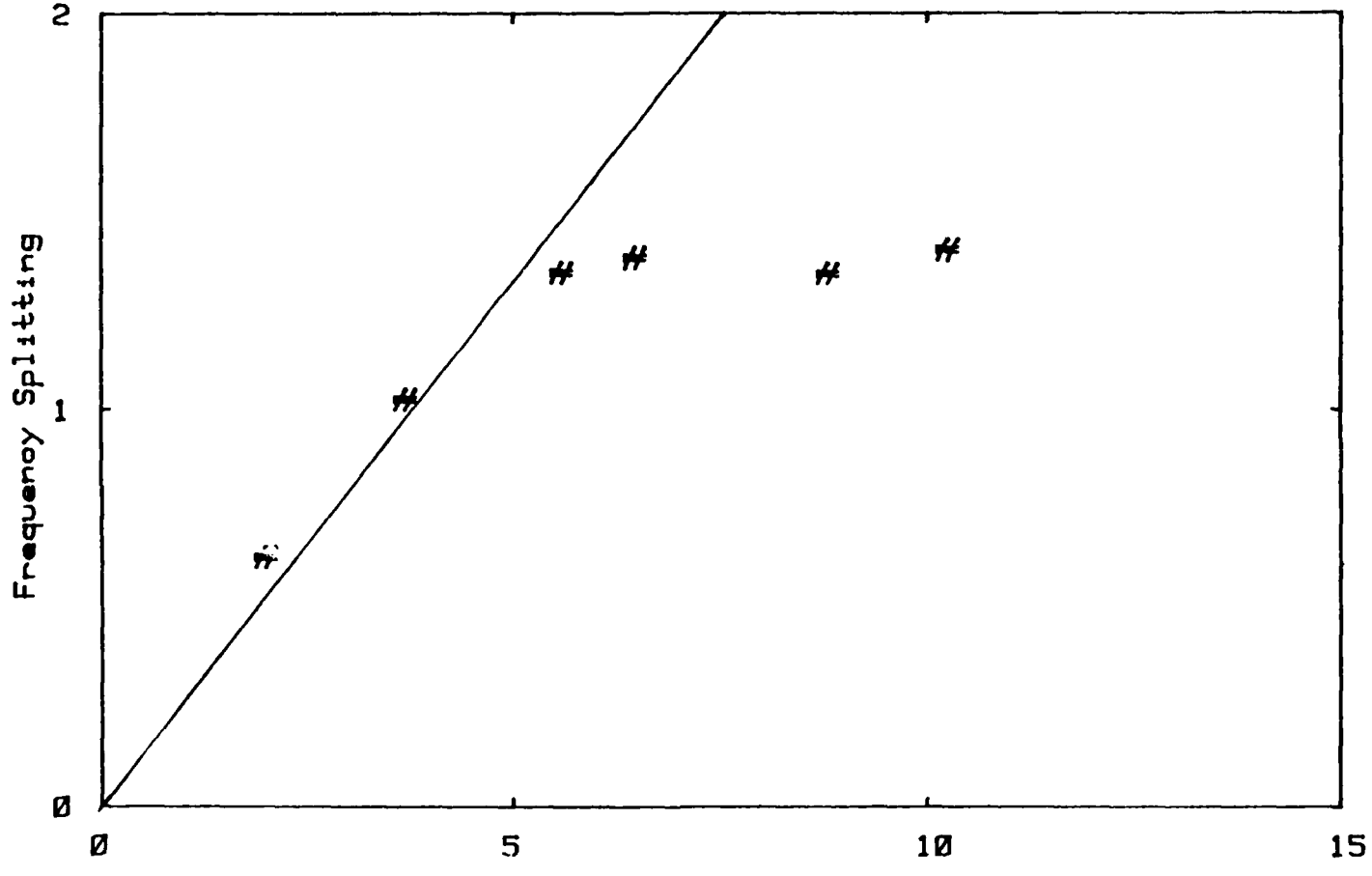

Figure IV.F.16 Landau Region Showing Fit of Equation IV.F.2
T = 1.29°K, f = 0.500, $\omega_i = 0$

observations. We conclude that this is the correct interpreatation.

There are two superfluid systems which we know about. The first is helium II and the second is superconducting electrons present in a superconductor. There are very strong similarities between the two systems. They both can be described by two fluid equations due to a normal and super component. In the case of superfluid helium the two components are the normalfluid and the superfluid which is thought to be a Bose fluid. In the superconductor there are the normal conducting electrons and the super-conducting electrons which form a Bose system as Cooper pairs. The general similarities have been known for some time. In 1950 and 1954 Fritz London wrote his two volume series titled 'Superfluids'. The first volume is 'The Macroscopic Theory of Superconductivity' and the second volume is 'The Macroscopic Thecry of Superfluid Helium'. He points out that the many strange properties common to both systems are due to quantum mechanics acting in the macroscopic regime.

There are several general comparisons which can be made between superfluid helium and superconductors. The first and most obvious comparsion is that a superfluid can flow with immeasurably small pressure gradients

(zero viscosity) while a supercurrent can flow in a superconductor with immeasurably small voltage differences (zero electrical resistance). Both systems have regions which exhibit curl free 'flow'. In superfluid helium there is the Landau state (see section IV.E) where the superfluid momentum is curl free (Landau restriction) and only potential flow exists. In a superconductor there is the Meissner state in which the supercurrent momentum is curl free (London restriction). In this state flux lines are excluded and only potential flow exists on the conductor's surface. Both systems exhibit quantized lines. In helium there are quantized vortex lines and in superconductors there are quantized flux lines. In each case the momentum is quantized by the Bohr-Sommerfeld quantization condition. Also in both cases the cores are considered to be made of the normal component of the system.

Kojima extends this general analogy to a much more specific comparison (Kojima). He compares the superfluid helium filled superleak with that of lead filled porous Vycor glass (Bean). This type of superconducting system is known as a high field type-II superconductor. The same comparison can be made to the partially filled superleak. Figure IV.F.17 shows a typical hysteresis curve from a helium filled superleak and a magnetic hysteresis curve from the lead filled

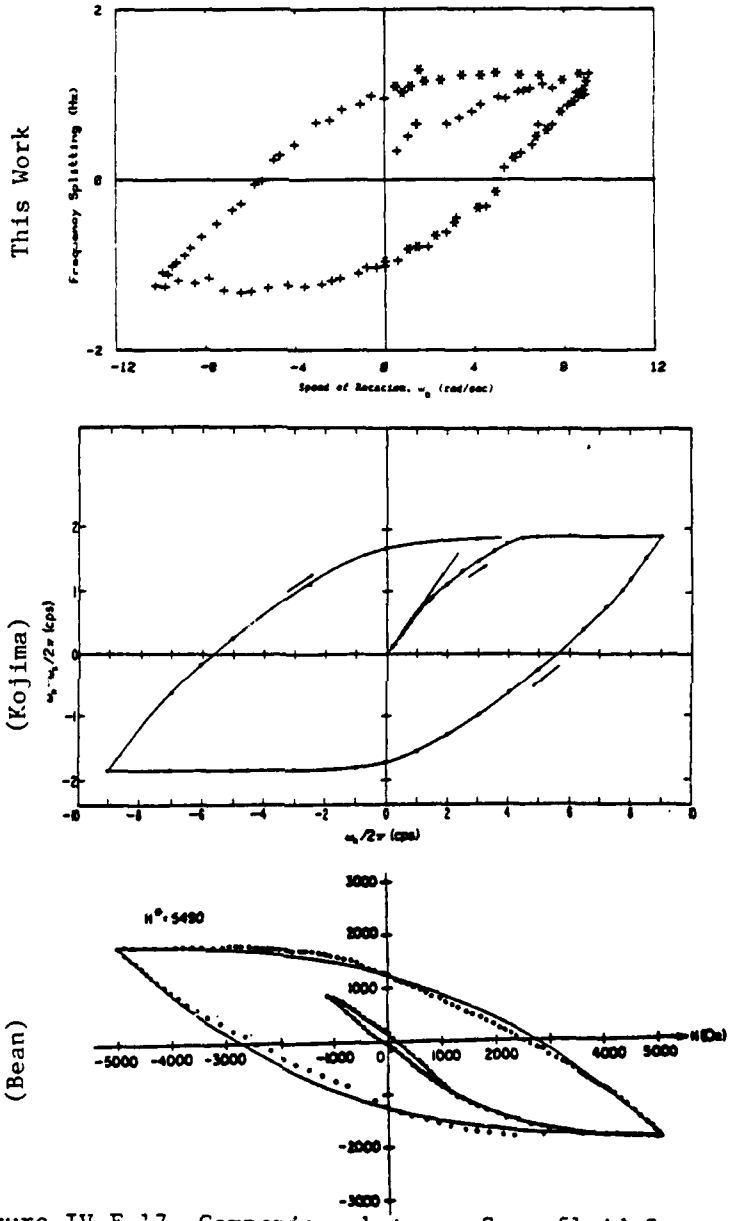

Figure IV.F.17 Comparison between Superfluid Systems and Highly Irreversible High Field Type-II Superconductors

Vycor (Bean). These two curves should be compared with figures IV.F.1 through IV.F.5 in the present work. The resembalance is certainly striking. The comparitive quantities are the frequency splitting ($\omega s - \omega n$) from the helium systems and the magnetization from the superconducting system. Also the speed of rotation (ωn) from the helium systems is directly analogous to the applied magnetic field in the superconducting system. This comparison again highlights the need to be able to make measurements of Ws-Wn while the system is rotating.

All three systems clearly show the curl free regions. In each case this is the only region which is strictly reversible. In all three systems this region ends at a critical number, ω_{c1} for the helium systems and H_{c1} for the superconducting system. Past this point quantized vortex lines enter the helium and quantized flux lines enter the superconductor. In both cases the quantized lines are pinned in their systems and give rise to the hysteresis.

Finally one more striking comparison should be made. As previously explained, if the superfluid system is cooled down below T-lambda while rotating at some initial velocity Wi the value of $\omega n - \omega s$ will remain zero as long as the value of ωi is unchanged. In an analogous manner the superconductor may be cooled below

its critical temperature with an applied magnetic field Ha. In this case the magnetization will remain zero as long as the field Ha remains fixed.

IV.G DECAY OF PERSISTENT CURRENTS

The decay of persistent currents have been studied in both superfluid and superconductor systems (Kojima, Kukich, Kim, Anderson). Kojima found that persistent currents in a helium II filled superleak are truly persistent and have projected lifetimes greater than the age of the universe (10 to the 17 sec). Kojima was able to measure the decay rate for both saturated and unsaturated persistent currents. He reported that the decay was logarithmic with time. A decay rate of 0.67% per decade was reported for the saturated currents while a rate as low as 0.2% was observed for unsaturated currents (87% of the saturated velocity). At the other extreme Hallock and co-workers (Hallock) have reported on decay rates for very thin film systems. They found decay rates which deviated strongly from the log t

behavior (for very large decay rates) seen in films (Telschow) and in filled superleaks (Kojima). The current work examines both saturated and unsaturated persistent currents in a superleak partialy filled with helium II. Results are reported for initial velocities from saturated (100%) to 77 percent of their saturated velocity.

After the filling fraction has been chosen and the correct amount of helium gas is transfered to the cell, the speed of rotation is set. The speed is chosen to give a saturated persistent current velocity or some percent of the saturated value. Since the current begins to decay a small amount once the probe is slowed it is necessary to use the following procedure to insure accurate results. The cell is then cooled to the operating temperature. The rotation of the probe may be slowed now, in order to make any final adjustments in the electronics, but not stopped. Once the final setting are made, the probe is rapidly (about 1 second) and smoothly brought to rest. Measurements are begun immediately and the first data point is usually within several seconds of the probe being brought to rest. The amount the probe may be slowed can easily be estimated from the hysteresis curves, it is just necessary that the increase in persistent current will easily cover any decay during the 60 seconds or so of adjustments.

Measurements are made as rapidly as possible in the begining of a run. As the run proceeds data points may be spaced further apart in time. Measurements were usually taken until the helium level dropped to the level of the regulating thermometer and it was no longer possible to regulate the temperature.

All experimental decay data was handled in the same manner. It was fit to equation IV.G.1 with a computerized least squares fit. The intercept A at one second and the decay coefficient B as well as their corresponding standard deviations were computed.

$$\frac{\Delta f}{m}(t) = A(1 - B \log t) \qquad \{IV.G.1\}$$

In figures IV.G.1 through IV.G.4 the data from a series of runs is shown. The frequency splitting divided by mode number is plotted against the log of the time in seconds. They are all for temperatures of 1.27 degrees Kelvin and a filling fraction of 0.60. The graphs are various intial velocities starting with IV.G.1 at 100 percent of the saturated value (Vs = 14.4 cm/sec). Figures IV.G.2 through IV.G.4 are for initial values of 88.6 percent, 84.5 percent and 76.9 percent respectively. All figures show the experimental points and a solid line which is the result of the least squares fit to the data. The results are summarized in the table shown in figure IV.G.5. The decay per decade

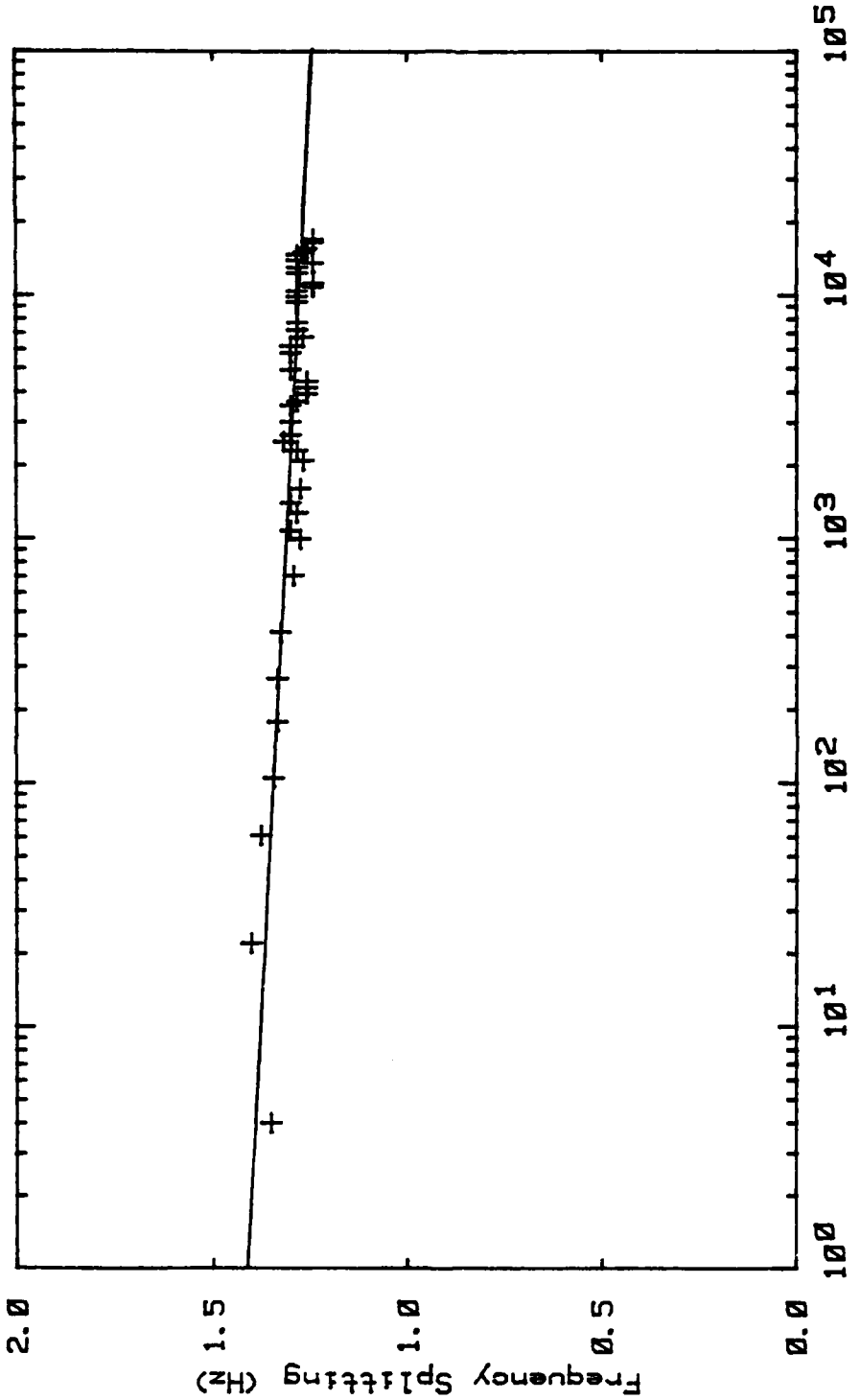

Figure IV.G.1 Decay, 100% of Saturated Velocity, T = 1.28°K, f = 0.600

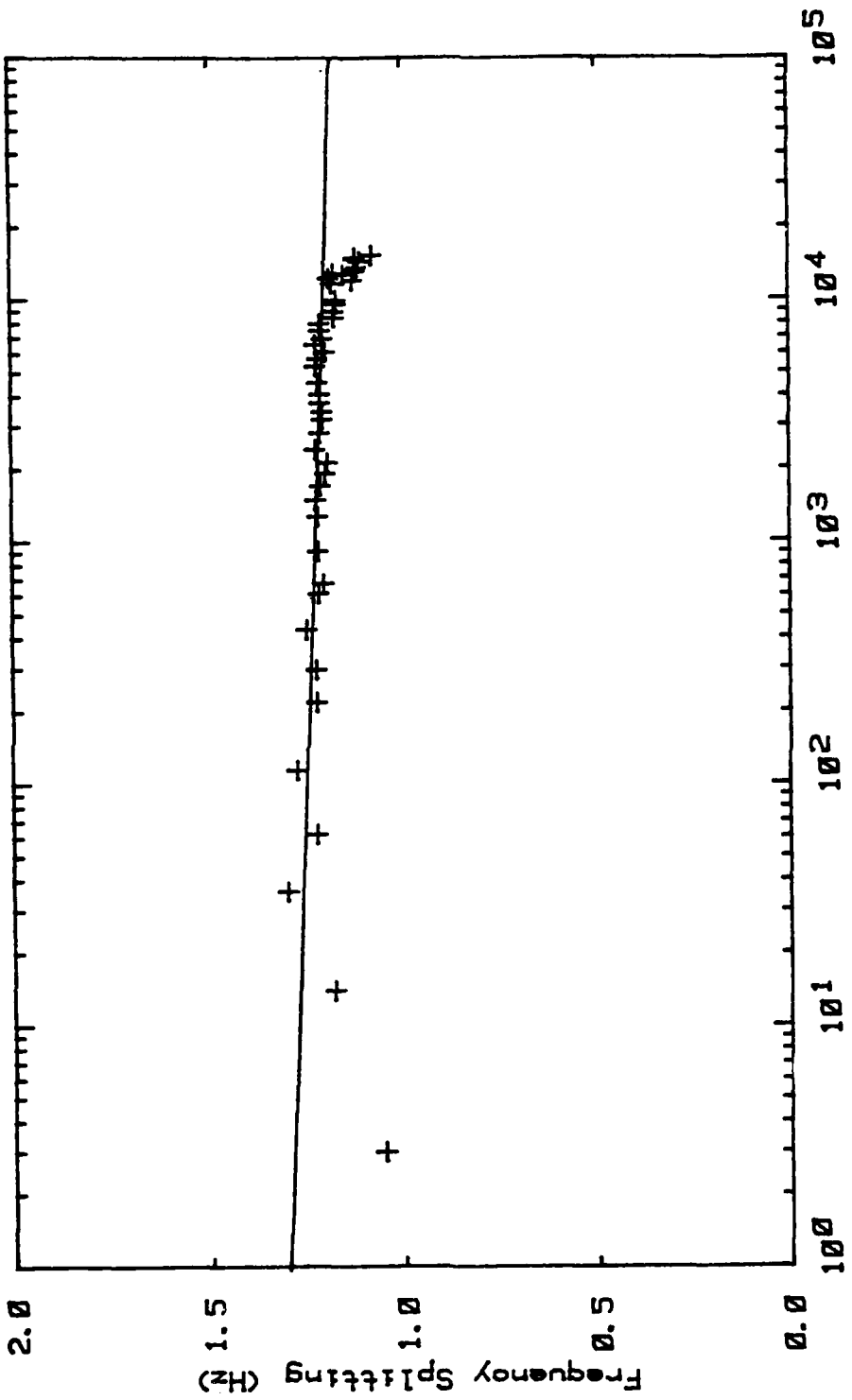

Figure IV.G.2 Decay, 88.6% of Saturated Velocity, T = 1.27°K, f = 0.600

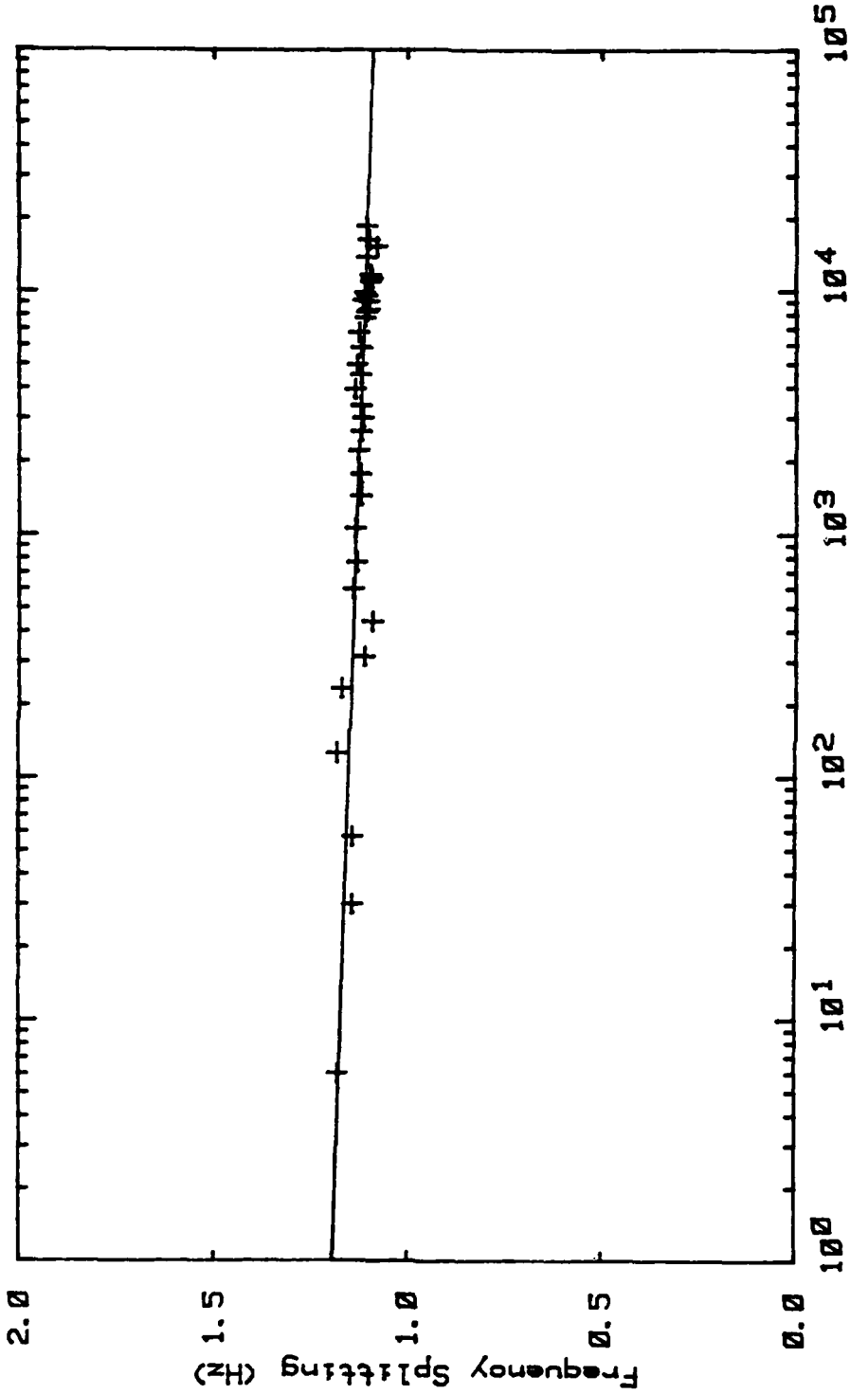

Figure IV.G.3 Decay, 84.5% of Saturated Velocity, T = 1.27°K, f = 0.600

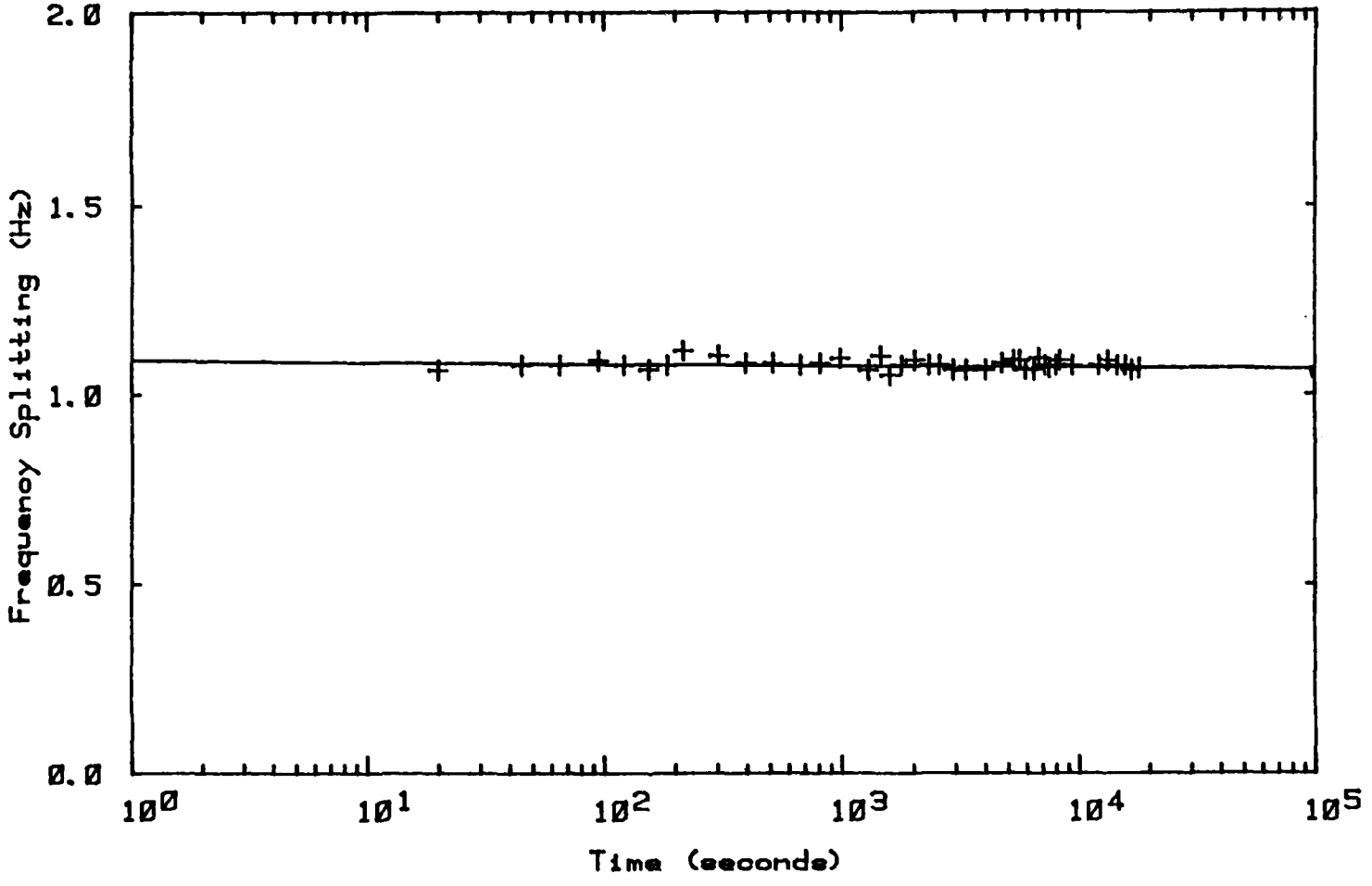

Figure IV.G.4 Decay, 76.9% of Saturated Velocity, T = 1.27°K, f = 0.600

TABLE IV.G.5

SUMMARY TABLE OF PERSISTENT CURRENT DECAY AS A FUNCTION OF INITIAL VELOCITY AS A PERCENTAGE OF ITS SATURATED VALUE FROM EQUATION IV.G.1
T = 1.27 degrees Kelvin and f = 0.600

INITIAL VELOCITY (cm/sec)		PERCENT DECAY PER DECADE	A	B
100%	14.38	2.47 ± 0.26 %	1.408 ± .013	0.0246 ± .0026
88.6%	13.3	1.90 ± 0.83 %	1.301 ± 0.029	0.0171 ± .0083
84.5%	12.2	1.76 ± 0.26%	1.189 ± 0.011	0.0176 ± .0026
76.9%	11.1	0.460 ± 0.23 %	1.083 ± .0084	.00163 ± .0023

of time is listed with its uncertainity. The value of the parameters A and B (from equation IV.G.1) are also shown with their uncertainity. The decay rate is highest for the persistent current which is initially saturated (maximum attainable velocity). The decay rate decreases as the initial velocity of the persisent current is reduced. The decay per decade is only 0.16 % for the persistent current with the lowest initial velocity (76.9 percent of saturation).

Figure IV.G.6 shows a comparision between our work and that of the helium filled superleak (Kojima). The plot shows the percent decay per decade of time plotted against the initial velocity as a percentage of the saturated value. The decay rates are greater in the partially filled superleak than the filled case. It will be seen however that as the filling fraction is increased the decay per decade tends toward the value from the filled superleak.

The next series of figures IV.G.7 through IV.G.10 again show the decay of the splitting plotted against the log of time. The series shows the decay rate as a function of the filling fraction at 1.27 degrees Kelvin and initial velocity is 100 percent of the saturated velocity. Figure IV.G.7 has a filling fraction of 0.798. The values of the filling fraction for figures

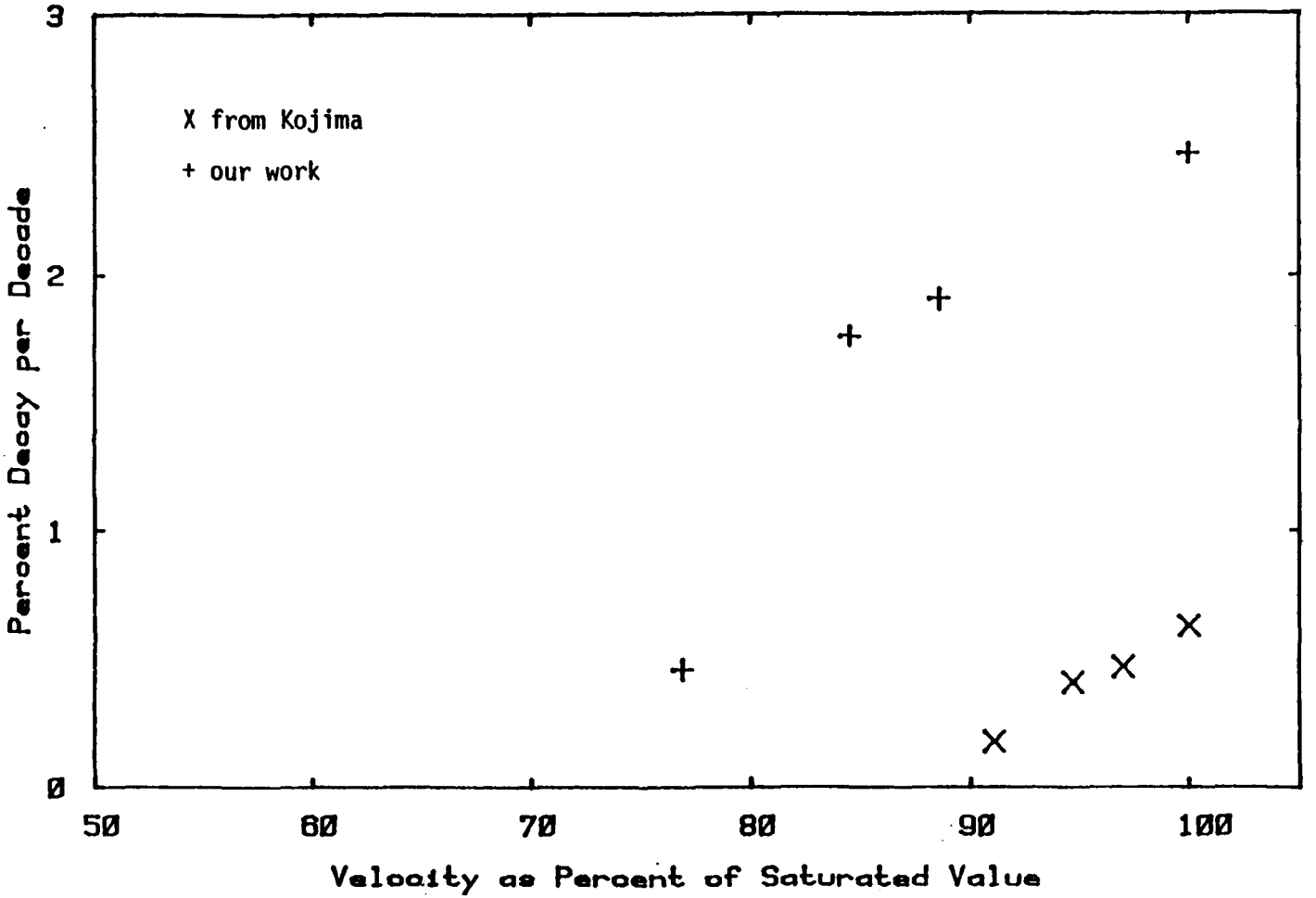

Figure IV.G.6 . Decay Comparison with Filled Cell (Kojima)

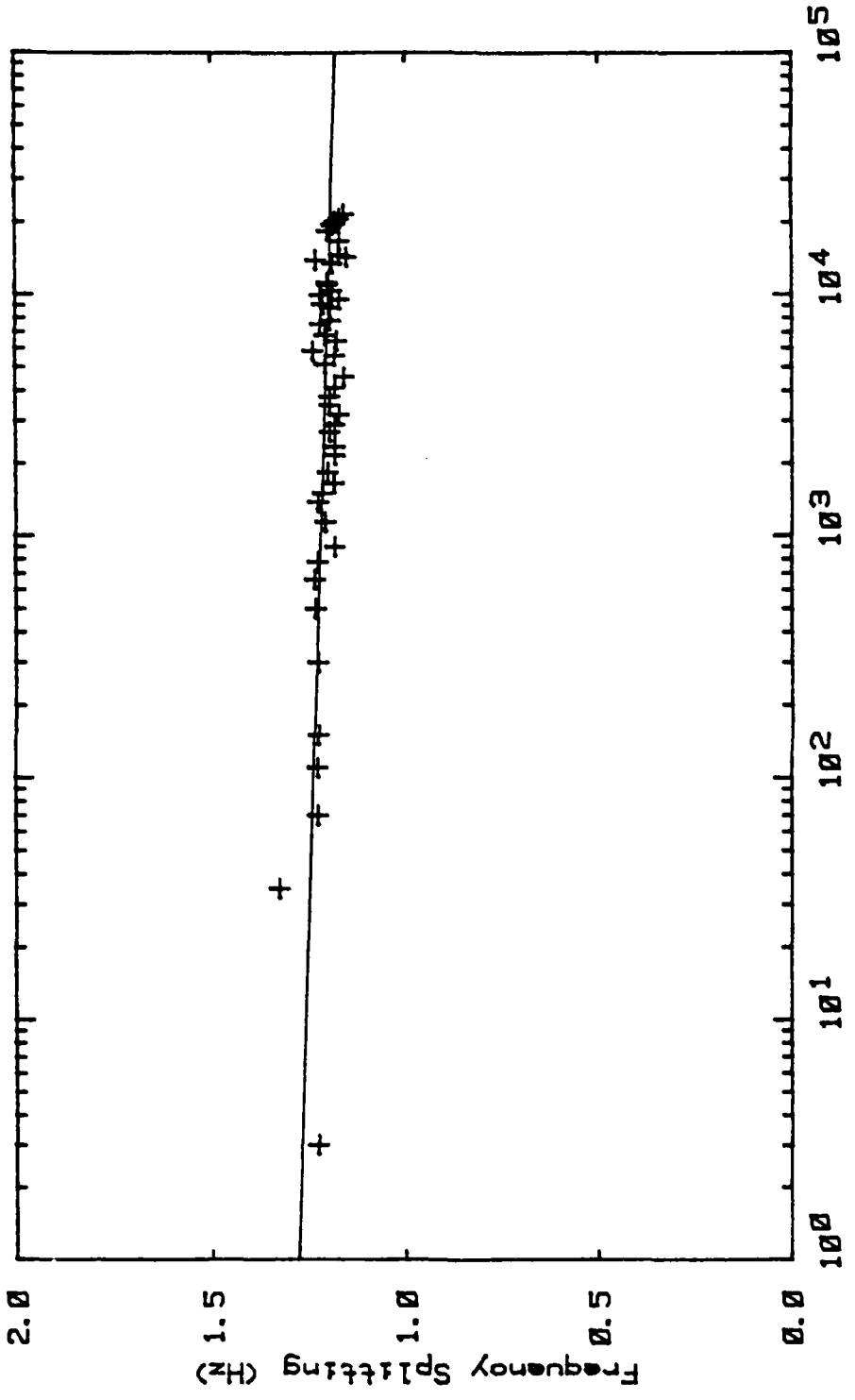

Figure IV.G.7 Decay, 100% of Saturated Velocity, T = 1.26°K, f = 0.798

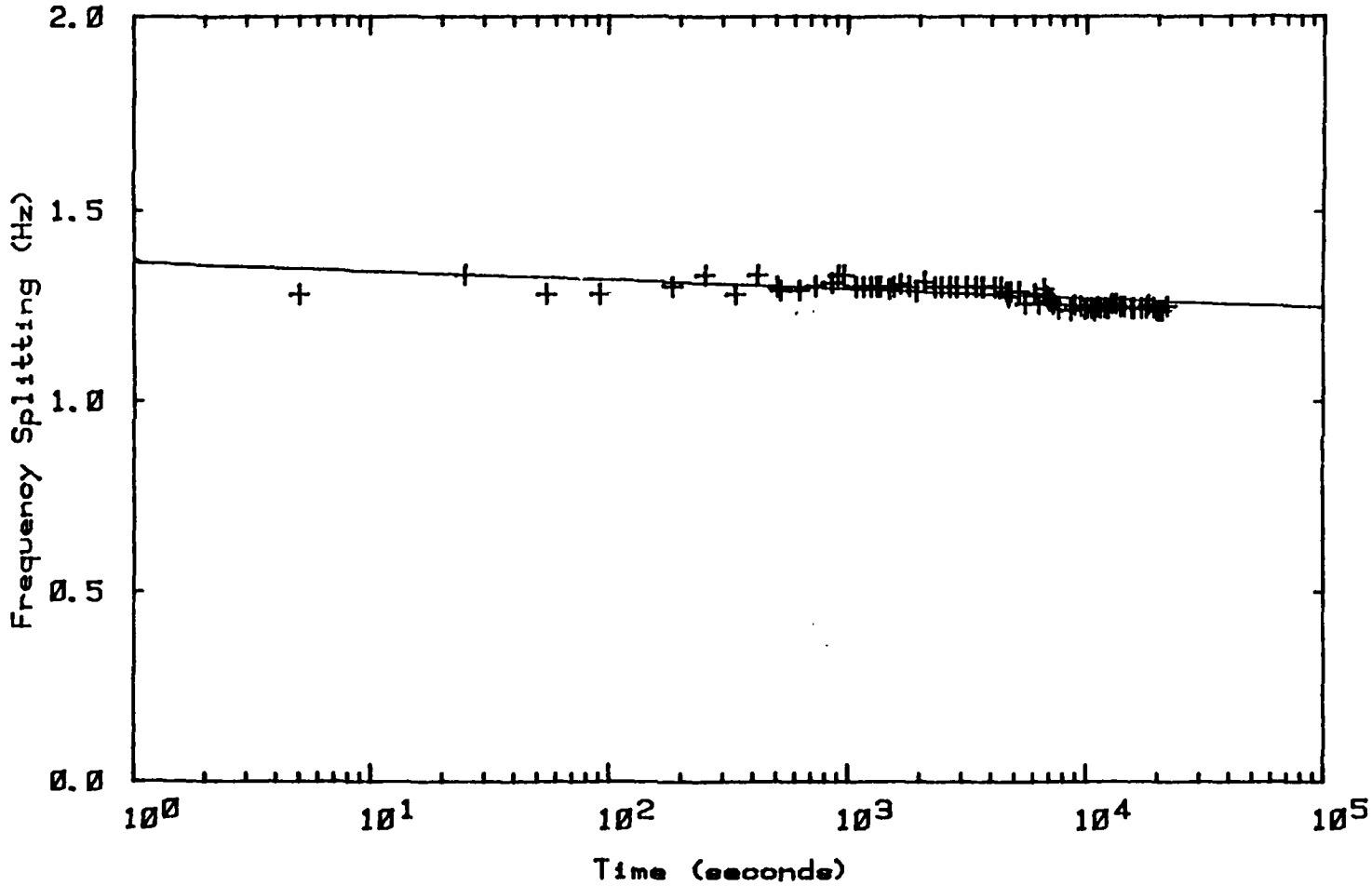

Figure IV.G.8 Decay, 100% of Saturated Velocity, T = 1.29°K, f = 0.702

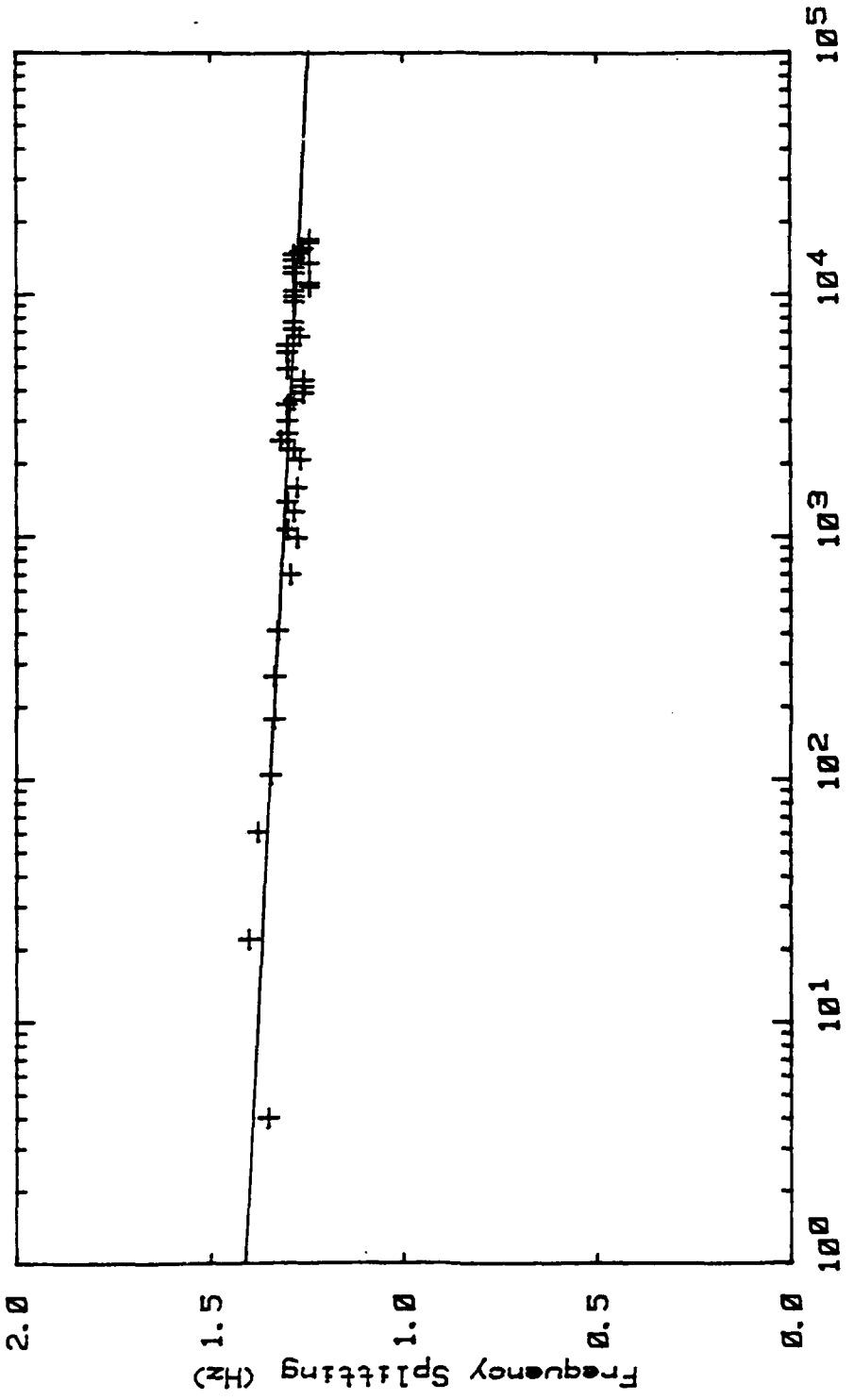

Figure IV.G.9 Decay, 100% of Saturated Velocity, T = 1.28°K, f = 0.600

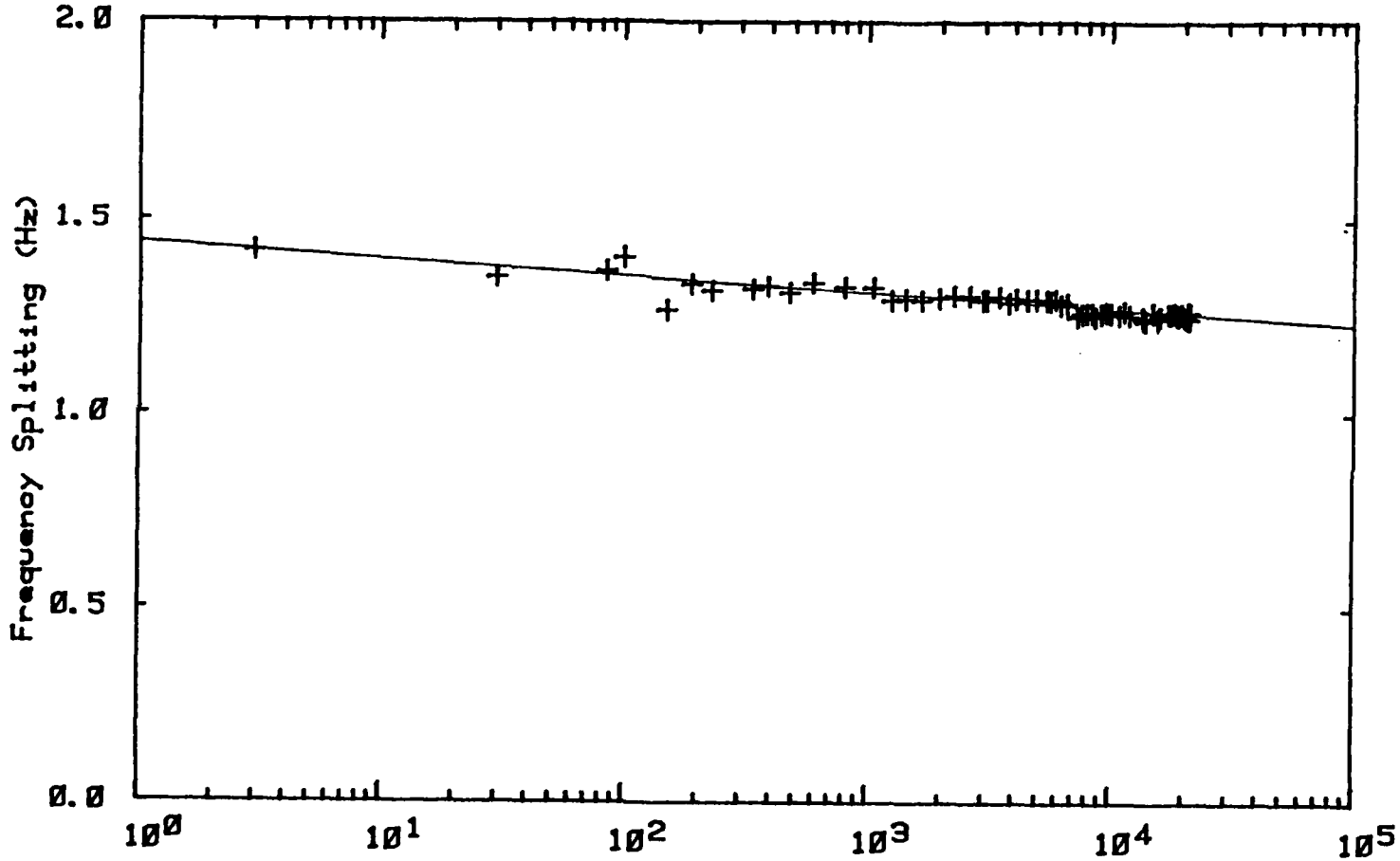

Figure IV.G.10 Decay, 100% of Saturated Velocity, T = 1.28°K, f = 0.500

IV.G.8 through IV.G.10 are 0.702, 0.600, 0.500 respectively. Here the trend is easy to pick out as the decay per decade decreases with increasing filling fraction. This is expected if the results are to match up with the results (0.67% per decade) of the filled superleak (Kojima). Table IV.G.11 is a summary table which lists the various filling fractions, the decay per decade, and the fit parameters A and B from equation IV.G.1.

There are several observations of a general nature which can be made regarding all the persistent currents in the present work. As Kojima found for the helium filled superleak the decay rates depend not only on the velocity of the persistent currents but on their intial state as well. This surprizing result means that the velocity of the persistent current is not enough to determine the decay rate for a given filling fraction (and given cell). Assuming that the logarithmic decay holds for long times then for the lowest decay rates observed the current would only decay 7.8 percent in the age of the universe (10 to the 17th seconds). The currents are truely are deserving of their name, persistent currents.

It was found during the course of investigation that the currents, especially those near their saturated

TABLE IV.G.11

SUMMARY TABLE OF PERSISTENT CURRENT
DECAY AS A FUNCTION OF FILLING FRACTION

FILLING FRACTION	PERCENT DECAY PER DECADE
0.798	1.71 ± 0.34 %
0.702	1.91 ± 0.12 %
0.600	2.47 ± 0.26 %
0.500	2.87 ± 0.19 %

values, were mechanically frail. If the dewar was sharply tapped or if nitrogen was abruptly added to the outer dewar, a sharp drop in the persistent current velocity was noted. However, after this intial loss they would seem quite stable to any further decreases in this manner. This can be readily seen in figures IV.G.2 and IV.G.8. The data past the sharp drops was left out of the fits using equation IV.G.1.

IV.H TEMPERATURE DEPENDENCE OF CRITICAL VELOCITIES

There are several critical velocities present in superfluid systems. The first is omega cee one, which marks the end of the Landau or reversible flow region. The next is omega sigma which marks the beginning of the vortex saturated flow region. Finally, omega cee two marks the point where superfluidity is lost from excessive Vn-Vs, however, this has never been observed in helium II. In this section the dependence of omega sigma on temperature is presented.

The experimental procedure to measure the temperature dependence of omega sigma is as follows. The probe is prepared as described in section IV.A. It is rotated above the lambda point fast enough so a saturated persistent current will result when the probe

is cooled to its operating temperature (1.2 degrees Kelvin). The probe is cooled and the splitting is recorded. The dewar is then warmed a little (0.15 degrees Kelvin) and recooled to the operating temperature. The splitting is then remeasured and any reduction is noted. The reduction in splitting is from the decrease of the critical velocity at the highest temperature. The procedure is repeated, warming up a little higher each time and the new splitting recorded. The results are shown for three different filling fractions in figure IV.H.1 (.344,.501,.803). The plot shows the frequency splitting divided by mode number plotted against the temperature is was raised to before recooling for each point. These results may be compared with the filled superleak (Kojima). This is shown in figure IV.H.2. The abruptness of the decrease is seen to depend on the filling fraction f. The larger the filling fraction the higher the critical velocity remains with increasing temperature.

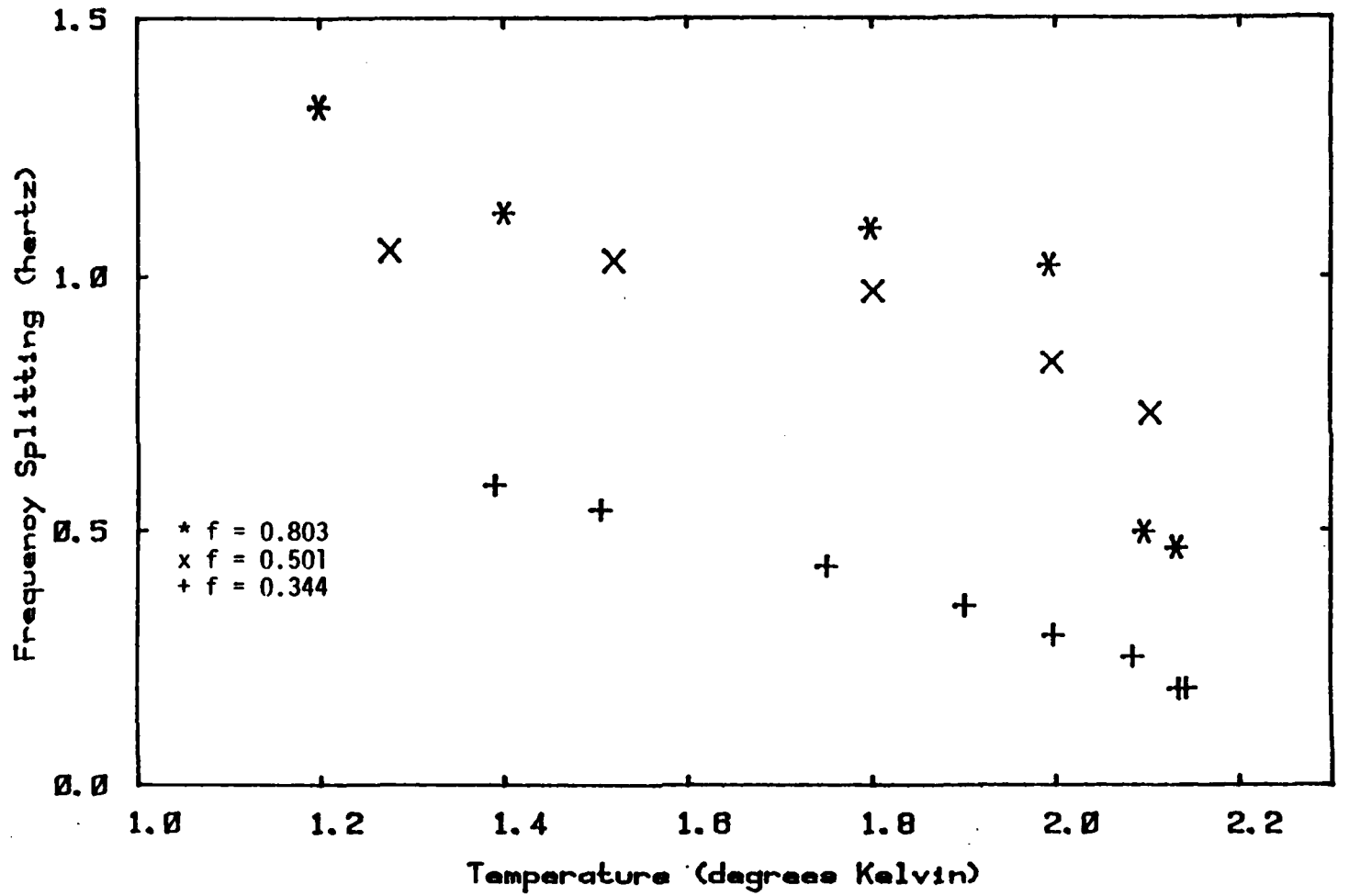

Figure IV.H.1 Critical Velocity ω_σ versus Temperature

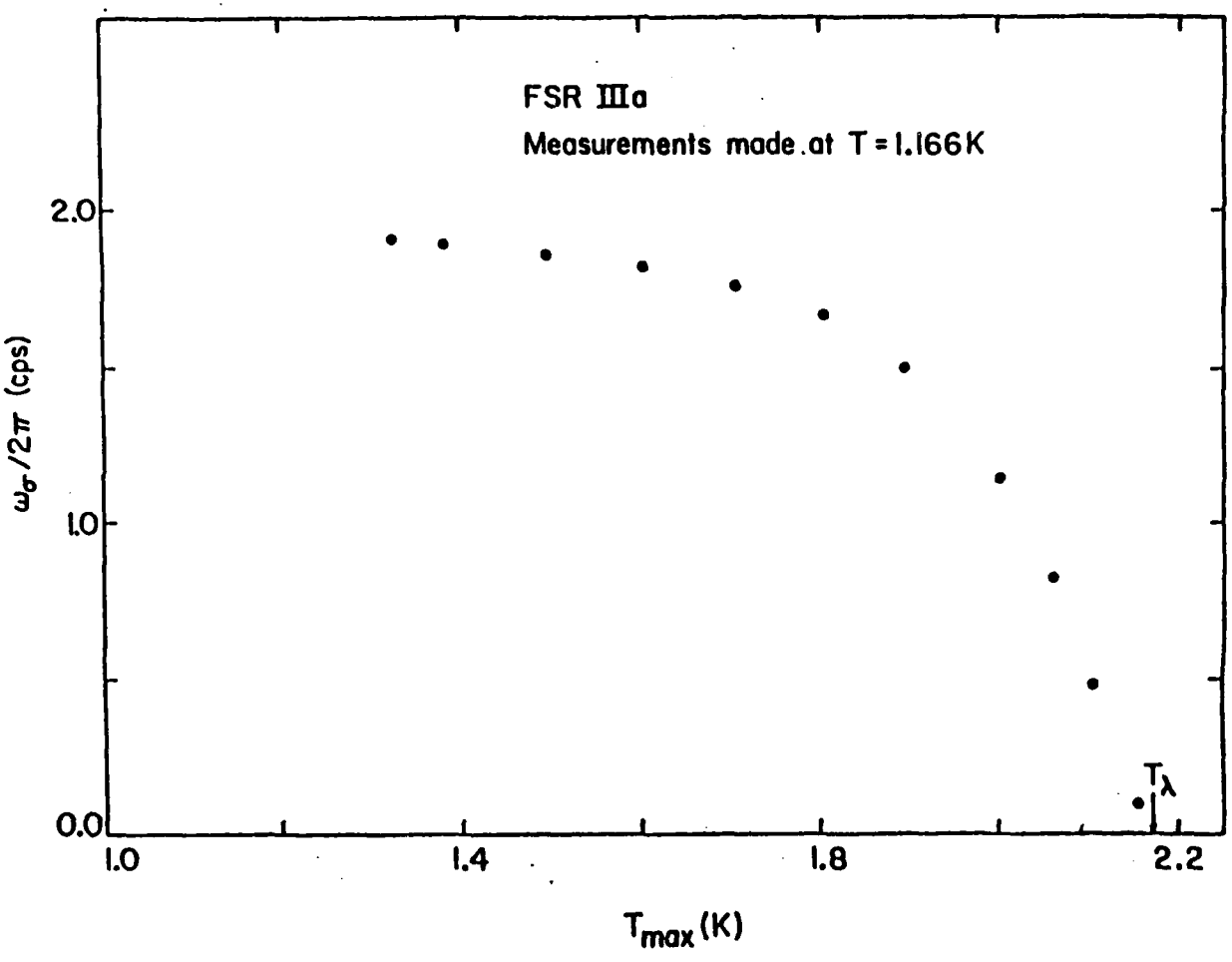

Figure IV.H.2 Saturated Critical Angular Frequency $\omega_\sigma/2\pi$ vrs Temperature

IV.I DEPENDENCE OF THE SOUND SPEED ON ROTATION SPEED

The frequency of any given mode is determined by the speed of sound in a given cell. If the speed is affected by the presence of a persistent current the center frequency will shift. This could be due to a change in the superfluid density as a function of the persistent current velocity as Kojima found.

The sound speed is calculated from the experimental frequency by equation II.B.5. The center, high and low frequencies for three runs are shown in figure IV.I.1 through IV.I.3. They show three sets of points on each graph. The top row is the frequency of the higher resonance, the middle row is the average and the lower row is the frequency of the lower peak. Within the accuracy of the measurements, there is no systematic change in the center frequency. This implies the velocity of the sound mode (or the value of the

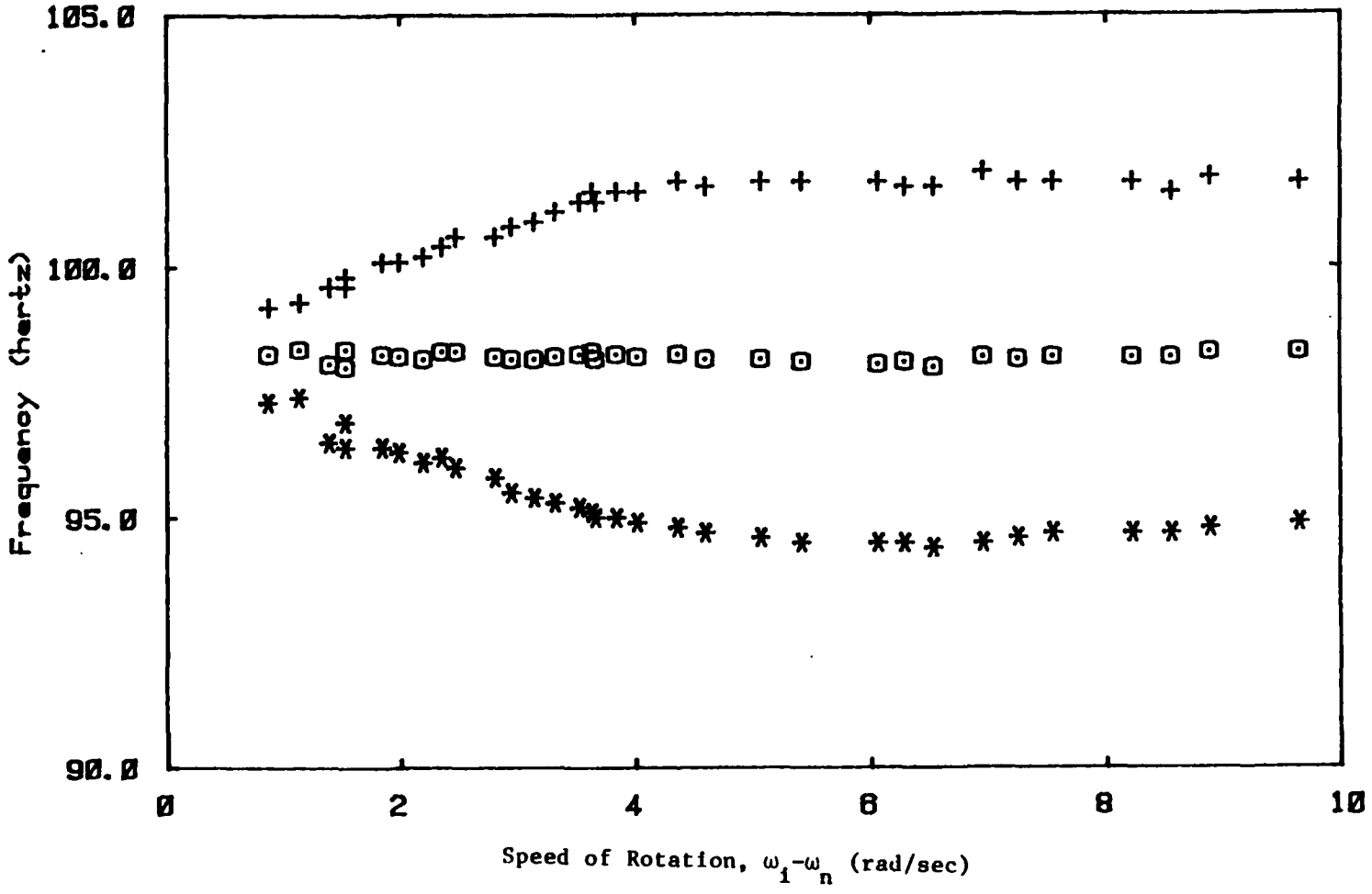

Figure IV.I.1 Frequency versus Speed of Rotation, T = 1.28°K, f = 0.700

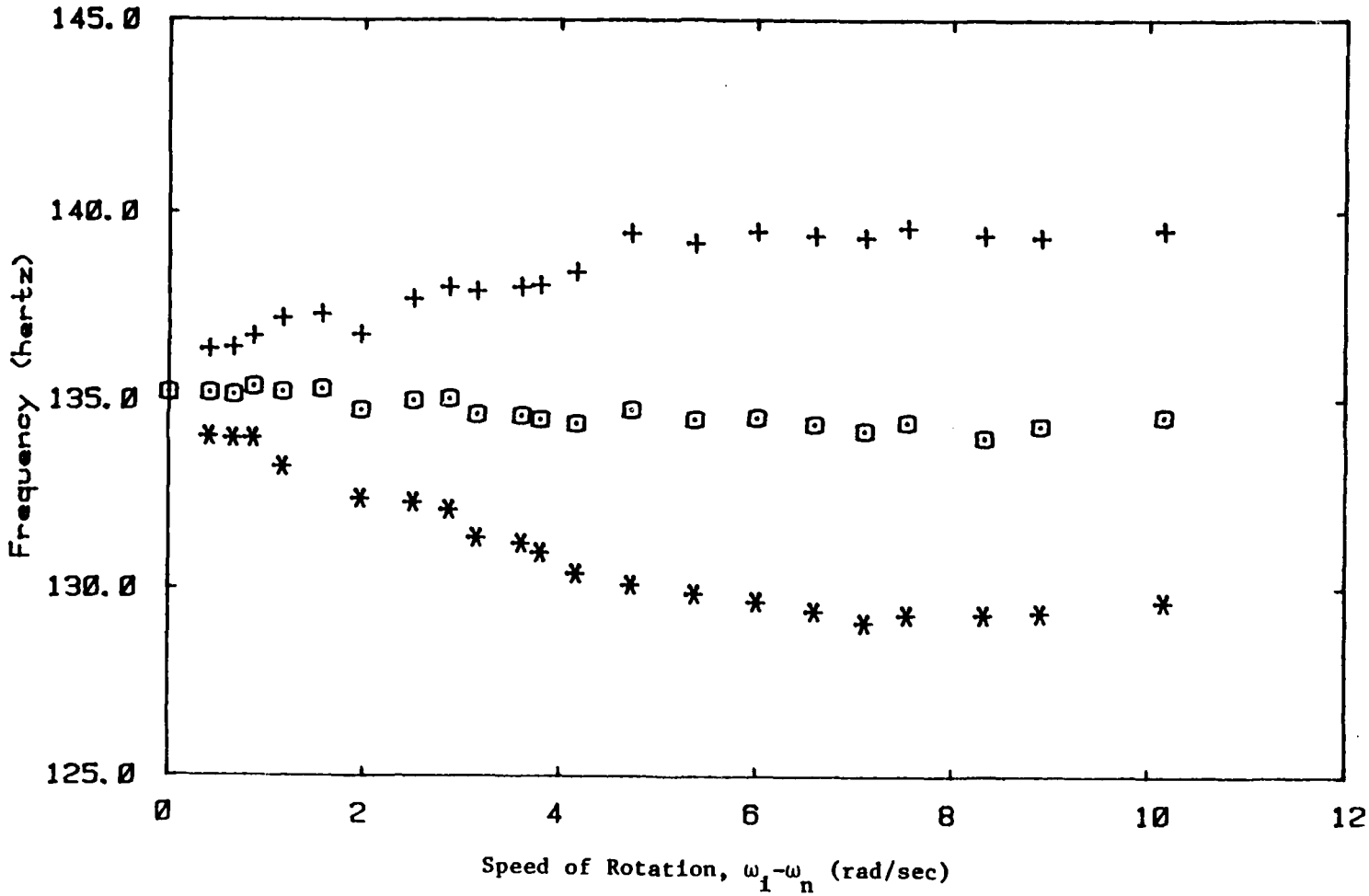

Figure IV.I.2 Frequency versus Speed of Rotation, T = 1.29°K, f = 0.500

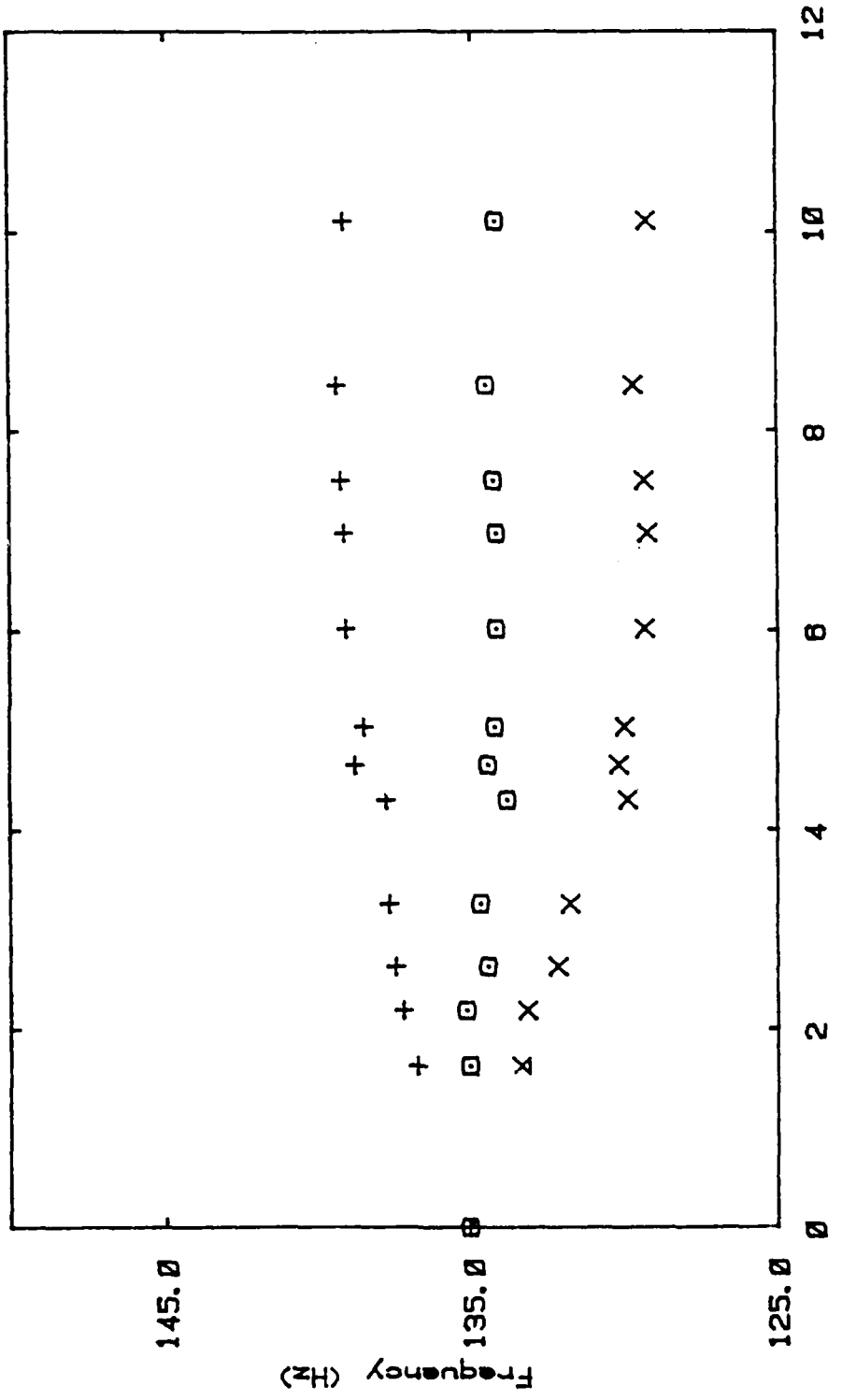

Figure IV.I.3 Frequency versus Speed of Rotation, T = 1.29°K, f = 0.500

superfluid fraction) is independent of the flow or rotation speed Wn within experimental error..

IV.J FREQUENCY SPLITTING VERSUS TEMPERATURE

Figure IV.J.1 shows the frequency splitting for a saturated persistent current plotted against increasing temperature. The splitting is observed to increase with increasing temperature. This begins about 1.4 degrees Kelvin. This is sooner than would be expected from figure II.C.2 which has been calculated from Landau's two fluid eqautions. At this time there is not a satisfactory explanation of this behavior.

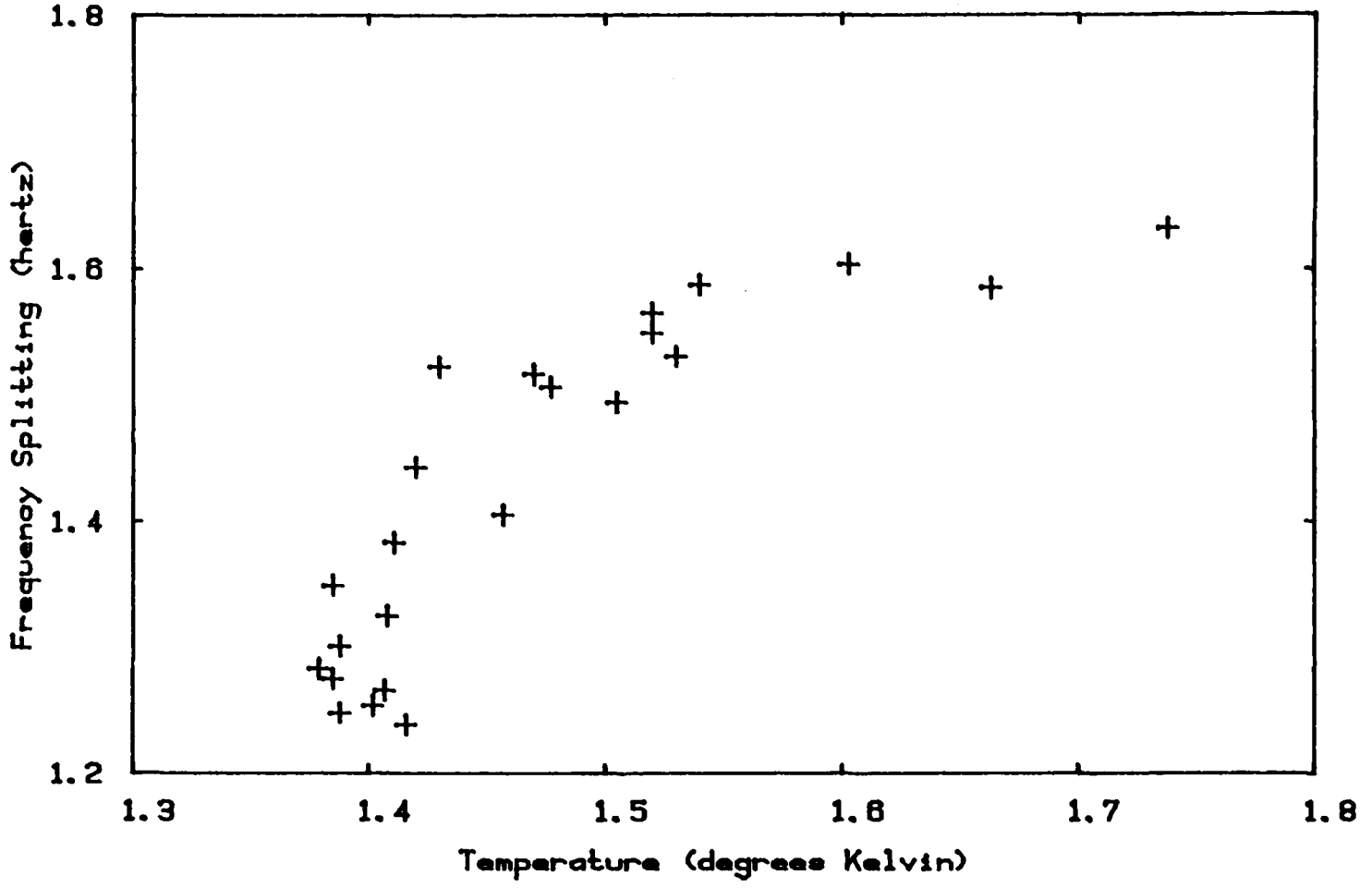

Figure IV.J.1 Frequency Splitting versus Temperature

V. CONCLUSIONS

Using acoustic techniques the properties of a superleak partially filled with He II have been investigated. The liquid He II forms a film which covers all the alumina powder grains (1 micron) which form the superleak. From the acoustic speed of the thickness wave in the helium II film the acoustic index of refraction, n, has been determined. Motivated by the idea that the scattering from the powder grains and the vapor spaces is independent a model has been proposed which is in excellent agreement with the data for $0.3 < f < 1.0$.

Using acoustic doppler-shift measurements the velocity of persistent superfluid currents have been studied. The potential flow region (Landau Region) has

been demonstrated at low rotational velocities (below about 0.5 Hz). At higher angular speeds quantized vortices enter the system becoming pinned in the superleak. This pinning leads to hysteresis in the relationship between the persistent current velocity and angular velocity of the cell.

Several critical velocities were determined. The first, omega cee one is the upper bound to the velocity of rotation for which the flow remains all potential (compare with Hc1 for the Meissner state). The second critical speed, omega sigma, is the angular velocity for which the value of Vn-Vs becomes a maximum. Further increases in the velocity of rotation do not increase the splitting (Vn - Vs). Finally the superfluid critical veloctiy was measured as a function of temperature and filling fraction. All the critical velocities were found to depend on the filling fraction and the temperature.

Persistent current velocity decay rates were determined. They were found to depend on the filling fraction, the temperature and the initial velocity of the persistent current rather than its instantaneous velocity. The decay was studied as a function of filling fraction for saturated initial persistent current velocities and the decay was found to decrease

for increased filling fraction. The deacy rate was also studied for fixed filling fraction and different initial persistent current velocities and was found to decrease for lower initial velocities. Decay rates varied from 0.5 percent to 2.9 percent per decade.

The partially filled superleak is directly comparable with both the filled superleak studied by Kojima and co-workers and also the magnetic properties of an irreversible high field type-II superconductor as studied by Bean, Kim and also Anderson. A one-to-one correspondence is made between the analogous properties of the three systems.

There are still several open questions. The persistent current velocity should be measured as a function of the filling fraction as a check of the quantization condition on Vs from equation I.B.7. The index of refarction measurements could be extended for a greater range of filling fractions by increasing the Q of the resonator and hence increasing the resolution. This would have the added benefit of increasing the ability to resolve small changes in persistent current velocities. This could be done by eliminating all vapor spaces in the cell. The vapor spaces are believed to be responsible for the acoustic losses.

A range of porosities could be studied to push

equation IV.D.5 to greater extremes. Powders of different microscopic geometries could be tried in order to more closely determine the validity of our interpretation of beta being a measure of the microscopic tortuosities of the superleak and vapor spaces. Finally the dependence on Vn - Vs on temperature does not have an adequate explanation.

APPENDIX ONE

$$C = C_o \pm (V_N - V_s) \frac{\partial C}{\partial V_s}$$

$$\frac{\partial C}{\partial V_s} \approx 1 , \qquad \frac{\Delta f}{m} = \frac{C}{2\pi r} ,$$

$$\frac{\Delta f}{M} = \frac{(V_N - V_s)}{\pi r}$$

$$\text{SLOPES FROM GRAPHS} = s = \frac{\Delta F/m}{\omega n}$$

$$S = \frac{V_N - V_s}{\pi r \omega_n} , \qquad \omega_x r = v_x$$

$$\frac{\omega_s}{\omega_n} = 1 - \pi s$$

REFERENCES

(Allen) J. F. Allen and A. D. Misener, Nature, Vol 141, No 75, 1938

(Anderson) P. W. Anderson, Phys. Rev. Lett. 9, 30,(1962)

(Atkins) K. R. Atkins, Phys Rev Vol III, No 4,Feb. 1958

(Bean) C. P. Bean, M. V. Doyle, and A. G.Pineus, Phys. Rev. Letters, Vol. 9, 93, 1962

(Biot) M. Biot, Journal of Applied Physics,Vol. 33, No. 4, 1962

(Clow) J. Clow, J.C. Weaver, D. Depatie and J.D. Reppy, Proc. LT 9, 1964, Plenum (New York, 1965)

(Depatie) J. D. Reppy and D. Depatie, Phy. Rev. Letters, Vol 12, 187, 1964

(Fraser) J. C. Fraser, Thesis, University of California Los Angeles, 1969

(Hall) H. E. Hall, Phil. Trans. Roy. Soc. (London),Vol. A250, 359, 1957

(Hallock) D. T. Ekholm and R.B.Hallock, Phys. Rev. B Vol.21,3902(1980)

(Kapitza) P. Kapitza, Nature, Vol 141,No 74, 1938

(Keesom) W. H. Keesom and G. MacWood, Physica, Vol 5, No 737, 1938

(Kim) Y. B. Kim, C. F. Hempstead, A. R. Strand, Phys. Rev. 0, 306(1962)

(Kojima) d. Kojima, Thesis, University of California, Los Angeles, 1972

(Kukich) G. Kukich, J. D. Reppy and R.P. Henkel, Phys. Rev. Lett. 21,(1968)197

(Landau) L. D. Landau, J. Phys., Vol 5, No 71, 1941

(Leonard) H.J.Seguin and R.W.Leonard, RSI,Vol 37, 1743-1745, 1966

(London) Fritz London, Nature 141, 913 (1938)

(Mehl) J. B. Mehl and W. Zimmermann Jr.,Phys. Rev. Letters, Vol 14, 815, 1965

(Morse) P. M. Morse and K. U. Ingard,Theoretical Acoustics, McGraw-Hill, 1968.

(Onsager) L. Onsager, Nuovo Cimento Suppl.,Vol 6, No 249, 1949

(Osborne) D. Osborne, Proc. Roy. Soc.(London), Vol A63, No 909, 1950

(Putterman) S. J. Putterman, Superfluid Hydrodynamics, North Holland, 1974

(Rayfield) G. W. Rayfield and F. Reif, Phys,. Rev. Letters, Vol 11, 305, 1963

(Reppy) G. Kukich, J. D. Reppy and R.P. Henkel, Phys. Rev. Lett. 21,(1968)197

(Rosenbaum et al) R. Rosenbaum, G. A. Williams, D. Heckerman,J. Marcus, D. Scholler, J. Maynard, and I. Rudnick,J. Low Temp. Phys., Vol. 35, No.5/6 (1979)

(Rudnick) I. Rudnick, UCLA Department of Physics, class " Advanced Physical Acoustics "

(Rudnick 76) I. Rudnick, Physical Acoustics at UCLA in the Study of Superfluid Helium, New Directions in Physical Acoustics, Soc. Italiana di Fisica Italy, 1976

(Sen) D. Johnson, and P. Sen, Phys. Rev. B, Vol 2, 5, 1981.

(Shapiro) K. A. Shapiro, Thesis, University of California Los Angeles, 1964.

(Telschow) K.L. Telschow and R.B. Hallock, Phys. Rev. Lett. Vol.37,1484 (1976)

(Tisza) Lazlo Tisza, Nature, Vol 141, No 913, 1938

(Verbeek 1974) H.J. Verbeek,E. Van Spronsen, H. Van Beelen, R. De Bruyn Ouboter and K.W. Taconis, Physica, Vol.77,131-133 (1974)

(Verbeek) H.J. Verbeek, Thesis, University of Leiden, 1980

(Vinen) W. F. Vinen, Proc. Roy. Soc. (London),Vol A260, 218, 1961

(Whitmore) S. C. Whitmore and W. Zimmermann Jr., Phys. Rev., Vol 166, No 181, 1968

(Williams 1974) G. A. Williams and R. Packard, Thesis, University of California Berkeley, 1974

(Williams 1979) G. A. Williams, Ralph Rosenbaum and Isadore Rudnick, Phys. Rev. Lett., Vol. 42, No. 19, 1979

REPORTS DISTRIBUTION LIST FOR ONR PHYSICS PROGRAM OFFICE
UNCLASSIFIED CONTRACTS

Director
Defense Advanced Research Projects Agency
Attn: Technical Library
1400 Wilson Blvd.
Arlington, Virginia 22209
3 copies

Office of Naval Research
Physics Program Office (Code
800 North Quincy Street
Arlington, Virginia 22217
3 copies

Office of Naval Research
Director, Technology (Code 200)
800 North Quincy Street
Arlington, Virginia 22217
1 copy

Naval Research Laboratory
Department of the Navy
Attn: Technical Library
Washington, DC 20375
3 copies

Office of the Director of Defense
Research and Engineering
Information Office Library Branch
The Pentagon
Washington, DC 20301
3 copies

U. S. Army Research Office
Box 12211
Research Triangle Park
North Carolina 27709
2 copies

Defense Technical Information Center
Cameron Station
Alexandria, Virginia 22314
12 copies

Director, National Bureau of Standards
Attn: Technical Library
Washington, DC 20234
1 copy

Commanding Officer
Office of Naval Research Western Regional Office
1030 East Green Street
Pasadena, California 91101
3 copies

Commanding Officer
Office of Naval Research Eastern/Central Regional Office
666 Summer Street
Boston, Massachusetts 02210
3 copies

Director U. S. Army Engineering Research and Development Laboratories Attn: Technical Documents Center Fort Belvoir, Virginia 22060	1 copy
ODDR&E Advisory Group on Electron Devices 201 Varick Street New York, New York 10014	3 copies
Air Force Office of Scientific Research Department of the Air Force Bolling AFB, D. C. 22209	1 copy
Air Force Weapons Laboratory Technical Library Kirtland Air Force Base Albuquerque, New Mexico 87117	1 copy
Air Force Avionics Laboratory Air Force Systems Command Technical Library Wright-Patterson Air Force Base Dayton, Ohio 45433	1 copy
Lawrence Livermore Laboratory Attn: Dr. W. F. Krupke University of California P.O. Box 808 Livermore, CAlifornia 94550	1 copy
Harry Diamond Laboratories Technical Library 2800 Powder Mill Road Adelphi, Maryland 20783	1 copy
Naval Air Development Center Attn: Technical Library Johnsville Warminster, Pennsylvania 18974	1 copy
Naval Weapons Center Technical Library (Code 753) China Lake, California 93555	1 copy
Naval Training Equipment Center Technical Library Orlando, Florida 32813	1 copy
Naval Underwater Systems Center Technical Center New London, Connecticut 06320	1 copy

AD-A123 522 PERSISTENT CURRENTS IN A ROTATING SUPERLEAK PARTIALLY FILLED WITH SUPERFLUID HELIUM(U) CALIFORNIA UNIV LOS ANGELES DEPT OF PHYSICS J S MARCUS DEC 82 TR-41 3/3

UNCLASSIFIED N00014-75-C-0246 F/G 20/4 NL

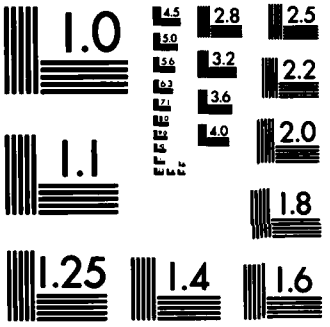

Commandant of the Marine Corps
Scientific Advisor (Code RD-1)
Washington, DC 20380 — 1 copy

Naval Ordnance Station
Technical Library
Indian Head, Maryland 20640 — 1 copy

Naval Postgraduate School
Technical Library (Code 0212)
Monterey, California 93940 — 1 copy

Naval Missile Center
Technical Library (Code 5632.2)
Point Mugu, California 93010 — 1 copy

Naval Ordnance Station
Technical Library
Louisville, Kentucky 40214 — 1 copy

Commanding Officer
Naval Ocean Research & Development Activity
Technical Library
NSTL Station, Mississippi 39529 — 1 copy

Naval Explosive Ordnance Disposal Facility
Technical Library
Indian Head, Maryland 20640 — 1 copy

Naval Ocean Systems Center
Technical Library
San Diego, California 92152 — 1 copy

Naval Surface Weapons Center
Technical Library
Silver Spring, Maryland 20910 — 1 copy

Naval Ship Research and Development Center
Central Library (Code L42 and L43)
Bethesda, Maryland 20084 — 1 copy

Naval Avionics Facility
Technical Library
Indianapolis, Indiana 46218 — 1 copy

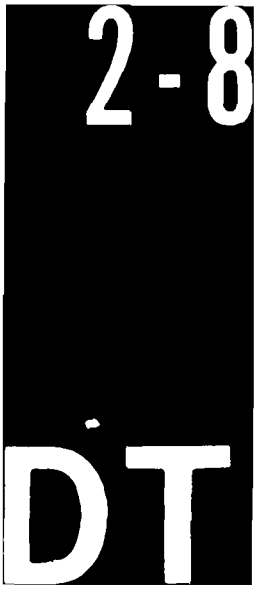
2-8
DT